DOSIMETRY OF ELECTRON SOURCES NEAR PLANAR TISSUE INTERFACES

DOSIMETRY OF ELECTRON SOURCES NEAR PLANAR TISSUE INTERFACES

BY

SIU-KI YU, B.Sc.

A Project Report

Submitted to the School of Graduate Studies

in Partial Fulfilment of the Requirements

for the Degree

Master of Science

McMaster University

MASTER OF SCIENCE (1989) McMASTER UNIVERSITY

(Physics) Hamilton, Ontario

TITLE : Dosimetry of Continuous Electron Sources near Planar Tissue Interfaces

AUTHOR : Siu-Ki Yu, B.Sc. (McMaster University)

SUPERVISOR : Dr. C.S. Kwok

NUMBER OF PAGES : xiii, 134

ABSTRACT

The beta dose distributions in red bone marrow equivalent material due to imbedded continuous sources were measured experimentally with ultra thin LiF thermoluminescent dosimeters near planar interfaces of cortical bone (CB) and red bone marrow (RBM), and RBM and air. It has been also investigated numerically by Cyltran, the Monte Carlo code.

In the Monte Carlo approach, the dose enhancement ratio for a planar CB-RBM interface increases with electron energy and reaches a plateau at 0.50 MeV while the dose reduction ratio for a planar vacuum-RBM interface decreases to a steady value from 1.00 MeV onwards.

With a semi-infinite source of ^{32}P, dose enhancement ratios at 0-9, 79-88, and 157-166 mg/cm^2 separations from a planar CB-RBM interface were measured to be 1.07 ± 0.01, 1.03 ± 0.03 and 0.99 ± 0.03 respectively. The dose reduction ratios at these separations from a planar AIR-RBM interface were found to be 0.82 ± 0.01, 0.94 ± 0.03 and 0.97 ± 0.03 respectively. Both the dose enhancement ratios and dose reduction ratios agree with the results calculated by the Monte Carlo approach within one standard deviation except for the dose reduction ratio at 0-9 mg/cm^2 from the AIR-RBM interface. The experimental result in this case is about three standard deviations less than the Monte Carlo results.

Using the same Monte Carlo code, the dose enhancement ratio at 0-20 micron separation from a planar CB-RBM interface due to a point or plane source of 0.50 MeV

electrons at the interface reaches saturation at approximately 0.22 times the CSDA range of 0.5 MeV electron in CB for both plane and point source configurations. The saturation dose enhancement ratio for both configurations is 1.06 ± 0.01.

ACKNOWLEDGMENTS

I would like to thank my supervisor, Dr. C.S.Kwok, for his guidance and advice throughout this project. I am also grateful to the opportunity and financial support from McMaster University and Dr. C.S.Kwok to complete this work.

A special thanks to Josane Nunes, Patrick Tam, and Vinay Jain for their constant encouragement and helpful suggestions.

Finally, it is with deep gratitude that I acknowledge the support my family has provided me in all my endeavor.

TABLE OF CONTENTS

LIST OF FIGURES

LIST OF TABLES

CHAPTER 1

INTRODUCTION

Recent advances in immunological technology lead to the use of tumor-associated monoclonal antibodies as carriers of beta radiation to small but widespread neoplasms for therapy. Owing to a combination of several factors including the radiosensitivity of the red bone marrow (RBM) and rapid entry of labeled antibody into bone marrow from the circulation, the RBM and to less extent the endosteal cells of the bone are likely to be the dose limiting tissues for systemic applications. Therefore, it is clinically important to quantitate their dose.

Although most tumors have soft tissue composition, their neighborhood may include air and bone interfaces with very different physical properties such as mass density. Electrons are backscattered more from bone than from soft tissue thereby increasing radiation dose to the tissues adjacent to bone. In contrast, dose to the soft tissue near an air interface drops. One goal of this work was to estimate the perturbation in dose distributions due to uniform semi-infinite sources of electrons at planar interfaces of cortical bone - red bone marrow, and soft tissue - air. It has been investigated by both experimental approach and Monte Carlo method.

The trabecular bone is composed of thin lamellae of cortical bone (CB) with a wide range of thicknesses. They are called trabeculae and they form a meshwork of interconnecting spaces which contain bone marrow. Another goal of the work was to investigate the effect of thickness of the trabeculae on the backscatter dose to the bone marrow imbedding uniform sources of electrons.

This chapter gives background material for this project. Chapter two describes the Monte Carlo code, the method of data analysis, and results of the Monte Carlo calculations. In chapter three, the materials, method, experimental procedure and experimental results are presented. Chapter four contains some essential findings in this project including the effect of trabecular bone thickness on electron backscatter dose. The final chapter discusses the Monte Carlo and experimental results and their comparison with other researchers' findings.

1.1 BONE MARROW STRUCTURE

The architecture of bone marrow is best understood in relation to its vascular anatomy. Figure 1.1 gives a schematic representation of a cross section of the shaft of a long bone containing hemopoietic marrow [23]. Hemopoietic marrow is largely confined to a zone adjacent to the endosteum.

The marrow cavities of the skull, vertebrae, ribs, sternum, pelvis and the articular ends of long bones contain numerous cancellous trabeculae in addition to marrow. In large mammals the hemopoietic activity of the marrow is not uniform in all bone cavities. Whereas the marrow of axial skeleton is intensely hemopoietic (red marrow), that of the limb bones of adults contains mainly adipose cells (yellow marrow). In addition, the general cellular content of the bone marrow is age-dependent. At birth, no adipose cells are present in the marrow.

Bone marrow is a well vascularized organ composed of hematopoietic parenchyma and a supporting stroma. Cellular exchange between the hematopoietic and the vasculature compartments occurs across the walls of the vascular sinusoids. The wall of the sinusoids is composed of a luminal layer of endothelial cells, which forms a complete inner lining, and a lining of adventitial reticular cells, which forms an incomplete outer coat. There is evidence that the sinusoids are permeable to large molecules such as plasma proteins, and the plasma proteins are also capable of moving back into bloodstream [16,17]. Whether circulating blood enters hematopoietic compartments through the wall of vascular sinusoids or from arterial terminals whose connection with the sinusoids has been disturbed is not clear. The permeability of the RBM to large molecules like antibodies plays a significant role in the rapidity of RBM uptake of radiolabeled antibodies and the residence time of the antibodies in the RBM. Whether the sinusoids are open or closed is still a controversial question. This is an essential feature of the bone marrow in radiolabeled monoclonal antibody dosimetry.

The bone marrow is the site for blood cell formation. The principal control of blood cell formation is exerted at the level of the stem cells. In the bone marrow, stem cells constitute a pool of self-perpetuating cells differing in specialization from being multi- or pluri- potential to being committed to one cell line only. Functionally, the multipotential stem cells have been identified by their capacity to repopulate the bone marrow after hematopoietic injury.

Radiation-induced bone marrow failure is considered to result primarily from the destruction of hemopoietic stem cells. Lord [18] reported a concentration gradient of the multipotential stem cells (CFU-S) in mouse bone marrow, the CFU-S concentration being threefold greater near the bone surface than near the central longitudinal axis of the femoral medullary cavity. However, Maloney [19] presented contrary results. The existence of a stem cell gradient is therefore still an open question. If there is a higher concentration of stem cells near the bone surface of the bone marrow, then the effect on bone marrow toxicity due to backscattering of electron at bone/marrow interfaces becomes more important.

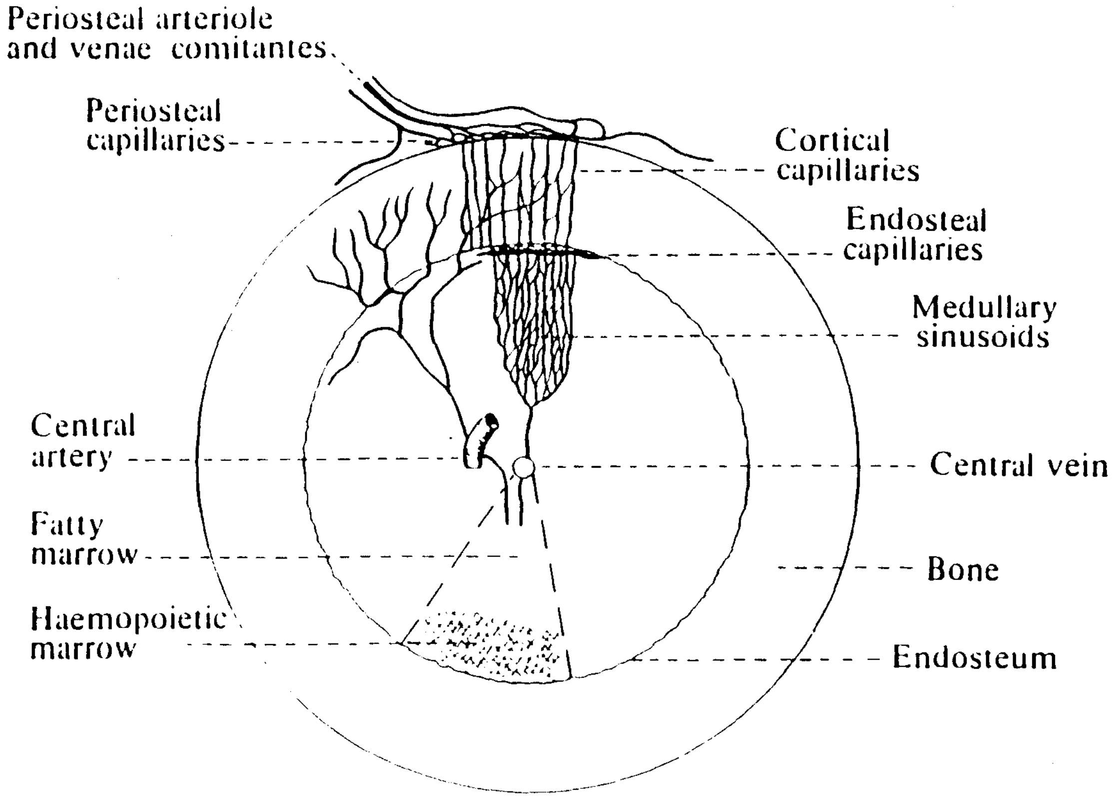

Figure 1.1. Organisation of bone marrow in a haemopoietically-active long bone

1.2 RADIOIMMUNOTHERAPY

Radioimmunotherapy (RIT) is the use of radiolabeled tumor-associated antibodies for cancer treatment. It is rapidly attracting interest as a potential weapon for cancer therapy. A first consideration in the use of radiolabeled antibody in diagnosis and therapy are the antigens, which are the potential targets of such antibody. In 1980, Order [13] described the delivery of therapeutic radiation in humans using ^{131}I-labeled polyclonal antibodies against tumor-associated antigens such as ferritin. Order [14] also showed a much higher specificity and affinity of monoclonal antibody over polyclonal antibody a year later.

Obviously, the success of any radiolabeled tumor-seeking antibody therapy will depend on the specificity and affinity of the antibody for the tumor. Monoclonal antibodies provide homogeneous molecules to be radiolabeled in order to target specific antigens. Indeed the specificity of antibody from a single cell clone is such that the antibody only reacts with a discrete portion and configuration of the antigenic molecule. A variety of tumor-seeking monoclonal antibodies can now be produced through the application of cell hybridization technology developed by Kohler and Milstein [10] in 1975. This technology opens the door for the effective development of the use of antibodies as carriers of radionuclides for cancer therapy.

The time factor is another important consideration such as the rapidity of tumor uptake, the biological half-life of the antibody in the tumor, and the speed of clearance from the normal tissues. In practice, the radiation dose to the tumor is dependent on both the physical properties of the labeling radionuclide and the biological half-life of the antigen-radiolabeled antibody complex. The toxic effect to normal tissue is logically less with a higher speed of clearance, and adminstration of larger therapeutic dose is allowed consequently.

The molecular size of intact immunoglobulin molecules does not allow them to move rapidly. This prolongs the time from injection to tumor uptake, thereby decreasing the radiation delivered to the tumor and increasing the total body dose. The solution of this problem is to use their active fragments for substitution. The active fragments can be produced by enzymatic digestion under appropriate conditions. Increases in the uptake of the radiolabeled monoclonal antibodies at the tumor site greatly enhance the ability of this technology to fight against tumor. However, a limiting factor in this modality is the lack of adequate blood flow at the tumor. The effects of induced hyperthermia on the uptake of radiolabeled monoclonal antibodies are being studied in human melanoma xenografts initiated in the hind legs of nude mice by Kwok et al. [28] and Stickney et al. [24].

Tumor morphologies are extremely varied, and antibody binding and retention will also vary depending on the antibody or antibody fragment used. To optimize the treatment of a particular cancer it may therefore be necessary to select a suitable antibody radiolabel to suit the individual tumor. Lists of suitable radionuclides for labeling tumor-associated or tumor-specific antibodies have been given by Wessels and Rogus [11], William and Irving [15], and Humm [12].

Organs that might commonly be expected to set upper limits on tumor dosage would include bone marrow because of the easy access of the antibody to the bone marrow and its high radiation sensitivity. Therefore, it is clinically important to quantitate the dose to this tissue.

1.3 BONE MARROW RADIATION DOSIMETRY

The absorbed dose to any target tissue in the body is the energy absorbed per unit mass of tissue. In the MIRD schema, the general equation employed is

$$D_T = A_0 \sum \tau_h S(T \leftarrow h) \tag{1.1}$$

where

D_T = the dose to target tissue T (mGy)
A_0 = the activity injected into the body (MBq)
$S(T \leftarrow h)$ = the absorbed dose in tissue T per disintegration in source region h (mGy/MBq-sec), called the S-value

τ_h = the residence time in source region h (sec). It also takes into account the fraction of A_0 taken up by h.

For RIT applications, the radiolabeled antibody is often metabolized by several organ systems, most notably those involved in excretory functions. Therefore, the blood, liver, kidneys, bladder, and possibly gastrointestinal organs may be significant source organs for irradiation of marrow. The marrow will also irradiate itself due to the activity in blood which can possibly enter the marrow space by either the capillary circulation of the bone marrow or extravascular diffusion of antibody through the sinusoidal walls. Since many possible candidates of radionuclides used for RIT applications involve a large beta and electron component, the dose from the marrow to itself may be of primary importance

Thus, the total marrow absorbed dose should be calculated as

$$D_{RM} = A_0\{\sum(\tau_h - (\tau_{RB} m_h / m_{RB}))S(RM \leftarrow h) +$$
$$(\tau_{RM} - (\tau_{RB} m_{RM} / m_{RB}))S(RM \leftarrow RM) +$$
$$(\tau_{RB} m_{TB} / m_{RB})S(RM \leftarrow TB)\} \qquad (1.2)$$

where terms have the same meaning as in Eqn. 1.1 except with specific source and target organs :

m = mass of organ
RM = red bone marrow
h = source region
TB = total body
RB = remainder of body

This system is attractive and convenient, however, it fails to be predictive when examining non-uniformly distributed particulate radiation in the subcentimeter range, at tumor boundaries, or at organ interfaces. Early modeling approaches typically assumed an absorbed fraction of 1.0 for nonpenetrating radiation, but all the energy emitted from high energy electrons within the marrow spaces would not be deposited in the marrow. Therefore, electrons cannot be classified as nonpenetrating radiation and the absorbed fraction of energy must be analytically, numerically , or experimentally determined.

1.4 INTERACTIONS OF ELECTRONS WITH MATTER

Interactions of electron with matter can be divided into three categories : electron-electron interactions, elastic interactions with nuclei, and inelastic interactions with nuclei.

1.4.1 Electron-electron interactions

Electrons traversing a medium transfer energy to orbital electrons of the medium. Impinging electrons lose energy and are deflected at some angle with respect to their original direction. An electron receiving energy may be raised to an excited state (excitation) or may be ejected from the atom (ionization).

The linear specific energy loss due to excitation and ionization has been derived by Bethe [1] as

$$-\left(\frac{dE}{dX}\right)_{c} = \frac{2\pi e^{4}NZ}{mV^{2}}\left(\ln\frac{mV^{2}E}{2I^{2}(1-\beta^{2})} - \ln 2\left(2(1-\beta^{2})^{\frac{1}{2}} - 1 + \beta^{2}\right) + (1-\beta^{2}) + \frac{1}{8}\left(1-(1-\beta^{2})^{\frac{1}{2}}\right)^{2}\right) \qquad (1.3)$$

where

e = electron charge
N = number density of the absorber atoms
V = velocity of electron
m = electron rest mass
E = impinging electron energy
I = average excitation and ionization potential of absorber
Z = atomic number of absorber atoms
$\beta = \frac{V}{C}$, and C is the speed of light in vacuum

1.4.2 Elastic interactions with nuclei

When an electron passes the neighborhood of a nucleus, it may undergo an elastic scattering. Backscattering of electron is primarily due to elastic scattering by nuclei, where electron undergoes sufficient deflection so that it re-emerges from the surface through which it entered. According to the Rutherford scattering formula,

$$\Xi d\omega = \frac{N}{A}\left(\frac{Ze^2}{4E}\right)^2 \frac{d\omega}{\sin^4\left(\frac{\theta}{2}\right)} \qquad (1.4)$$

where

$\Xi d\omega$ = probability per g-cm^2 of an electron scattered into the solid angle $d\omega$ about θ (from its original direction)

The probability of elastic interactions with nuclei varies with Z^2 of the absorber and approximately with ($1/E^2$), where E represents the kinetic energy of the incident electrons. Thus, backscattering is most pronounced for electrons with low incident energy and absorbers with high atomic numbers.

1.4.3 Inelastic interactions with nuclei

An electron passing near a nucleus (i.e. distance of approach is smaller than the atomic radius but larger than nuclear radius) may be deflected with reduced velocity. The interaction is inelastic if energy is released as electromagnetic radiation during the encounter. Radiative energy loss is caused by an acceleration of the electron under the influence of the electric field of a nearby nucleus. The radiated energy is known as bremsstrahlung. The linear specific energy loss through this radiative process [1] is

$$-\left(\frac{dE}{dX}\right)_r = \frac{NEZ(Z+1)e^4}{137m^2C^4}\left(4\ln\frac{2E}{mC^2}-\frac{4}{3}\right) \qquad (1.5)$$

where the terms have the same meaning as in the preceding equation.

From the specific energy loss equation for collision processes and for radiative processes, it is obvious that collision energy loss increases with Z and lnE while radiative energy loss increases with Z^2 and E. Therefore, radiative loss are always a small fraction of energy losses due to ionization and excitation for low electron energies (less than a few MeV), and are significant only in absorber materials of high atomic number. As the electron energy increases, radiative energy loss becomes significant. At a certain energy called the critical energy, the two are equal. The ratio of the specific energy losses [1] is

$$\frac{\left(\frac{dE}{dX}\right)_r}{\left(\frac{dE}{dX}\right)_c} \cong \frac{EZ}{700} \qquad (1.6)$$

where E is electron energy in MeV

The effective atomic number for RBM is 5.93 [21] so that the critical energy should be approxiamtely 118 MeV according to equation (1.6). Thus, the radiative stopping power for electron in RBM is negligible in the range of electron energy considered in this work (note that the maximum electron energy considered in this work is 1.75 MeV).

The total linear stopping power for electrons is

$$\frac{dE}{dX} = \left(\frac{dE}{dX}\right)_c + \left(\frac{dE}{dx}\right)_r \qquad (1.7)$$

1.4.4 Electron range

The continuous-slowing-down-approximation (CSDA) is a schematization in which the rate of energy loss at each point along an electron trajectory is assumed to be equal to the mean energy loss given by the Bethe stopping power formula [2].

The CSDA range R_E can be defined as follows

$$R_E = \int_E^0 \frac{dE}{\left(\frac{dE}{dX}\right)_E} \tag{1.8}$$

where

E = initial electron energy

$\left(\frac{dE}{dX}\right)_E$ = Bethe stopping power for electron with energy E

However, this formula ignores multiple scattering and only suitable for heavy charged particles or low energy electrons (e.g. 0.1 MeV to critical energy in polystyrene). For electron energies much larger than the critical energy, the concept of electron range is meaningless because of cascade shower production. In addition, electrons are also subject to range straggling, defined as the fluctuation in path length for individual electrons of the same initial energy. This is caused by statistical fluctuations of the rate of energy loss along the electron track. Some energy is transported to distances greater than the CSDA range because of this energy loss straggling.

1.5 Back Scattering of Electrons

When a stream of electrons is directed against a solid target, most of the electrons penetrate into the target but some come out again. Most of the returning electrons are members of the original beam which have penetrated to a greater or lesser extent into the target, suffered elastic or inelastic collisions or both, and returned to the entrance surface of the target. Of course there are a few secondary electrons escaping from the target as well, however, they are generally having an energy less than 50 eV. Holiday et al. [26] reported that electron backscattering depends on the atomic number of the target material at energies above approximately 5 KeV. They suggested that research on electron backscatter dose at the interface should be focused on electron energies higher than 5 KeV.

There are two existing theories namely Diffusion Theory and Large Angle Single Elastic Scattering Theory to explain this phenomenon [27].

According to the Diffusion theory, electrons are supposed to travel straight into the target up to a certain specified distance, after which they diffuse evenly in all directions. It acknowledges the fact that an electron's progress eventually becomes random due to multiple collisions. However, it ignores the possibility of electrons undergoing large single reflections somewhere between the surface and the depth of complete diffusion. The depth of complete diffusion is defined as the depth at which the average cosine between the actual direction of the primary beam becomes 1/e (i.e. the directions differ by an angle of 68.4°). Suppose a stream of monoenergetic electrons is moving towards the center of a sphere and starts to move equally in all directions at the depth of complete diffusion. The electrons can only escape from the sphere within a solid angle such that their overall paths are equal to or less than their full range. The ratio of this solid angle to the solid angle of the complete sphere (i.e. 4 pi) is defined as the back-scattering coefficient. The back-scattering coefficient R deduced by this theory is

$$R = \frac{(7Z-80)}{(14Z-80)} \qquad (1.9.1)$$

where Z is the atomic number of the target

According to the Large Angle Elastic Scattering Theory, electrons are supposed to travel straight into the target, suffering retardation and also undergoing elastic collisons in accordance with Rutherford's law of scattering, but it ignores the diffusing effect of multiple scattering. Only those reaching the surface before fulfilling their total range escape from the target. The relevent back scattering coefficient R_E is

$$R_E = \frac{(a-1+0.5^a)}{(a+1)} \qquad (1.9.2)$$

where

$$a = \frac{\pi Z^2 e^4 N_A}{m^2 cA}$$

$$c = \left(\frac{16\pi N_A e^4 Z}{m^2 A}\right) \ln\left(\frac{2E}{J}\right)$$

N_A = Avogadro's number

J = 11.5 Z eV

m = electron mass

E = electron energy in eV

Archard [27] combined the above theories and the combination of the theories is composed of three regions. For low Z target (below Z=11) the depth of complete diffusion (Xd) is large compared to the range of the electrons in the target material (Xr) so that Large Single Elastic Scattering Theory predominates for this range of Z. As Z rises, the ratio of Xd/Xr falls and many more electrons diffuse back to the surface. In regions of high Z (above Z=60) the ratio of Xd/Xr is very small; electrons become diffused almost immediately and there is little chance for large single elastic scattering. Therefore, Diffusion Theory predominates in this region. In the region of medium Z ($11 < Z < 60$) Archard found that the mean of the two theories agreed well with experimental results. All materials used in this investigation have effective atomic numbers less than 11 (Ze for CB and RBM are 10.50 and 5.93 respectively [1]), thus Large Single Elastic Scattering Theory applies to this work.

1.6 THERMOLUMINESCENT DOSIMETRY

Thermoluminescence (TL) has been used as a useful means of radiation dosimetry since the early 1950's [8,9]. During exposure to radiation, electrons in the crystalline structure of a thermoluminescent phosphor are excited to higher energy levels. Some of the electrons fall into and stay in so called "traps" where they remain after the irradiation. The traps are created by the inherent impurities and defects in the crystal. If the distance of the trap energy level below the conduction band is sufficiently large, there is only a small probability per unit time at ordinary room temperatures that the electron will escape the trap by being thermally excited back to the conduction band.

When the irradiated sample is sufficiently heated, trapped electrons migrate to combine with holes or holes migrate to combine with trapped electrons releasing photons. If the photon energy is about 2 to 3 eV, the emitted photons are in the visible region. It is this portion of the light spectrum which is normally used in thermoluminescence. The amount of light emitted is directly proportional to the irradiation dose. The light yield as a function of temperature is recorded in a "glow curve". Therefore, the area under the glow curve is proportional to the irradiation dose.

In practice, not all the electron traps are of the same energy level. The shallow traps are somewhat unstable even at ordinary room temperature. Therefore, it is necessary to allow the thermoluminescent dosimeter (TLD) to "fade" before reading out. In the readout process, TLD is heated to a sufficient temperature to deplete most of the electron traps. In order to ensure that all the traps have been depleted, the TLD must be annealed before reuse.

In this project, ultra thin LiF TLD discs, 50 microns thick, were used to measure the dose distribution near planar interfaces of air - red bone marrow (AIR-RBM), and cortical bone - red bone marrow (CB-RBM). Of all TLD materials, LiF has proved to be the most popular because of its small fading at room temperature and its low average atomic number, which does not differ greatly from that of air or tissue. The minimum sensitivity of LiF is about 10^{-4} Gy. The TL output of LiF as a function of energy absorbed is linear up to about 10 Gy, and then becomes superlinear.

The basic components of most commercial TLD reading systems are illustrated in Figure 1.1. The commercial system which was used in this project is the Harshaw TLD system 4000.

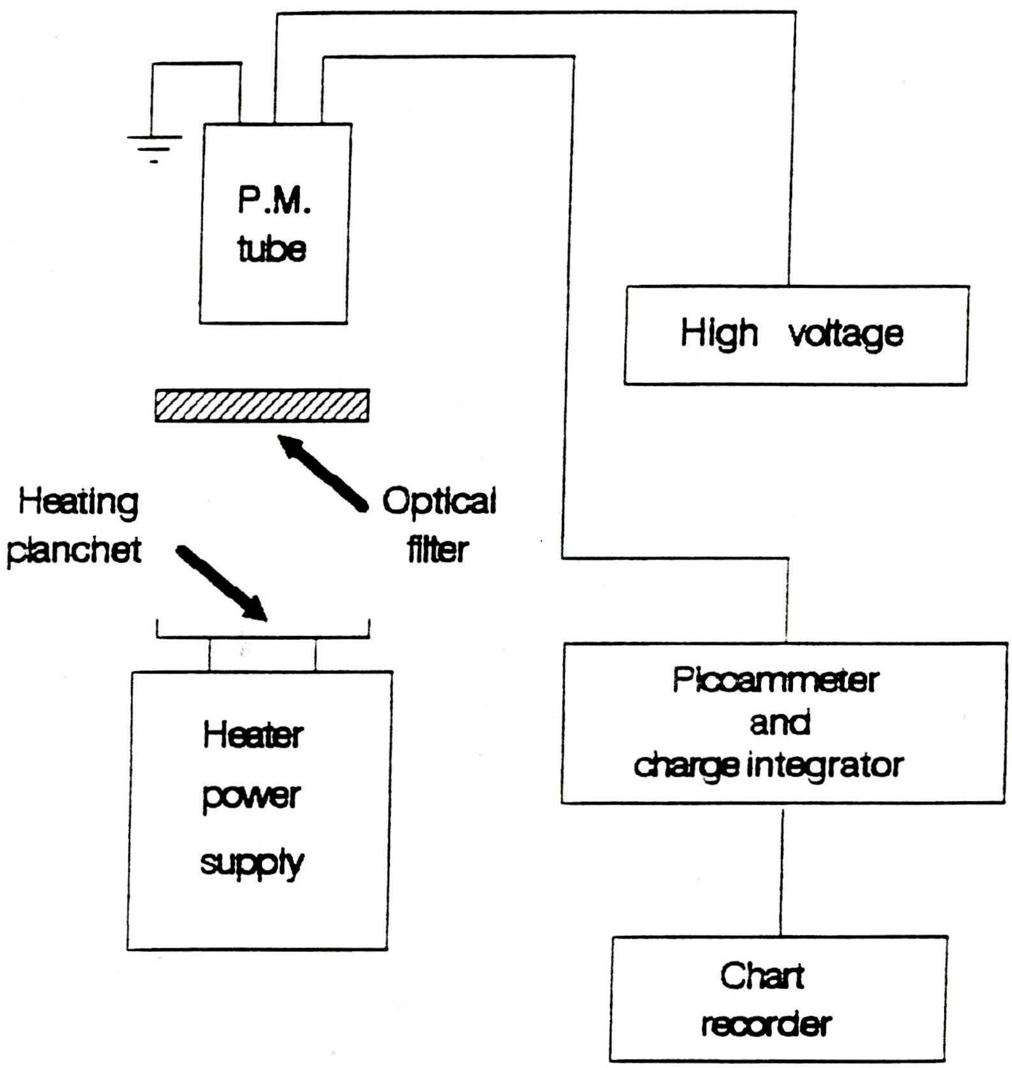

Figure 1.2 Basic components of a typical thermoluminescent readout system

CHAPTER 2

MONTE CARLO CALCULATIONS

A Monte Carlo electron transport code, Cyltran [29], was used in this work to calculate the backscatter dose as a function of distance from planar CB-RBM and AIR-RBM interfaces due to a semi-infinite uniform source of monoenergetic electrons. Since Cyltran has a built-in algorithm for selecting the appropriate step size for electron trajectories and it is several times faster than EGS [30], it was used in this work. The backscatter dose in a scoring region with inhomogeneous geometry (CB-RBM or VAC-RBM geometry) was divided by the dose in the same region with homogeneous geometry (RBM-RBM geometry) to yield a dose ratio. Variation of the dose ratio with electron energy of the semi-infinite source was also investigated. The dose ratio at three particular distances from the interfaces due to a semi-infinite uniform source of ^{32}P was also calculated in order to compare with experimental results.

Since low energy beta nuclides could be used to label anti-tumor antibodies for treating occult micrometastases and single tumor cells, the calculation was extended to low energy beta emitters such as ^{204}Tl and ^{147}Pm.

2.1 MONTE CARLO CODE AND GEOMETRY

Cyltran was obtained from Oak Ridge National Laboratory. Being one of the base codes of the Integrated TIGER Series (ITS) [29], Cyltran employs a fully three-dimensional description of particle trajectories within an axisymmetric cylindrical material geometry. The ITS is a group of multimaterial and multidimensional Monte Carlo codes designed to provide a description of the production and transport of the electron/photon cascade. Its base codes were primarily designed for transport at primary source energies from a few tens of MeV down to 1.0 and 10 KeV for electrons and photons, respectively. The ITS consists of an electron/photon cross section data file (XDATA), a cross section generation program (XGEN), and several Monte Carlo program files (e.g. Cyltran in this work). Program XGEN looks for the cross section and atomic data in XDATA while it is being executed to create cross section input for the specified Monte Carlo program. In addition, a problem specific input file must be provided. The values of the keywords in the input file for this work are described in the following.

```
GEOMETRY [parameter(1)]
    [parameter(2)][parameter(3)].....[parameter(5)]
          .            .             .
          .            .             .
          .            .             .
```

This keyword signals the beginning of the geometry information. [parameter(1)] is the number of input zones. Immediately after the keyword line there must follow a series of [parameter(1)] lines, one for each input zones. [parameter(2)] through [parameter(5)] specify the minimum z boundary, the maximum z boundary, the minimum radius, the maximum radius and the material, respectively.

DIRECTION [parameter(1)][parameter(2)]

[parameter(1)] and [parameter(2)] are the spherical polar angles in degrees that defined the source reference direction.

Default values, zero for both parameters, were used to define source reference position at positive z direction in this work

ISOTROPIC [parameter(1)]

Defines angular distribution of source particles as being isotropic with respect to the reference direction.

[parameter(1)] = 180.0 (i.e. a 4 pi isotropic source) in this work

ELECTRONS

This keyword defines the source particles to be electrons rather than photons.

ENERGY [parameter(1)]

This keyword specifies a monoenergetic source of energy [parameter(1)] in MeV.

[parameter(1)] = 0.1, 0.2, 0.35, 0.50, 0.75, 1.00, 1.25, 1.50, or 1.75 in this work

POSITION [parameter(1)][parameter(2)][parameter(3)]

[parameter(1)] through [parameter(3)] are the x, y and z coordinates of the center of the source, respectively, in cm.

[parameter(1)] = [parameter(2)] = 0 in this work

[parameter(3)] = 0, 1/18, 1/9, 1/6, 2/9, 1/3, 2/3,

1, 10/9, or 4/3 times the CSDA
range of the electron source
in this work

RADIUS [parameter(1)]

This keyword defines the radius [parameter(1)] in cm of a disk source with the reference position at its center. The normal to the disk will be the reference direction as defined by the DIRECTION keyword.

[parameter(1)] = 2 in this work

CUTOFFS [parameter(1)][parameter(2)]

[parameter(1)] and [parameter(2)] are the cutoff energies (MeV) at which electron and photon histories are terminated, respectively.

[parameter(1)] = [parameter(2)] = 0.001 in this work

HISTORIES [parameter(1)]

[parameter(1)] is the number of primary particle histories to be followed.

[parameter(1)] = 50000 in this work

BATCHES [parameter(1)]

[parameter(1)] is the number of batches of primary particles to be run. The total number of histories is divided into [parameter(1)] batches containing an equal number of source particles in order to obtain estimates of statistical uncertainties.

[parameter(1)] = 10 in this work

Some keywords other than the above had not been specified and default settings were then automatically activated such that histories of knock on delta rays were followed; histories of all bremsstrahlung photons and relaxation radiation resulting from electron impact ionization were followed; electron loss straggling was taken into account.

As illustrated in Figure 2.1 and 2.2, the cylindrical regions of cortical bone, red bone marrow, and vacuum simulate the cortical bone equivalent plastic, gelatin, and air which were used in the experiments. Twelve small disc-like dose scoring regions (DSR) in RBM were equally spaced from the interfaces up to 11/9 times the CSDA range. They were defined in the geometry of the Monte Carlo calculations to simulate the LiF TLD used in the experiments. The mass density of the TLD was assumed to be 2.39 g/cm^3 according to the specifications from the manufacturer. The dose scoring regions had the same mass thickness of 12 mg/cm^2 as the 50 microns thick TLD but the radius was set to be 1 cm in RBM (mass density 1.047 g/cm^3) so as to improve counting statistics in the DSRs. Note that the composition of the scoring regions was RBM instead of LiF. It has been proven that there is no significant difference in the dose ratio of inhomogeneous geometry to homogeneous geometry by using RBM to imitate the LiF TLD in experiment [21]. By defining two distinct materials in the simulation instead of three, it was shown that the CPU time for each Monte Carlo run was decreased by 23% [21].

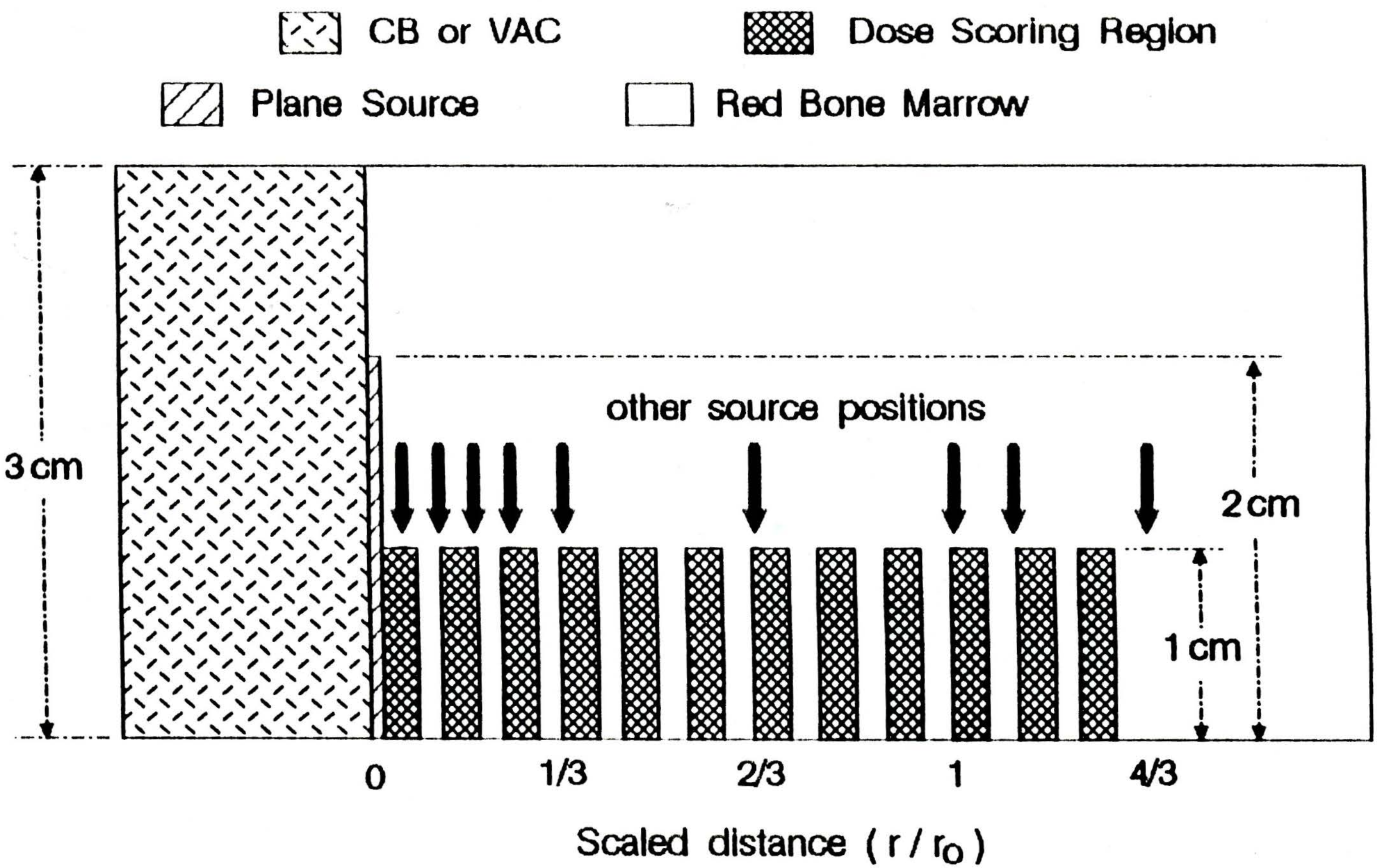

Figure 2.1 Geometry of the upper half cross section in the Monte Carlo calculations

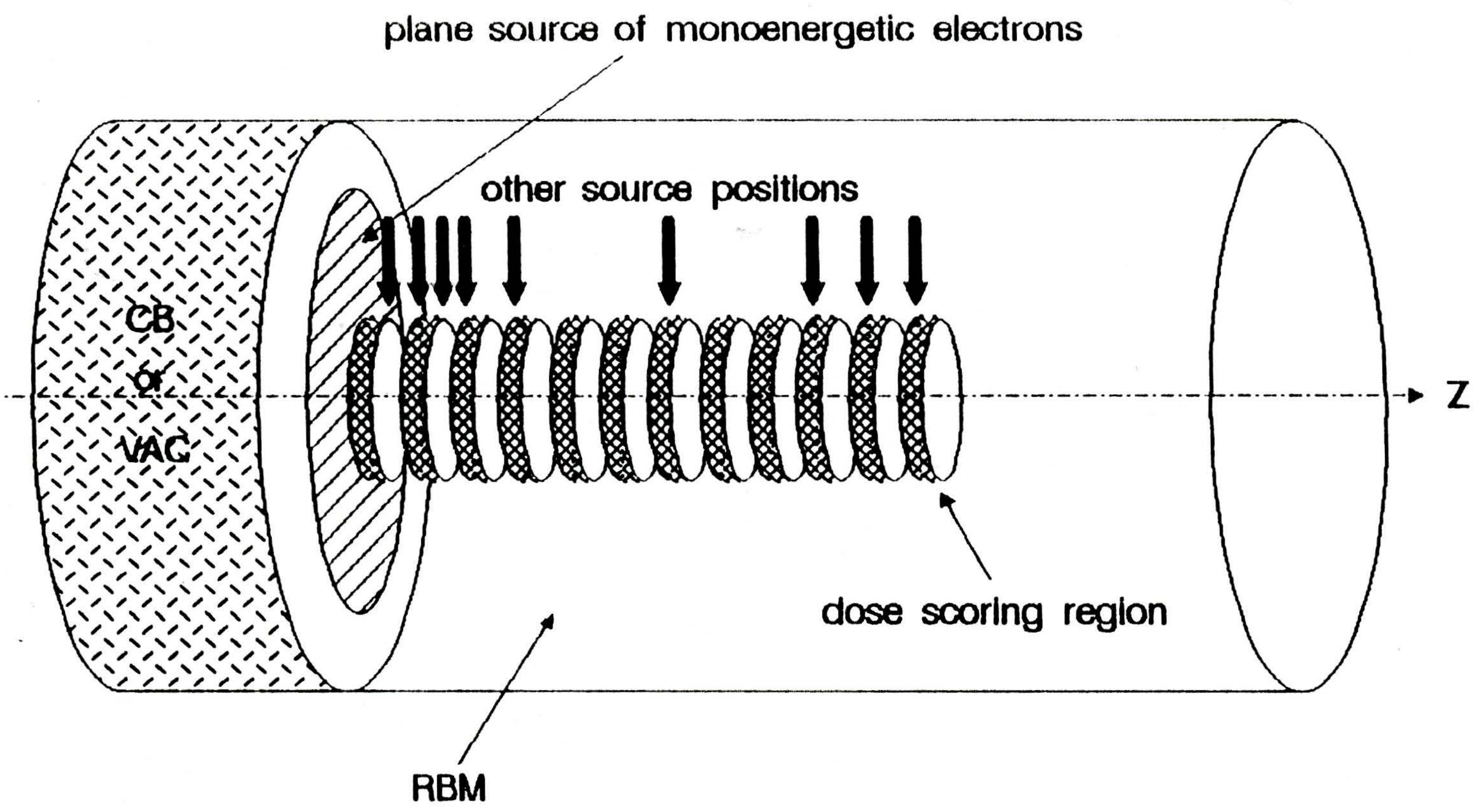

Figure 2.2 Three-dimensional view of the geometric specifications used in the Monte Carlo calculations

Note that the radius of the DSR was set to be 1 cm instead of the actual radius of the TLD (i.e. 0.3 cm) because as long as the radius of the source is much larger than that of the DSR the absorbed dose in the DSR is independent of its actual magnitude. The radius of the plane source was set to be 2 cm. Since the maximum CSDA range (i.e. for 1.75 MeV electron) in RBM is about 0.84 cm, the radius of the plane source had more than one maximum CSDA range than the radius of the dose scoring regions. Therefore, the plane source could be treated as infinitely large with respect to the DSRs. Similarly, the lateral dimensions of the RBM, CB and vacuum region were greater than the diameter of the DSR by 4 cm. Thus, these regions act as infinite media to the DSRs and the plane source. There were ten source positions (i.e. P = 0, 1/18, 1/9, 1/6, 2/9, 1/3, 2/3, 1, 10/9, 4/3 CSDA range) in the Monte Carlo calculations.

2.2 DATA ANALYSIS

270 Monte Carlo calculations had been done for the spatial distribution of absorbed dose in RBM with or without a heterogeneous interface due to the plane sources of monoenergetic electrons at different source positions and at different energies. Fifty thousand electron histories were followed for each Monte Carlo run. The results are presented in appendix A. The absorbed dose in the DSRs is expressed as a function of their scaled distance from the interface, the scaled source position, and electron energy. The scaled distance S and the scaled source position P are defined as the ratio of the absolute distances from the interface to the CSDA range $r_o(E)$ of electrons with energy E in RBM. These scaled quantities facilitate interpolation to any source energy and distance from the interface.

The dose to any one of the DSRs due to a semi-infinite uniform source of monoenergetic electrons in RBM could be calculated as the integral of the dose contributed by the plane sources with the source position.

$$D_{SI}(S,E) = \int_0^{4/3} D_P(S,P,E)\ dP + \int_{4/3}^{S+4/3} D_P(S,P,E)\ dP \qquad (2.1)$$

where

$D_{SI}(S,E)$ = dose in a DSR at scaled distance S due to a semi-infinite uniform source of electrons with energy E

$D_P(S,P,E)$ = dose in the same DSR at scaled distance S due to a plane source of electrons with energy E at scaled source position P

The first term on the right hand side of equation (2.1) calculates the dose to the DSR at S due to electron sources in the region from the interface to the scaled distance of 4/3. Note that there is less than 4/3 times the CSDA range from the DSR to the end of the region (i.e. scaled distance = 4/3) except for the DSR at the interface. Therefore, the second term on the right hand side of equation (2.1) is introduced to calculate the dose to the DSR from a second source region which is from scaled distance of 4/3 to 4/3 times the CSDA range from the DSR.

Let U=P−S,

$$\int_{4/3}^{S+4/3} D_P(S,P,E)\,dP \Rightarrow \int_{4/3-S}^{4/3} D_P(S,U+S,E)\,dU$$

$$\Rightarrow \int_{4/3-S}^{4/3} D_P^{RBM-RBM}(0,U,E)\,dU \qquad (2.1)$$

Since the second source region is at a distance more than 4/3 times the CSDA range away from the interface, the dose to the DSR due to the second source region is equivalent to the dose to the DSR at the interface due to a source region from scaled distance of (4/3-S) to scaled distance of 4/3 in RBM-RBM geometry.

$D_P(0,P,E)$, was fitted by weighted least-squares method to a degree six polynomial function or to a cubic spline function for comparison. The reason of using a degree six polynomial is that the largest decrease of residual variance occurred in going from degree five to degree six. The residual variance is the sum of squares of the residual values divided by the degree of freedom. $D_P(0,P,0.5)$ for the three different geometries were plotted in Figure 2.3 for illustration.

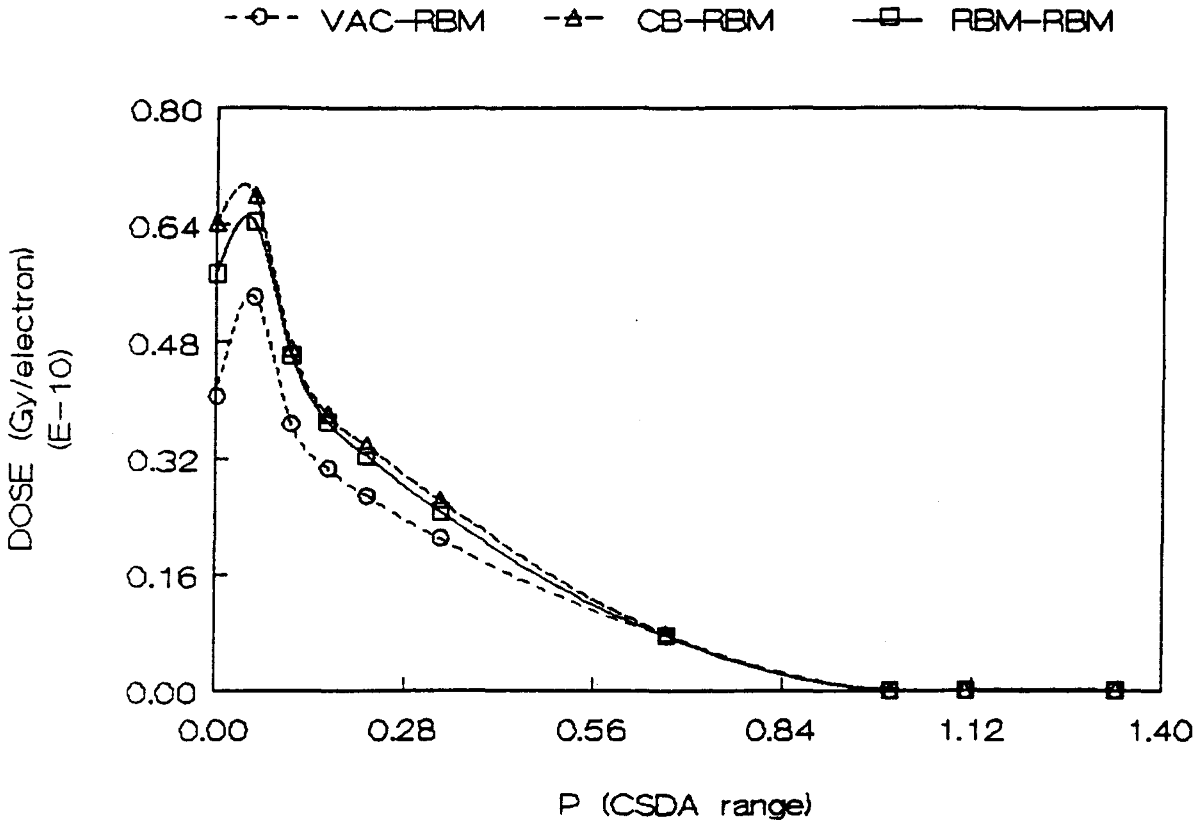

Figure 2.3 Dose at 0-12 mg/cm² from the respective interface due to a plane source of 0.5 MeV electrons as a function of plane source position P

Fitting function : cubic spline

The uncertainty of the integration was estimated in two ways. The first was to calculate the standard error of the sum from the coefficients and their associated uncertainties of the polynomial function. The general equation of an N degree polynomial function is :

$$Y = \sum_{i=1}^{N} P_i X^{i-1} \tag{2.2}$$

where P_i = coefficent of the term X^{i-1} of the polynomial

The integral I of the function in the interval a to b is

$$I = \int_a^b Y\,dX = I_a + I_b = \sum_{i=1}^{N} \frac{P_i b^i}{i} - \sum_{i=1}^{N} \frac{P_i a^i}{i} \tag{2.3}$$

The absolute standard error $\sigma(I)$ of the integral is

$$\sigma^2(I) = \sum_{i=1}^{N}\sum_{j=1}^{N}\left(\frac{dI_b}{dP_i}\right)\left(\frac{dI_b}{dP_j}\right)\sigma^2(P_{ij}) +$$

$$\sum_{i=1}^{N}\sum_{j=1}^{N}\left(\frac{dI_a}{dP_i}\right)\left(\frac{dI_a}{dP_j}\right)\sigma^2(P_{ij}) \tag{2.4}$$

$\sigma^2(P_{ij})$ = **element i,j in the variance-covariance matrix**

A computer program was written to perform the polynomial fitting, integration of the fitted curve and error estimation; it is listed in appendix B.

The second way is an approximate method whereby the absolute error is expressed as the absolute difference of two area integrations divided by 2 as follows.

$$ERR_{SI}(S,E) = \frac{A1 - A2}{2} \qquad (2.5)$$

where

$$A1 = \int_0^{4/3} D_P(S,P,E)\{1+RELERR(S,P,E)\}\,dP + \int_{4/3-S}^{4/3} D_P^{RBM\text{-}RBM}(0,P,E)\{1+RELERR(0,P,E)\}\,dP$$

$$A2 = \int_0^{4/3} D_P(S,P,E)\{1-RELERR(S,P,E)\}\,dP + \int_{4/3-S}^{4/3} D_P^{RBM\text{-}RBM}(0,P,E)\{1-RELERR(0,P,E)\}\,dP$$

$ERR_{SI}(S,E)$ = absolute error of $D_{SI}(S,P,E)$

$RELERR(S,P,E)$ = relative error of $D_P(S,P,E)$

In the approximate method, curves of dose $\pm$ one standard deviation versus source position were fitted by cubic spline function. This method was used for the rest of the integrations even though this method over-estimates the uncertainty of the integration because the polynomial function is not always a good fitting function to the data. On the contrary, the cubic spline function is a more flexible fitting function in general.

Since the separations of the dose scoring regions were expressed in terms of the CSDA range, the corresponding scaled distance X(E) of an absolute distance r for electron energy E can be calculated as

$$X(E) = \frac{(\rho_{RBM})r}{r_0(E)} \qquad (2.6)$$

where

$X(E)$ = scaled distance for electron energy E

ρ_{RBM} = density of RBM

$= 1.047 g/cm^2$

r = absolute distance from interface

$= 0.075 cm$ or $0.15 cm$

$r_0(E)$ = CSDA range for energy E in water; unit = g/cm^2

The doses due to a semi-infinite source at absolute distances of 0.75 mm and 1.50 mm from the interface were obtained by interpolation to the $D_{SI}(S,E)$ with respect to S. Curves were fitted by weighted least-squares method to the discrete values of $D_{SI}(S,E)$ and the choice of the fitting function depended upon the shape of the curves. The fitting functions for these curves are listed in appendix C. $D_{SI}(S,0.5)$ for VAC-RBM, RBM-RBM and CB-RBM were plotted in Figure 2.4 as examples.

Let $D_I(r,E)$ be the dose at an absolute distance r from the interface as a function of electron energy E for the inhomogeneous geometry and $D_H(r,E)$ be that for the homogeneous geometry. $D_I(r,E)$ and $D_H(r,E)$ were assumed to be increased linearly with electron energy from 0 to 0.1 MeV. The fitting functions for $D_I(r,E)$ and $D_H(r,E)$ are listed in appendix C. Figure 2.5 illustrates $D_I(0,E)$ for the VAC-RBM, and CB-RBM geometries and $D_H(0,E)$ for the RBM-RBM geometry. The dose ratio R(r) of the inhomogeneous geometry to the homogeneous geometry due to a semi-infinite beta source was evaluated for an absolute distance r from the interface.

$$R(r) = \frac{\int_0^{E_0} D_I(\mathrm{r,E})\mathrm{B(E)}\ \mathrm{dE}}{\int_0^{E_0} D_H(\mathrm{r,E})\mathrm{B(E)}\ \mathrm{dE}} \tag{2.7}$$

where B(E) is the beta spectrum of ^{32}P (E_o = 1.71 MeV), ^{204}Tl (E_o = 0.766 MeV) or ^{147}Pm (E_o = 0.224 MeV). The former two nuclides have allowed transitions while the last one has first-forbidden transition. A computer program has been developed by W.V. Prestwich, Ph.D. to evaluate the beta spectra. Integration of a beta spectrum with D(r,E) is required for determining the average dose per beta decay and it was done numerically by using a program developed by P.J. Bialobzyski [3].

The error $\sigma(R)$ in R is given by

$$\left(\frac{\sigma\{R(r)\}}{R(r)}\right)^2 = \left(\frac{\sigma\left\{\int D_I(\mathrm{r,E})\mathrm{dE}\right\}}{\int D_I(\mathrm{r,E})\mathrm{dE}}\right)^2 + \left(\frac{\sigma\left\{\int D_H(\mathrm{r,E})\mathrm{dE}\right\}}{\int D_H(\mathrm{r,E})\mathrm{dE}}\right)^2 \tag{2.8}$$

where

$$\sigma\left\{\int D(\mathrm{r,E})\mathrm{dE}\right\} = \sum_{i=1}^{N}\sum_{j=1}^{N}\left(\frac{\mathrm{d}\left\{\int D(\mathrm{r,E})\mathrm{dE}\right\}}{dP_i}\right)\left(\frac{\mathrm{d}\left\{\int D(\mathrm{r,E})\mathrm{dE}\right\}}{dP_j}\right)\sigma^2(P_{ij})$$

and

P_i = coefficient of the ith term in the fitting function

$\sigma^2(P_{ij})$ = element i,j in the variance-covariance matrix

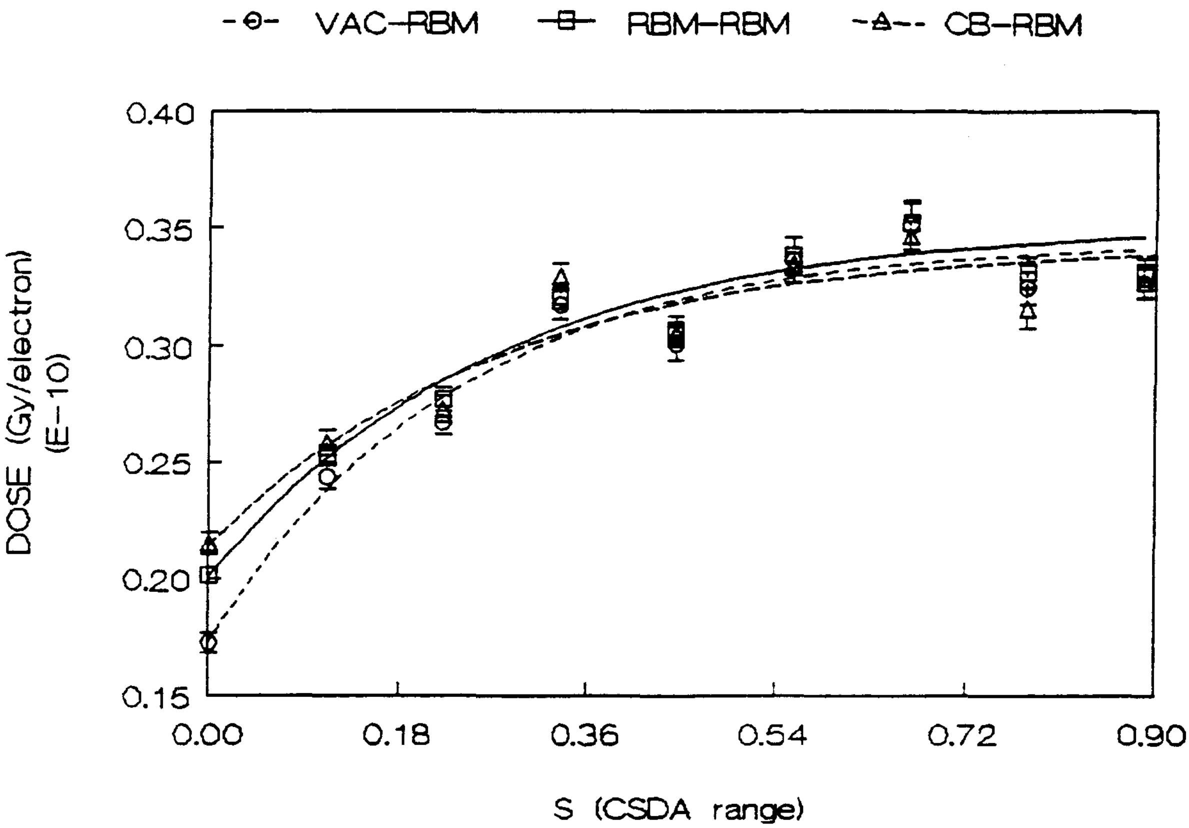

Figure 2.4 Dose distribution near the respective interface due to a semi-infinite sources of 0.5 MeV electrons as a function of scaled distance S

Fitting function : listed in appendix C

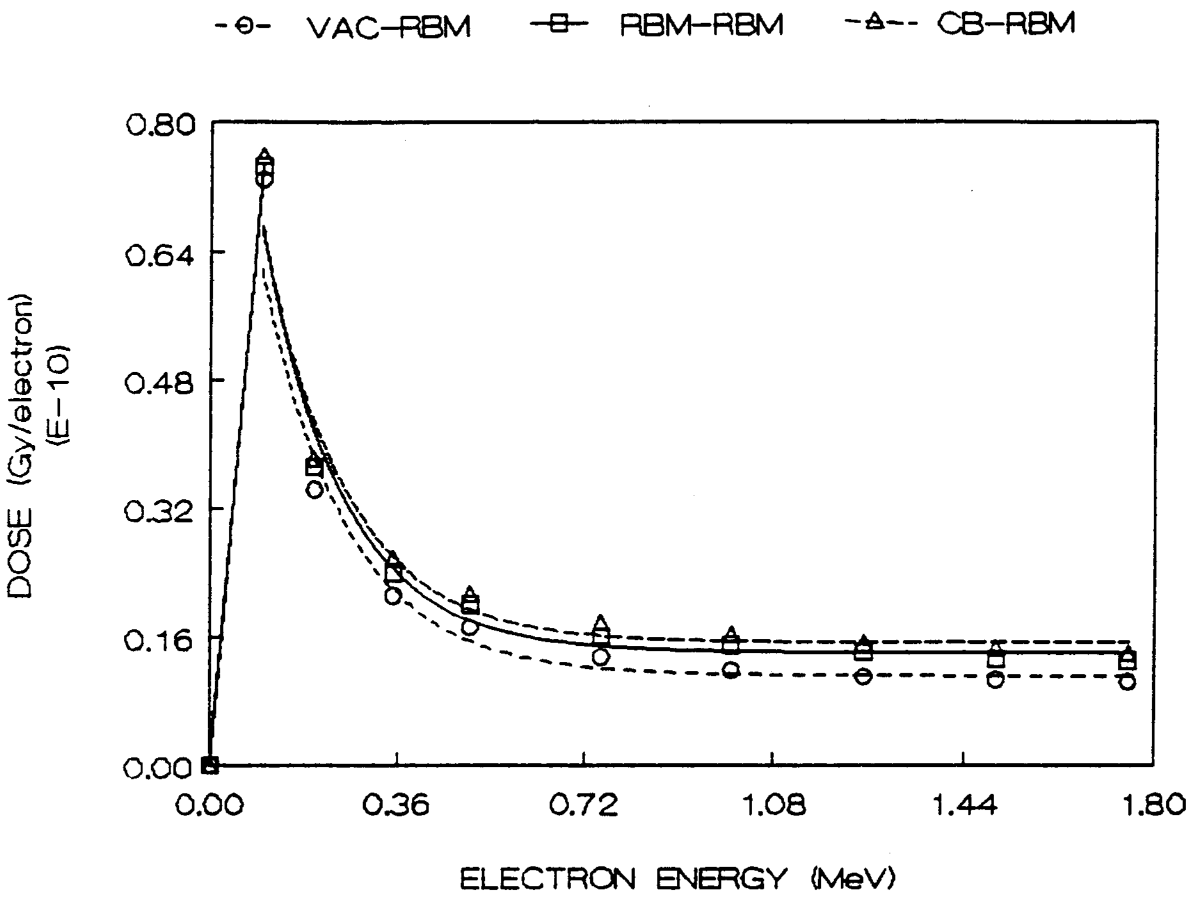

Figure 2.5 Dose at 0-12 mg/cm^2 from the respective interface due to a semi-infinite sources of electrons as a function of electron energy

Fitting function : listed in appendix C

2.3 RESULTS

Tables 2.1, 2.2 and 2.3 list $D_{SI}(0,E)$ for the RBM-RBM, CB-RBM and VAC-RBM geometries respectively and their corresponding estimated uncertainties for the dose scoring region located at 0-12 mg/cm^2 from the interface using the polynomial fit or the cubic spline fit respectively. Obviously, the estimated uncertainties for curves fitted by the cubic spline function are significantly higher than the uncertainties estimated by the other method.

TABLE 2.1

$D_{SI}(0,E)$ at 0-12 mg/cm^2 or 0-0.05 mm in RBM for the RBM-RBM geometry

Electron energy (MeV)	(1) Cubic spline dose*	(1) Cubic spline % error	(2) Polynomial dose*	(2) Polynomial % error	% difference $\frac{\lvert(2)-(1)\rvert \times 100\%}{(2)}$
0.10	7.4546	1.12	7.4861	0.50	0.4
0.20	3.7097	1.70	3.7301	0.69	0.5
0.35	2.4119	1.93	2.3691	0.77	1.8
0.50	2.0129	1.65	1.9919	0.69	1.1
0.75	1.6078	2.01	1.6054	0.91	0.1
1.00	1.4994	1.99	1.4985	0.89	0.06
1.25	1.4133	2.28	1.4109	1.00	0.2
1.50	1.3271	3.26	1.3474	1.46	1.5
1.75	1.3081	2.45	1.3086	0.94	0.04

* The unit of dose is 10^{-11} Gy per electron

TABLE 2.2

$D_{ax}(0,E)$ at 0-12 mg/cm^2 or 0-0.05 mm in RBM for the CB-RBM geometry

Electron energy (MeV)	(1) Cubic spline		(2) Polynomial		% difference
	dose*	% error	dose*	% error	$\frac{\lvert(2)-(1)\rvert}{(2)}$x100%
0.10	7.5830	1.43	7.6014	0.84	0.2
0.20	3.8126	1.64	3.8238	0.66	0.3
0.35	2.5834	1.49	2.5893	0.67	0.2
0.50	2.1510	2.19	2.1337	1.02	0.8
0.75	1.7881	2.44	1.7655	0.95	1
1.00	1.6296	1.70	1.6240	0.59	0.3
1.25	1.5254	2.16	1.5385	0.91	0.9
1.50	1.4652	2.30	1.4686	0.92	0.2
1.75	1.4082	2.49	1.4116	1.07	0.2

* The unit of dose is 10^{-11} Gy per electron

TABLE 2.3

$D_{SI}(0,E)$ at 0-12 mg/cm^2 or 0-0.05 mm in RBM for the VAC-RBM geometry

Electron energy (MeV)	(1) Cubic spline		(2) Polynomial		% difference
	dose*	% error	dose*	% error	$\frac{\lvert(2)-(1)\rvert}{(2)} \times 100\%$
0.10	7.2878	1.13	7.3040	0.51	0.2
0.20	3.4271	1.34	3.4357	0.60	0.3
0.35	2.1272	1.69	2.1223	0.74	0.2
0.50	1.7222	2.42	1.7252	0.87	0.2
0.75	1.3565	2.07	1.3531	0.99	0.3
1.00	1.1880	2.69	1.1737	0.81	1
1.25	1.1081	2.12	1.1064	1.04	0.2
1.50	1.0732	2.52	1.0695	1.12	0.3
1.75	1.0409	2.02	1.0417	0.79	0.08

* The unit of dose is 10^{-11} Gy per electron

Tables 2.4 and 2.5 show the variation of the dose with electron energy at absolute distances of 0.75 mm and 1.50 mm, respectively.

TABLE 2.4

$D_{SI}(X(E),E)$ at 79-91 mg/cm^2 or 0.75-0.80 mm in RBM

Electron energy (MeV)	VAC-RBM		RBM-RBM		CB-RBM	
	dose*	% error	dose*	% error	dose*	% error
0.10	8.7906	1	8.7965	1	8.7980	1
0.20	5.5306	1	5.5321	1	5.5355	1
0.35	4.3222	2	4.3498	2	4.4063	1
0.50	3.1927	2	3.2280	2	3.1791	2
0.75	2.4437	2	2.4507	2	2.4669	2
1.00	1.8129	3	1.9586	2	2.0420	2
1.25	1.5990	2	1.7934	2	1.8575	2
1.50	1.4759	2	1.6499	2	1.7468	2
1.75	1.3441	2	1.4944	3	1.5582	2

* The unit of dose is 10^{-11} Gy per electron

TABLE 2.5

$D_{SI}(X(E),E)$ at 157-169 mg/cm^2 or 1.50-1.55 mm in RBM

Electron energy (MeV)	VAC-RBM		RBM-RBM		CB-RBM	
	dose*	% error	dose*	% error	dose*	% error
0.10	8.5996	1	8.7965	1	8.7980	1
0.20	5.1106	1	5.5321	1	5.5355	1
0.35	4.3422	2	4.3498	2	4.3496	1
0.50	3.4093	2	3.4620	2	3.3845	2
0.75	2.8540	2	2.8507	2	2.8167	2
1.00	2.3062	2	2.3304	2	2.3712	2
1.25	1.9634	2	2.0696	2	2.0928	2
1.50	1.7612	2	1.8677	2	1.9363	2
1.75	1.5822	3	1.6838	3	1.7364	2

* The unit of dose is 10^{-11} Gy per electron.

Dose enhancement ratio and dose reduction ratio can be defined respectively as the dose ratio of the CB-RBM geometry and VAC-RBM geometry to the RBM-RBM geometry due to the semi-infinite sources of electrons.

The dose enhancement ratio and dose reduction ratio at 0-12 mg/cm^2 separation from the respective interface are plotted as a function of the energy of an isotropic source of monoenergetic electrons in Figure 2.6. The dose enhancement ratio increases with electron energy and reaches a plateau at 0.50 MeV while the dose reduction ratio decreases and becomes steady from 1.00 MeV onwards. The maximum dose enhancement ratio and dose reduction ratio are 1.10 $\pm$ 0.03 and 0.79 $\pm$ 3 respectively.

Tables 2.6, 2.7 and 2.8 summarize the dose ratios at 0-12, 79-91 and 157-169 mg/cm^2 from the planar interfaces for nuclides ^{32}P, ^{204}Tl and ^{174}Pm respectively. Neither dose enhancement nor dose reduction were observed at 157-169 mg/cm^2 (i.e. 0.15 cm) from the interfaces for the three nuclides and at 79-91 mg/cm^2 for the last two nuclides as well. The dose enhancement ratios, are 1.07 $\pm$ 0.01, 1.04 $\pm$ 0.01 and 1.02 $\pm$ 0.01 at 0-12 mg/cm^2 (i.e. 0 cm) for ^{32}P, ^{204}Tl and ^{174}Pm, respectively. The dose enhancement ratio and the dose reduction ratio are 1.02 $\pm$ 0.03 and 0.97 $\pm$ 0.03 respectively at 79-91 mg/cm^2 (i.e. 0.075 cm) for ^{32}P.

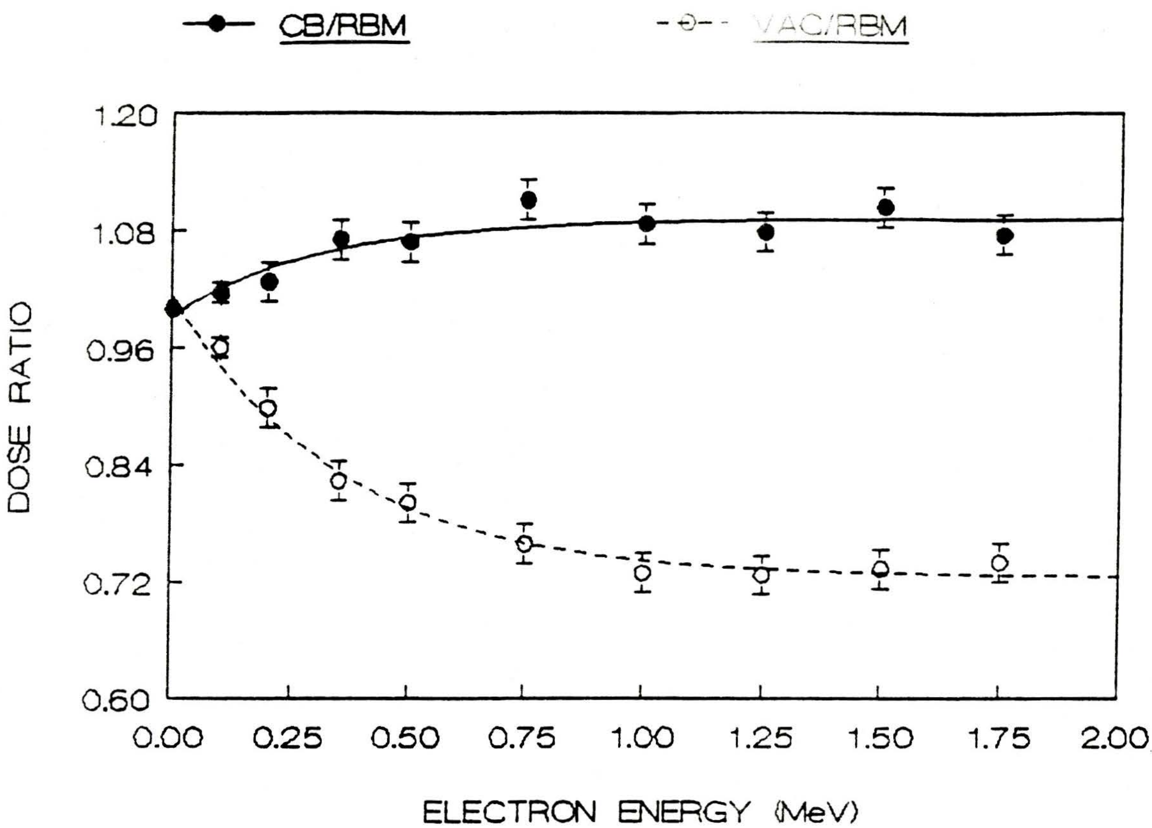

Figure 2.6 Dose enhancement ratio and dose reduction ratio at 0-12 mg/cm^2 from the respective interface due to a semi-infinite sources of electrons as a function of electron energy

Fitting function :

$$Y = A + B(1-\exp(-CX)) \text{ for dose enhancement ratio}$$

$$Y = A + B * \exp(-CX) \text{ for dose reduction ratio}$$

where Y = dose ratio

X = electron energy (MeV)

A, B and C are fitting parameters

For dose enhancement ratio

$A = 0.994 \pm 0.009$

$B = 9.87 \pm 0.01$

$C = 3.4 \pm 0.9$

For dose reduction ratio

$A = 0.724 \pm 0.005$

$B = 0.290 \pm 0.009$

$C = 2.8 \pm 0.2$

TABLE 2.6

Numerical dose ratio near the interfaces for ^{32}P

Distance from interface (mm, mg/cm^2)	Dose enhancement ratio for CB-RBM interface	Dose reduction ratio for VAC-RBM interface
0-0.05, 0-12	1.07 ± 0.01	0.87 ± 0.01
0.75-0.80, 79-91	1.02 ± 0.03	0.97 ± 0.03
1.50-1.55, 157-169	1.00 ± 0.03	1.00 ± 0.03

TABLE 2.7

Numerical dose ratio near the interfaces for ^{204}Tl

Distance from interface (mm, mg/cm^2)	Dose enhancement ratio for CB-RBM interface	Dose reduction ratio for VAC-RBM interface
0-0.05, 0-12	1.04 ± 0.01	0.93 ± 0.01
0.75-0.80, 79-91	1.00 ± 0.03	1.00 ± 0.03
1.50-1.55, 157-169	0.99 ± 0.03	1.00 ± 0.03

TABLE 2.8

Numerical dose ratio near the interfaces for ^{147}Pm

Distance from interface (mm, mg/cm^2)	Dose enhancement ratio for CB-RBM interface	Dose reduction ratio for VAC-RBM interface
0-0.05, 0-12	1.02 $\pm$ 0.01	0.96 $\pm$ 0.01.
0.75-0.80, 79-91	1.00 $\pm$ 0.03	1.00 $\pm$ 0.03
1.50-1.55, 157-169	1.00 $\pm$ 0.03	1.00 $\pm$ 0.03

CHAPTER 3

EXPERIMENTAL MEASUREMENTS OF DOSE DISTRIBUTION NEAR INTERFACES

With a uniform continuous source of ^{32}P inside a well designed phantom, beta doses at various separations from the AIR-RBM, and CB-RBM planar interfaces were measured by groups of ultra thin LiF thermoluminescent dosimeters (TLDs). The dose near the planar interfaces due to changes in the backscattering of electrons is then compared with the dose in homogeneous RBM. Due to the long half-lifes of ^{147}Pm(2.623 years) and ^{204}Tl(3.779 years), experiments for these two nuclides were not performed. In this chapter, the materials, experimental procedure and results are presented.

3.1 MATERIALS AND METHOD

A cortical bone equivalent plastic plate, 78 x 78 mm^2 in area and 12 mm in thickness, was used as a substitute for cortical bone. The plastic was obtained from Dr. Rodney Bigley, Sloane Kettering Cancer Center, New York, New York and it has the same number of electrons per gram and mass density as real cortical bone [3]

As a substitute for RBM containing uniformly distributed ^{32}P, Knox gelatin solution [5], 50 gram per litre of water in concentration, was mixed uniformly with a sodium phosphate ^{32}P solution. The source of ^{32}P was purchased from Merck Frosst Canada Inc., Kirkland, Quebec. The gelatin solution was mainly a very diluted mixture of water-soluble proteins composed of atoms with low atomic numbers.

Therefore, the effective atomic number (Ze) of the mixed solution should be comparable to the Ze of water. The Ze of RBM, RBM equivalent plastic, polystyrene and water are 5.93, 5.53, 5.29 and 6.6 respectively [21]. The specific activity of the mixed solution was in the range of 185-262 KBq/ml and the final volume of the solution was 200 ml. A volume of 0.15 ml of formaldehyde was also added into the solution not only to prevent bacterial invasion during the experiments, but also to increase the melting point of the gelatin [4].

The solubility of LiF in water, although slight, makes it unsuitable for dosimetry when it is in contact with aqueous solution because the solution will etch the surface and perhaps release the energy previously stored [6]. The TLDs would become contaminated while in contact with the ^{32}P gelatin source. Thus, a group of five TLDs were sandwiched by two mylar sheets (13.4 micron in thickness each) mounted firmly on two polystyrene frames as shown in Figure 3.1, and air between the mylar sheets was evacuated. Since the CSDA range of the end point energy E_o of ^{32}P in water is about 0.84 cm [20], the TLDs were separated from the inner edge of the frames and from each other by at least 1.5 cm (i.e. more than 1.5 times the CSDA range) in order to prevent mutual interaction.

A polystyrene rectangular phantom was used in these experiments. Dimensions of the phantom are greater than twice the CSDA range of E_o of ^{32}P so that charged particle equilibrium is established at the center region of the phantom. As shown in Figure 3.2, the piece of CB equivalent plastic was inserted into the phantom against a sidewall, and the assembled frames were inserted vertically into the phantom. The portable slab was removed after the mixed solution had solidified so that the phantom had a CB-RBM interface on one side and an AIR-RBM interface on the opposite side.

Three groups of TLDs were used in the experiments. Group (A) and group (C) were used to measure the dose at a distance less than one CSDA range from the CB-RBM and AIR-RBM interfaces respectively. Group (B) was located between the other two groups at a distance more than one CSDA range away from each of them. Group (B) therefore measured the dose in an infinite medium of RBM. The positions of the groups of TLDs were varied by placing known thicknesses of polystyrene frames (1.5 mm thick each) and mylar frames (0.25 mm thick each) between the groups of TLDs and the interfaces.

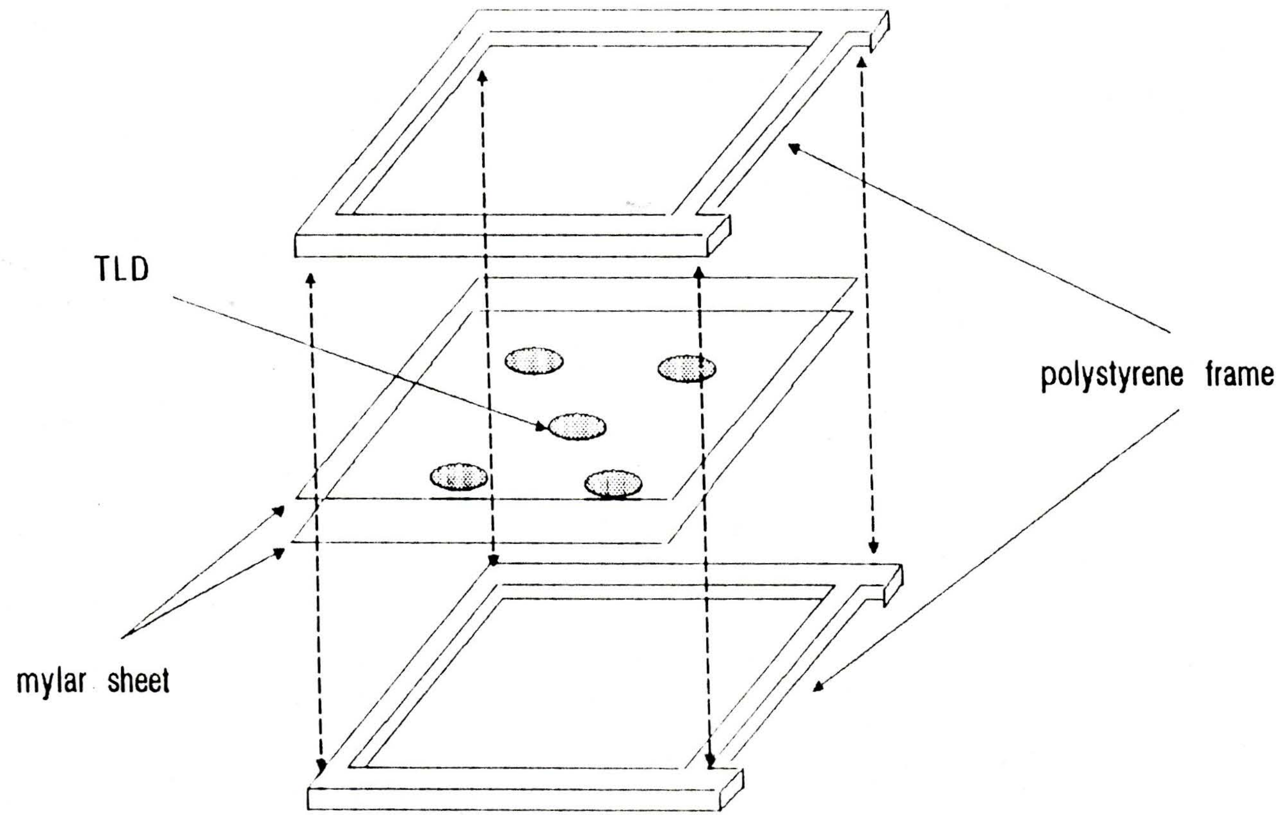

Figure 3.1 Assemble Process of a Group of TLD

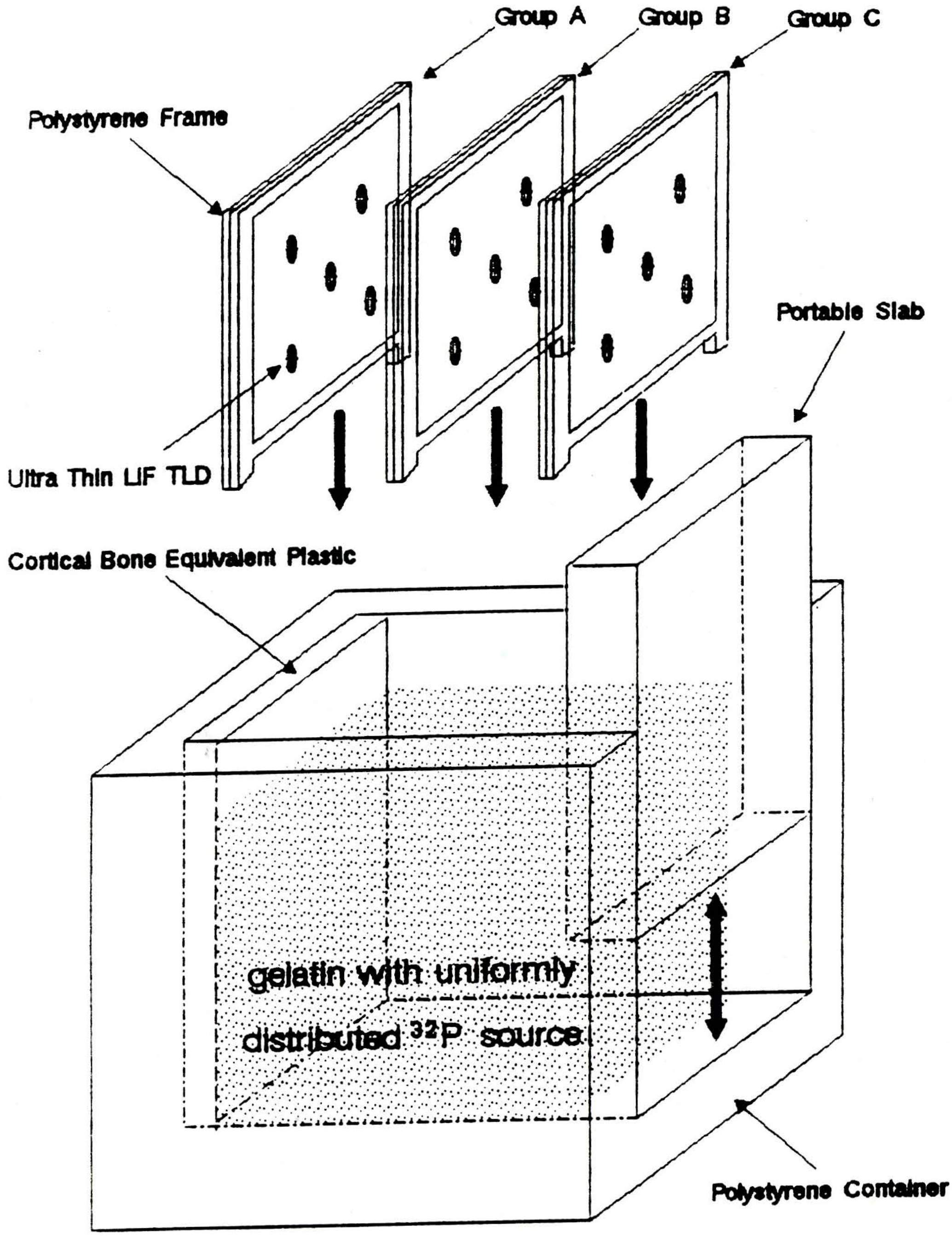

Figure 3.2 Experimental setup for measuring backscatter dose near planar tissue interfaces

3.2 EXPERIMENTAL PROCEDURE

3.2.1 TLD Calibration

The TLDs, 6 mm diameter x nominal 50 micron thickness, were purchased from Teledyne Isotopes, Westwood, New Jersey. 110 TLDs were annealed in an annealing oven for two hours at $(300 \pm 1)^{\circ}C$ and then 24 hours at $(80 \pm 1)^{\circ}C$. One hundred of the TLDs were calibrated individually with 3 Gy of ^{60}Co gamma rays five times. The remaining ten TLDs were not irradiated and were used to monitor the background radiation.

Irradiated TLDs were allowed to fade for 24 hours and then read out consecutively with a Harshaw TLD system 4000 TLD reader. The parameters for the programmed heating cycle during readout had been set to : heating rate, $10^{\circ}C/s$; preheating annealing constant temperature, $150^{\circ}C$ for 5 s; constant temperature for reading, $240^{\circ}C$ for 20 s. TLDs were washed with 70% ethanol before readout in order to remove possible build up of electrostatic charge and dirt on the surface of the TLDs.

The sensitivity of the TLDs could be defined as the TLD response (i.e. light output) divided by the calibration dose. The TLDs were annealed after each calibration. The sensitivity of an individual TLD in each calibration was recorded, and the records of the sensitivity and history were kept. Only those TLDs with less than 1% change of sensitivity in the last three consecutive calibrations were used for experiments.

Each unirradiated TLD was placed in the aluminum planchet of the TLD reader and read twice. A small transparent pyrex glass slab was placed on the top of the TLD to ensure that it made good thermo-contact with the planchet. The initial background reading was acquired and it was read again for the residual background after the planchet was cooled down to 30°C. The total background reading is calculated to be the sum of the initial and residual readings. Each irradiated TLD was read twice in the same way for the initial and residual readings. Thus, the TLD response could be calculated as the difference of the total readings and the total background readings.

3.2.2 Dose Measurement In Phantom

After the phantom had been assembled as illustrated in Figure 3.2, the radioactive gelatin solution was poured into the phantom. The phantom was then stored in a refrigerator at 4°C for one hour in order to solidify the gelatin. A TLD was placed on the inside surface of the portable slab to monitor the dose to the group (C) TLDs during solidification. This dose is named as solidification dose. The TLD was covered by a sheet of mylar. The phantom was then put on the floor of an isolated room without any other scattering material except the floor in a radial distance of at least 1 m. Two TLDs were placed underneath the phantom for measuring background radiation. Since the thickness of the walls of the phantom was 2 cm (i.e. more than twice the CSDA range of E_o of ^{32}P in RBM), the TLDs for background counting would not be irradiated by the beta particles of ^{32}P.

The TLDs in the phantom were irradiated for 3 days in order to obtain a less than 1% noise to signal ratio. Since the group (B) TLDs measured the dose due to an infinite source of ^{32}P, a correction factor, C1(z), must be multiplied to the dose of group (B) TLDs to convert it to the dose at a distance z within a semi-infinite source of ^{32}P. Thus, the dose ratio due to a semi-infinite source of ^{32}P at a distance z from the interface can be calculated.

Let D_o be the equilibrium absorbed dose rate that would prevail everywhere in an unbounded homogeneous water medium if an uniform isotropic source of ^{32}P were distributed throughout the entire medium. Let D(z) be the corresponding absorbed dose rate at a depth $z > 0$ in water if the source were confined to the half-space $z \leq 0$. A reduction factor G(z) for ^{32}P in a water medium can be expressed as follows

$$G(z) = \frac{D(z)}{D_o} \tag{3.1}$$

Dose distributions in the water medium were found by convolution of the beta dose point kernel for ^{32}P with the activity distribution of the source. The beta dose point kernel for ^{32}P has been calculated by Prestwich et al. [22] and the results were fitted by a lognormal-cum-exponential function. A program called TDRD which has been developed by Dr. C.S. Kwok was used to calculate D(z) and D_o. A simplified algorithm of TDRD can be found in Figure 3.3

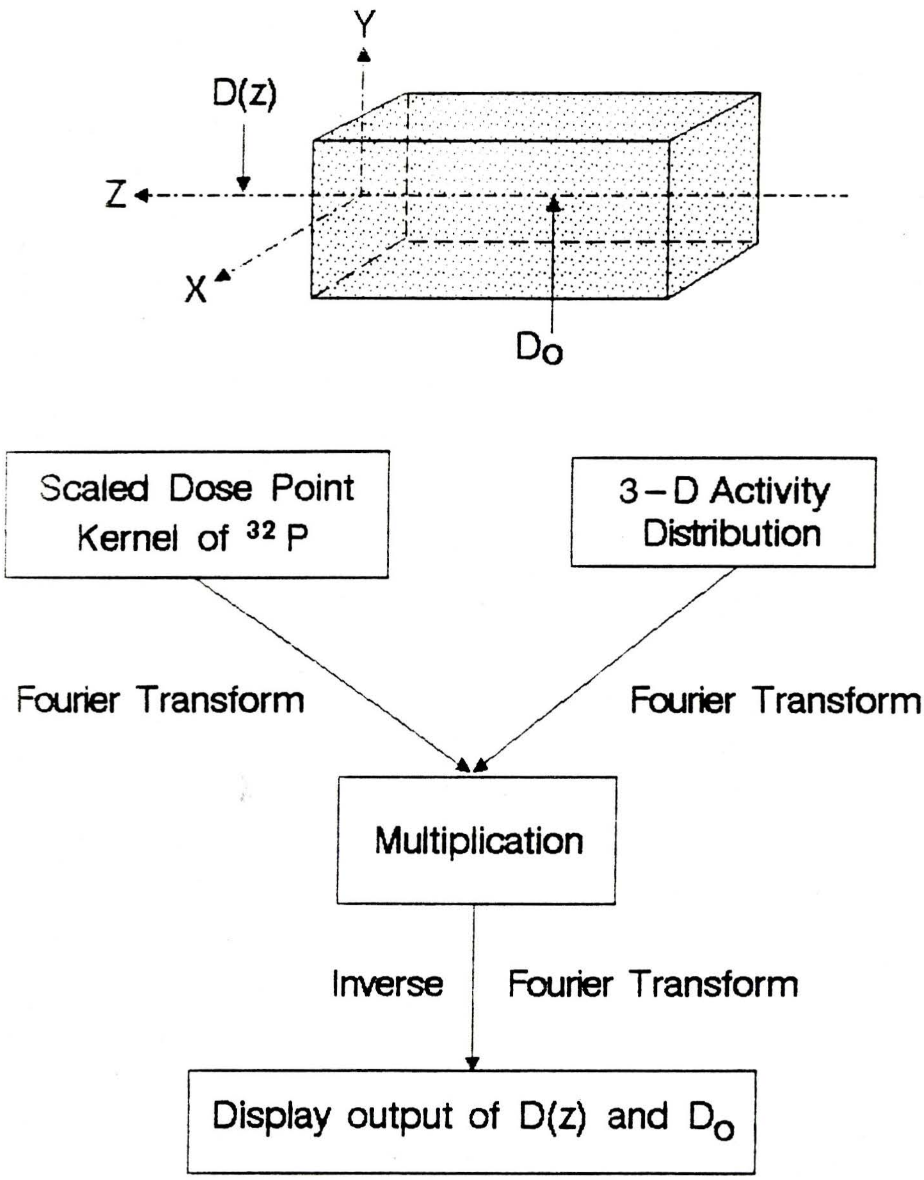

Figure 3.3 Simplified algorithm of TDRD and 3 – D geometry of the activity distribution

In the experiments, TLDs were placed at 0, 0.075 and 0.15 centimeters away from the interfaces. Since the nominal thickness of the TLDs is 50 microns, the 'distance intervals' (i.e. front side to back side) of the TLDs from the interface in mg/cm^2 are

$$z = \rho_{gel} d \rightarrow (\rho_{gel} d + \rho_{TLD} T) \qquad (3.2)$$

where

ρ_{gel} = density of the gelatin
ρ_{TLD} = density of the TLDs
d = absolute distance from the interface
= 0, 0.075 or 0.15 cm
T = the TLD thickness
= 0.005 cm

Thus, the distance intervals of the TLDs are 0-9, 79-87 and 157-166 mg/cm^2 corresponding to the absolute distance of 0, 0.075 and 0.15 cm.

The density of the TLDs was measured to be 1.71 g/cm^3. Density of the gelatin was measured to be approximately 1.05 g/cm^3.

$$\text{Thus, } Cl(z) = 1 - G(z) \qquad (3.4)$$

C1(0 cm) = C1(0-9 mg/cm^2) = 0.50
C1(0.075 cm) = C1(79-87 mg/cm^2) = 0.749252
C1(0.15 cm) = C1(157-166 mg/cm^2) = 0.903633

The dose enhancement ratio at z from the CB-RBM interface was then calculated as follows:

$$R_{CB\text{-}RBM}(z) = \frac{A}{B}\left(1 \pm \left(\left(\frac{\sigma(A)}{A}\right)^2 + \left(\frac{\sigma(B)}{B}\right)^2\right)^{\frac{1}{2}}\right) \qquad (3.5)$$

where

A = mean dose of the group (A) TLDs

B = (mean dose of the group (B) TLDs) x C1(z)

And the dose of either group TLD = (TLD response - background)/(sensitivity factor)

Similarly, the dose reduction ratio at z from the AIR-RBM interface was calculated by

$$R_{AIR\text{-}RBM}(z) = \frac{C}{B}\left(1 \pm \left(\left(\frac{\sigma(C)}{C}\right)^2 + \left(\frac{\sigma(B)}{B}\right)^2\right)^{\frac{1}{2}}\right) \qquad (3.6)$$

where

C = mean dose of the group (C) TLDs

B = (mean dose of the group (B) TLDs) x C1(z)

For this equation,

the dose of group (C) TLD = (TLD response - background - solidification dose)/(sensitivity factor)

and

the dose of group (B) TLD = [(TLD response - background) x C2]/(sensitivity factor)

$$\text{where } C2 = 1 - \frac{\text{dose received during solidification}}{\text{total dose recieved}}$$

$$= 1 - \frac{\left(1 - \exp^{-\left(\lambda \cdot \frac{1}{24}\right)}\right)}{\left(1 - \exp^{-(\lambda \cdot 3)}\right)} \qquad (3.7)$$

λ = decay constant of ^{32}P in the unit of day^{-1}

3.3 RESULTS

Table 3.1 summarizes the results of the experiment. The experimental results in table 3.1 and the Monte Carlo results in table 2.6 are presented in Figure 3.4 and Figure 3.5 for the CB-RBM and AIR-RBM interfaces respectively. The data points in Figure 3.4 are fitted by linear functions, while the data points in Figure 3.5 are fitted well by exponential functions. The experimental results agree with the Monte Carlo results except for the dose reduction ratio at 0-12 mg/cm^2, where the experimental result (i.e. 0.82 $\pm$ 0.02) shows about three standard deviations less than the Monte Carlo result (i.e. 0.87 $\pm$ 0.01)

TABLE 3.1

Experimental dose ratio near the interfaces

Distance from interface (mm, mg/cm^2)	Dose enhancement ratio for CB-RBM interface	Dose reduction ratio for AIR-RBM interface
0-0.05, 0-9	1.07 $\pm$ 0.01	0.82 $\pm$ 0.02
0.75-0.80, 79-87	1.03 $\pm$ 0.03	0.94 $\pm$ 0.03
1.50-1.55, 157-166	0.99 $\pm$ 0.03	0.97 $\pm$ 0.03

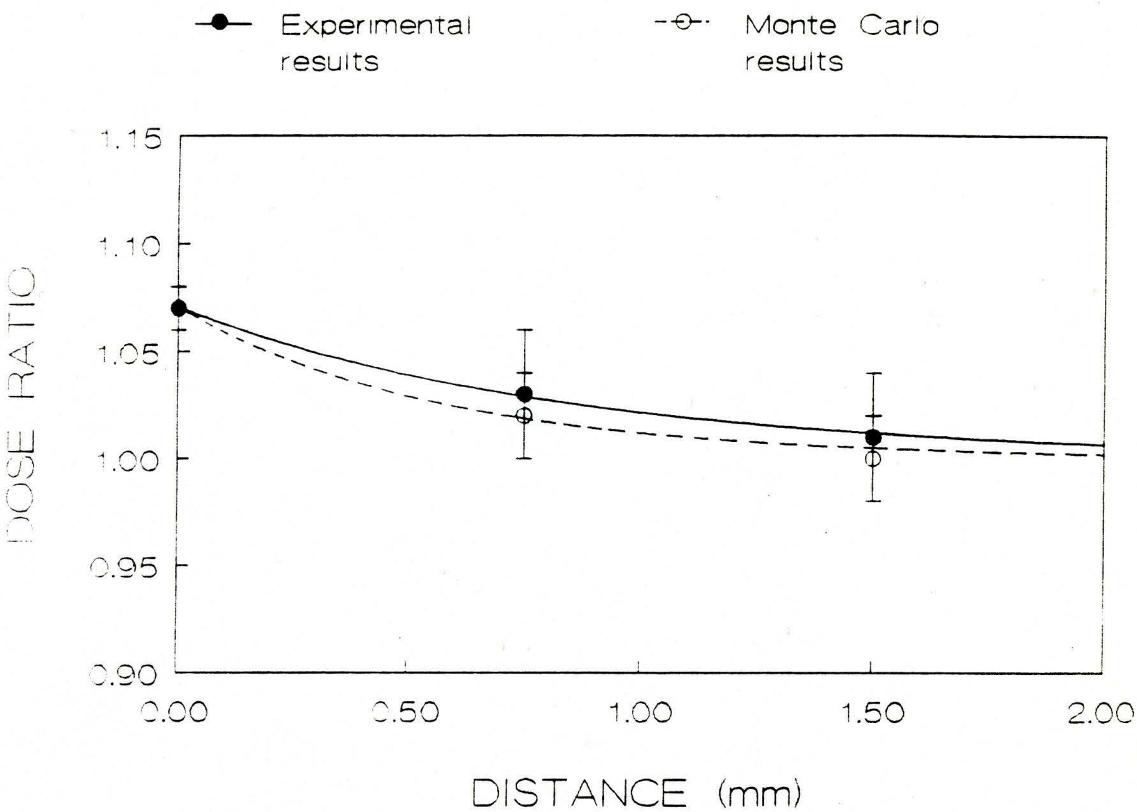

Figure 3.4 Experimental and Monte Carlo calculated results of dose enhancement ratio as a function of absolute distance from the planar CB-RBM interface

Fitting function : Y = 1 + A*EXP(-B*X) for both curves

where Y = dose ratio

X = absolute distance

A and B are fitting parameters

for solid line

A = 7.0401E-2

B = 1.1948

chi square = 1.134E-2

for dotted line

A = 7.0474E-2

B = 1.7725

chi square = 6.577E-4

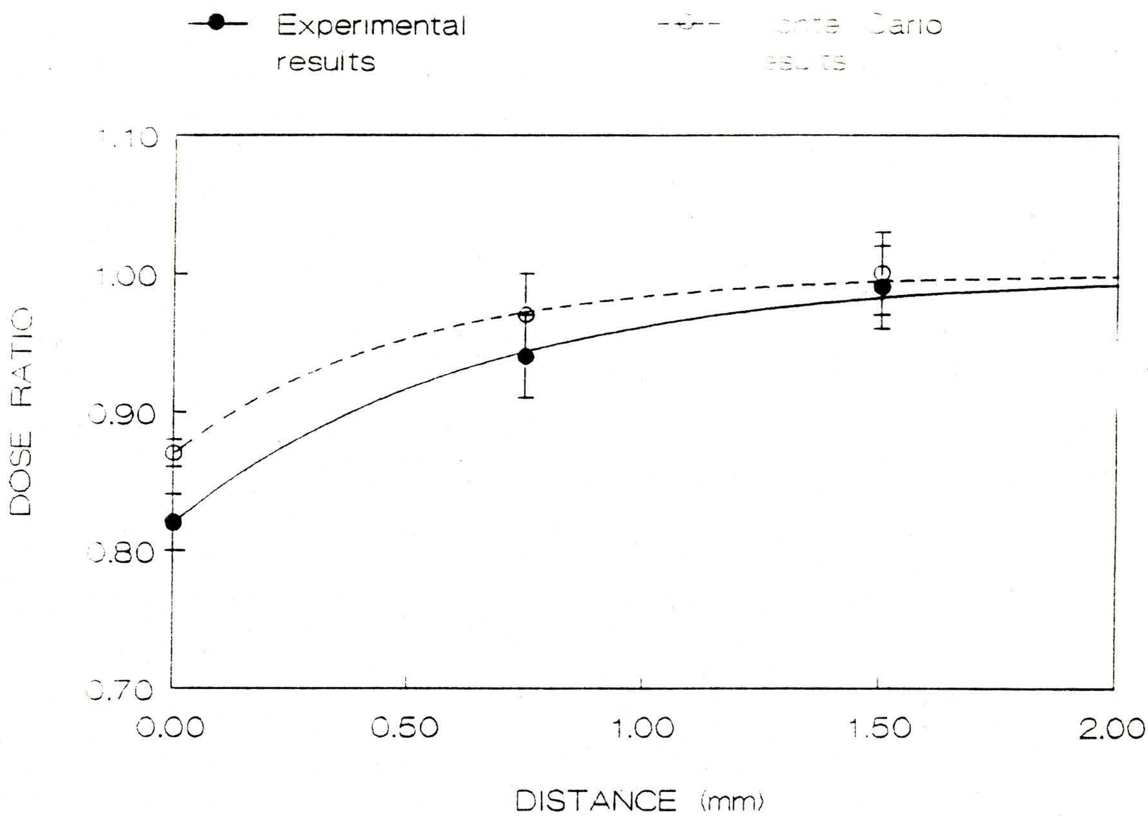

Figure 3.5 Experimental and Monte Carlo calculated results of dose reduction ratio as a function of absolute distance from the planar AIR-RBM interface

Fitting function : Y = 1 - A*EXP(-B*X) for both curves

where Y = dose ratio

X = absolute distance

A and B are fitting parameters

for solid line	for dotted line
A = 1.8060E-1	A = 1.3028E-1
B = 1.5514	B = 2.0532
chi square = 1.859E-1	chi square = 1.013E-1

CHAPTER 4

SUPPLEMENTARY FINDINGS WITH POINT SOURCES OR PLANE SOURCES AT INTERFACE

4.1 EFFECT OF CORTICAL BONE THICKNESS ON ELECTRON BACKSCATTER DOSE

Since trabecular bone is composed of a network of fine lamellae of cortical bone with a wide range of thicknesses and numerous cavities which contain the red marrow, it will be essential to repeat Monte Carlo calculations for sources of electrons in such cavities surrounded by different thicknesses of bone. Previous Monte Carlo calculations assumed infinitely thick layers of bone surrounding the cavities.

The same Monte Carlo transport code, Cyltran, was used to investigate the electron backscatter dose as a function of scaled cortical bone slab thickness which is defined as the thickness divided by the CSDA range of the electron in bone. The geometry of the Monte Carlo calculations was similar to the one described in chapter 2 except for the following. (a) A point source or a plane source of isotropically emitting electrons of 0.50 MeV at the junction of the CB-RBM interface was used. (b) 2.094 mg/cm^2 instead of 12 mg/cm^2 thick dose scoring regions were defined. (c) Vacuum or a thick slab of RBM was placed behind the CB slab in this simulation. Figure 4.1 gives details of the geometry. The scaled CB slab thickness was varied from more than 9 to 0.03. Fifty thousand electron histories were followed in each Monte Carlo run.

In table 4.1, Monte Carlo results for the dose enhancement ratio at 0-20 micron separation from the interface with different bone thicknesses are given. As expected, the dose ratio increases rapidly with thickness until a saturation value of 1.06$\pm$0.01 is reached. The results are also presented in Figures 4.2, 4.3 and 4.4 for the point source and RBM-CB-RBM system, the plane source and RBM-CB-RBM system, and the point source and VAC-CB-RBM system, respectively. The saturation dose ratio for all these systems agrees with the dose ratio for infinitely thick CB within one standard deviation. At 99% saturation, the scaled thicknesses of the CB slab are (0.22 $\pm$ 0.05), (0.3 $\pm$ 0.1) and (0.22 $\pm$ 0.01) for the point source and RBM-CB-RBM system, the plane source and RBM-CB-RBM system, and the point source and VAC-CB-RBM system, respectively. It may then be concluded that the saturation thickness of CB is approximately 0.22 times the CSDA range for 0.5 MeV electrons for both the point source and plane source confrigurations. The range of the dose ratio for the VAC-CB-RBM system (i.e 0.89 to 1.07) is greater than that for the RBM-CB-RBM system (i.e. 1 to 1.07). Therefore, the VAC-CB-RBM system is suggested to be used in further investigations for other electron energies.

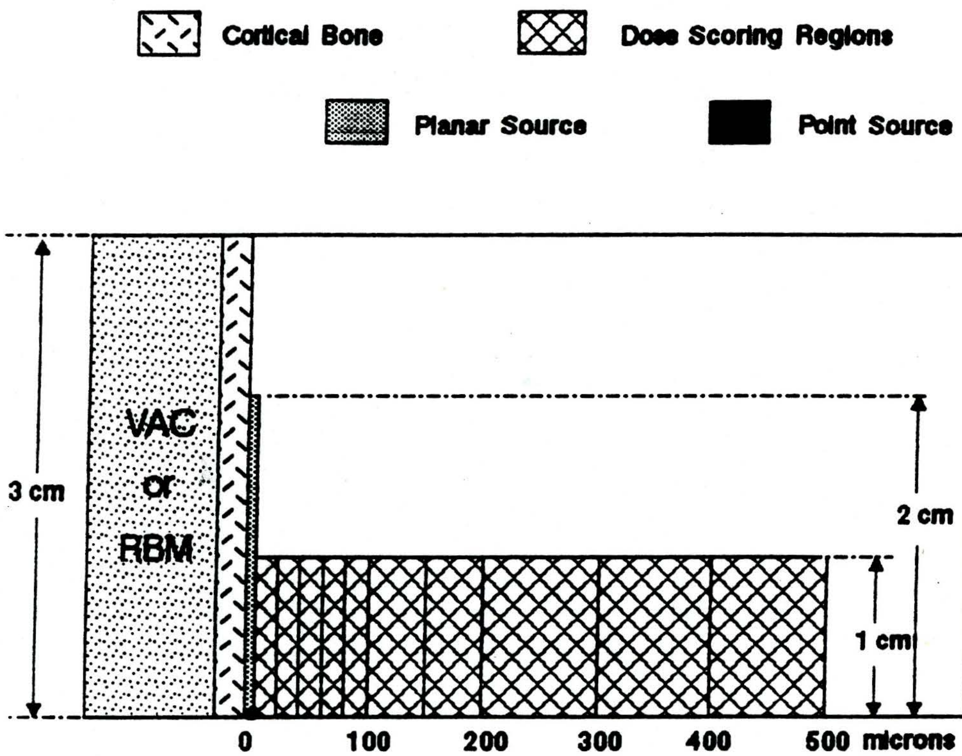

Figure 4.1 Geometry of the upper half cross section in the Monte Carlo calculations

TABLE 4.1

Dependence of electron backscattering from a point or a plane source of 0.5 MeV electrons on CB slab thickness

Scaled CB thickness	Dose enhancement ratio at 0-20 micron separation from interface		
	RBM-CB-RBM		VAC-CB-RBM
	point source	plane source	point source
0.03		1.00 ± 0.02	0.89 ± 0.01
0.05	1.02 ± 0.01	1.01 ± 0.03	0.93 ± 0.01
0.07			0.98 ± 0.01
0.10	1.03 ± 0.01	1.01 ± 0.02	1.00 ± 0.01
0.13			1.02 ± 0.01
0.15	1.04 ± 0.01	1.05 ± 0.01	1.05 ± 0.01
0.17	1.05 ± 0.01		1.04 ± 0.01
0.20	1.06 ± 0.01	1.05 ± 0.03	1.04 ± 0.01
0.25	1.05 ± 0.01	1.05 ± 0.01	1.06 ± 0.01
0.30	1.05 ± 0.01	1.05 ± 0.02	1.06 ± 0.01
0.35		1.07 ± 0.02	1.07 ± 0.01
0.40	1.05 ± 0.01		1.07 ± 0.01
more than 9	1.07 ± 0.01	1.06 ± 0.02	1.07 ± 0.01

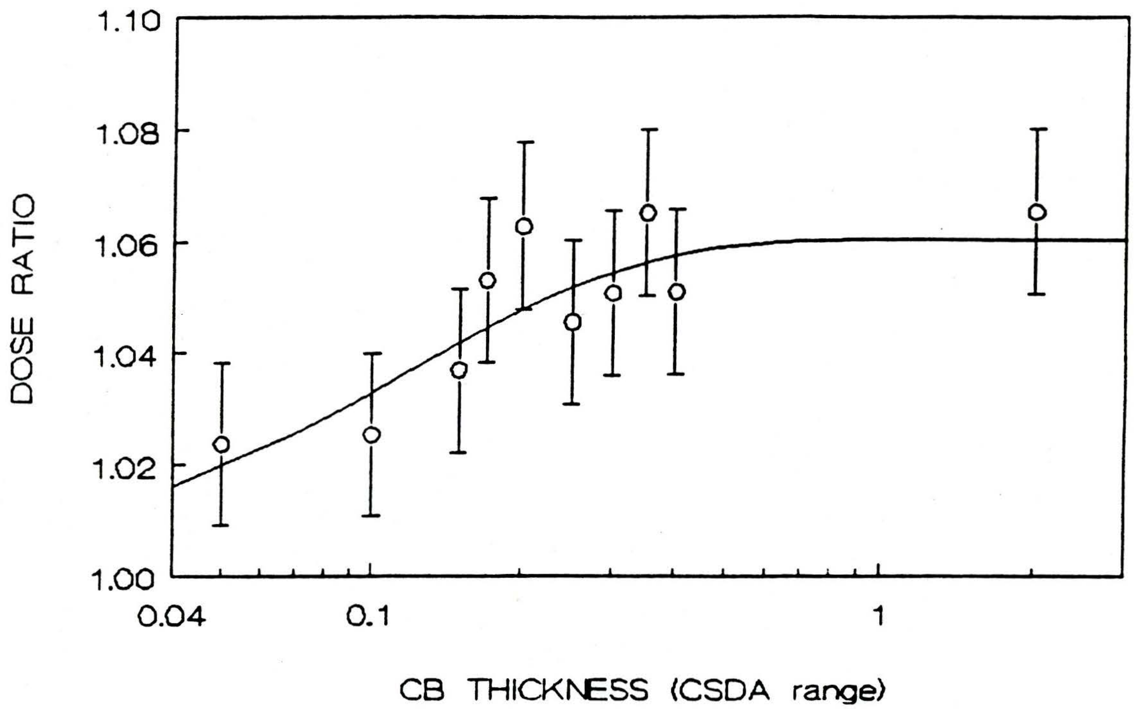

Figure 4.2 Dose enhancement ratio as a function of scaled CB thickness at 0-2.094 mg/cm² from planar CB-RBM interface for the point source and RBM-CB-RBM system

Fitting Function : $Y = A + B (1 - EXP(-CX))$

Where Y = Dose ratio

X = CB thickness in CSDA range

A, B and C are fitting parameters

$A = 1.000 \pm 0.002$

$B = 0.060 \pm 0.006$

$C = 8 \pm 2$

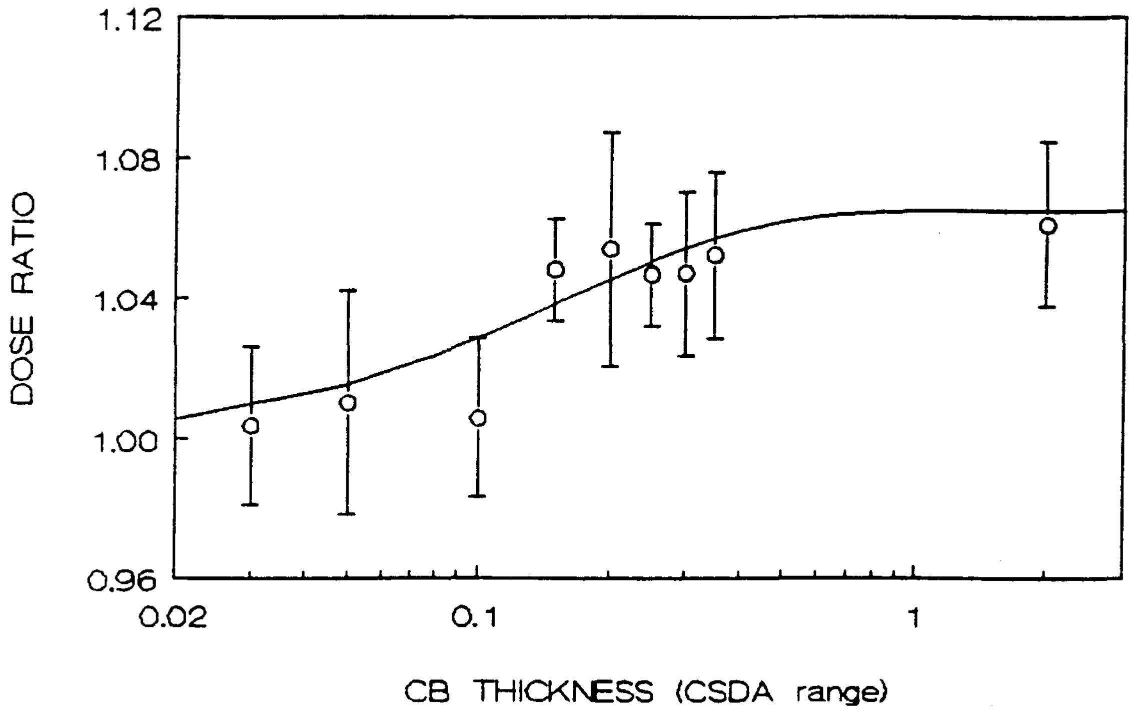

Figure 4.3 Dose enhancement ratio as a function of scaled CB thickness at 0-2.094 mg/cm² from planar CB-RBM interface for the plane source and RBM-CB-RBM system

Fitting Function : $Y = A + B (1 - EXP(-CX))$

Where Y = Dose ratio

X = CB thickness in CSDA range

A, B and C are fitting parameters

$A = 0.9981 \pm 0.005$

$B = 0.067 \pm 0.01$

$C = 6 \pm 2$

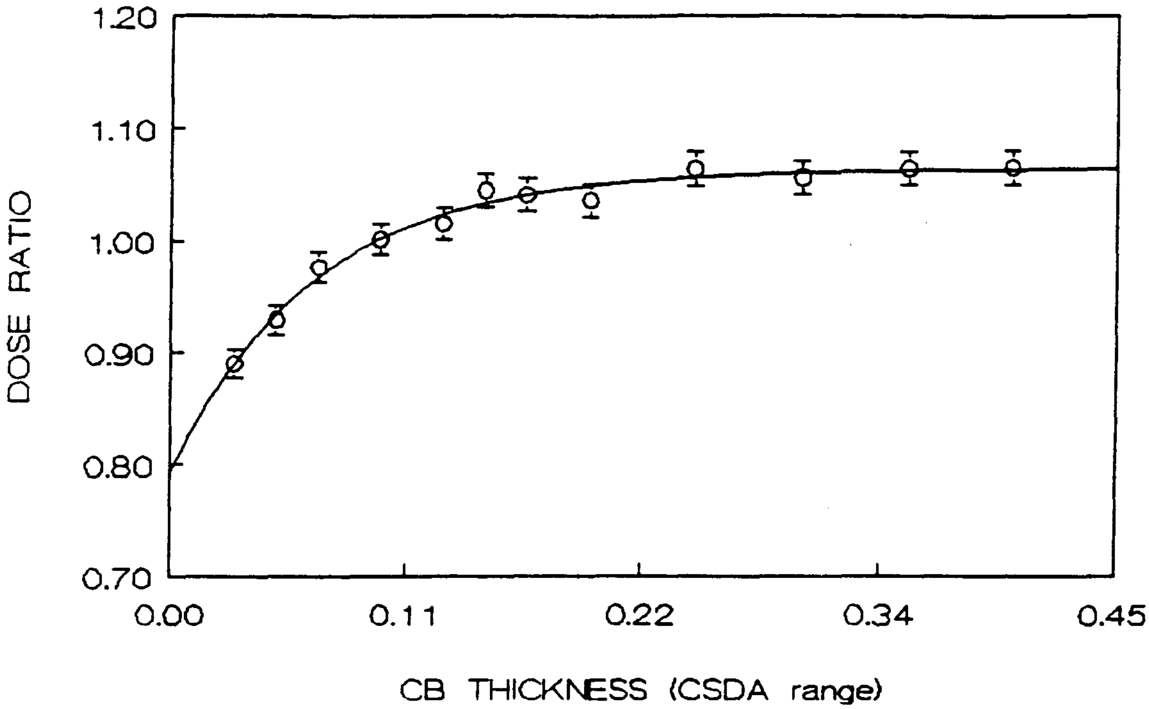

Figure 4.4 Dose enhancement ratio as a function of scaled CB thickness at 0-2.094 mg/cm² from planar CB-RBM interface for the point source and VAC-CB-RBM system

Fitting Function : Y = A + B (1 - EXP(-CX))

Where Y = Dose ratio

X = CB thickness in CSDA range

A, B and C are fitting parameters

A = 0.79 $\pm$ 0.01

B = 0.27 $\pm$ 0.01

C = 14.7 $\pm$ 0.8

4.2 DOSE RATIO FOR POINT SOURCES OF ELECTRONS AT A VAC-RBM INTERFACE

The dose distribution of a beta point source at a planar interface of air and polystyrene has been studied by Kwok et al. [3,21]. They found experimentally that the beta dose at 0-12 mg/cm² from the air-polystyrene interface decreased by (23 ± 2)% and (14 ± 3)% respectively for point sources of ^{204}Tl and ^{147}Pm compared with the dose in an unbounded polystyrene medium. However, the corresponding dose reductions according to their Monte Carlo calculations were respectively (6 ± 1)% and (2 ± 1)%. Unfortunately, they used a wrong cross section data file for polystyrene in the Monte Carlo calculations. There is another reason for repeating the calculations. The mass density of the TLD had been assumed to be 2.39 g/cm³ in the previous work according to the manufacturer's specification, but the mass density of the TLDs used in the experiments was measured to be (1.71 ± 0.03)g/cm³.

The geometry for the repeated Monte Carlo calculations is illustrated in Figure 4.5. Six electron energies ranging from 0.1 to 0.75 MeV were used. Forty thousand electron histories were followed for each Monte Carlo run.

A comparison of the dose ratio for different mass densities of the dose scoring region resulting from a point source of monoenergetic electrons at the VAC-PST (where PST stands for polystyrene) interface is presented in Table 4.2. The dose reduction ratios for the two different mass densities of DSR agree within one standard deviation except at 0.2 MeV where the dose ratio for the DSR with greater mass density (i.e. 0.94±0.01 for 2.39 mg/cm³) is about two standard deviation greater than the dose ratio for the DSR with smaller mass density (i.e 0.91 ± 0.01 for 1.71 mg/cm^3). Curves of dose versus electron energy in the range of 0.1 MeV to 0.75 MeV for homogeneous and inhomogeneous geometries were fitted by weighted least-squares method to a polynomial function. Linear functions were used in the region below 0.1 MeV. The fitting functions, listed in appendix D, were integrated with the beta spectra of ^{204}Tl and ^{147}Pm. The dose ratio for the beta sources was calculated by equation 2.8 and is given in Table 4.3. There is no significant effect of the change of mass density of the TLD on the dose reduction ratio since the two sets of Monte Carlo calculation results agree within one standard error. However, a significant discrepancy between Monte Carlo results and experimental results was still observed and the cause of this discrepancy remains unexplained.

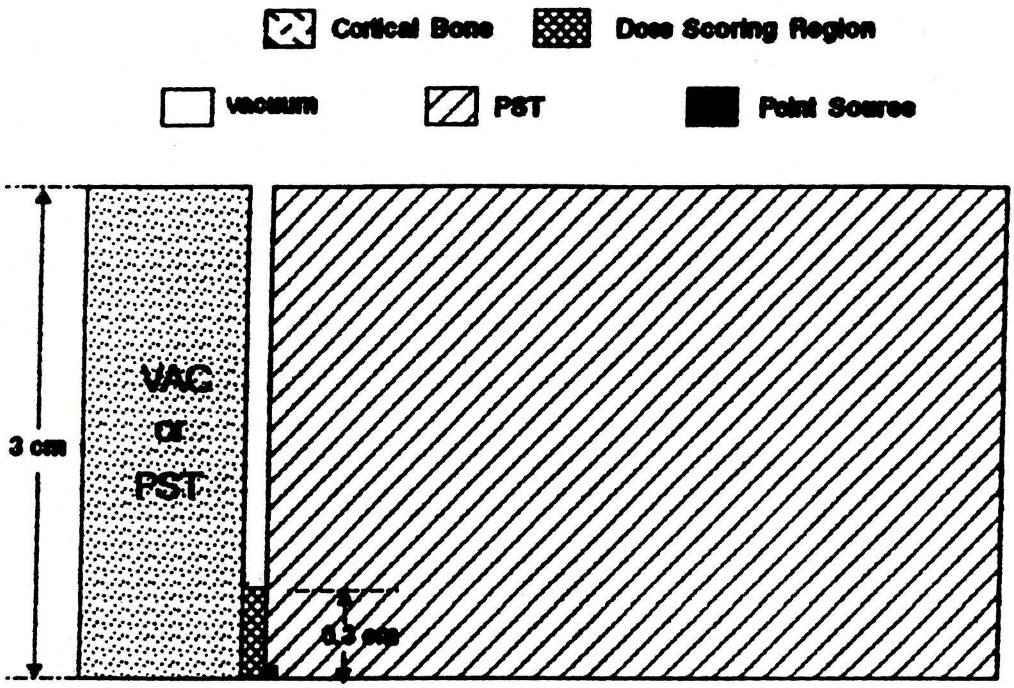

Figure 4.5 Geometry of the upper half cross section in the Monte Carlo calculations

TABLE 4.2

Dose reduction ratio for different mass density of dose scoring region resulting from a point source of monoenergetic electrons at a VAC-PST interface

Electron energy (MeV)	Mass density = 2.39 mg/cm^3	Mass density = 1.71 mg/cm^3
0.1	1.01 ± 0.01	1.00 ± 0.01
0.15	0.97 ± 0.01	0.95 ± 0.01
0.2	0.94 ± 0.01	0.91 ± 0.01
0.25	0.90 ± 0.01	0.88 ± 0.01
0.35	0.87 ± 0.01	0.86 ± 0.01
0.50	0.84 + 0.01	0.84 + 0.01
0.75	0.83 ± 0.01	0.84 ± 0.01

TABLE 4.3

Dose reduction ratio for different mass densities of dose scoring region with a point source of ^{204}Tl OR ^{147}Pm at the VAC-PST interface

Isotope	Mass density = 2.39 mg/cm^3	Mass density = 1.71 mg/cm^3	Experimental results
^{204}Tl	0.91 ± 0.01	0.91 ± 0.01	0.77 ± 0.07
^{147}Pm	0.99 ± 0.01	0.98 ± 0.01	0.9 ± 0.1

4.3 EFFECT OF MYLAR USED IN EXPERIMENTS ON DOSE RATIO

There was a difference in the geometry between the Monte Carlo calculations and the experiment. In the experiment, TLDs were sandwiched by two thin layers of mylar and they had not been taken into account in the Monte Carlo calculations. Thus, it is essential to investigate the effect of the presence of these layers of mylar on the dose ratio, especially the dose reduction ratio at the VAC-RBM interface.

Two geometries were used in the Monte Carlo calculation as shown in Figure 4.6. In geometry (1) a plane source of 0.1 MeV electrons was set at the VAC-RBM interface and a dose scoring region with equivalent mass density of 2.39 mg/cm³ was defined just behind the plane source. It has the same geometry and the same assumed value of mass density of TLD described in chapter 2. Fifty thousand electron histories were followed. Geometry (2) is the same as geometry (1) except that a layer of PST with equivalent thickness (i.e. 13.4 micron) and mass density (i.e. 1.66 g/cm³) of the mylar used in the experiment was placed in front of the plane source, and the mass density of the dose scoring region was 1.71 mg/cm³ (i.e. the same as the TLDs used in the experiment). One hundred and fifty thousand electron histories were followed.

Electrons with energy of 0.1 MeV were chosen because they have the shortest CSDA range among those used in the Monte Carlo calculations described in chapter 2. Therefore, the thickness of the mylar represented the biggest fraction of the CSDA range. The method of calculating dose ratio is the same as in the previous section. The dose reduction ratios calculated by using geometry (1) or (2) are 0.79 ±

0.02 and 0.83 ± 0.04 respectively. They are not statistically different. It justifies not including the mylar in most of the Monte Carlo calculations. If the thin layers of mylar does not affect the dose reduction ratio, it is expected not to cause any change to the dose enhancement ratio previously obtained as well.

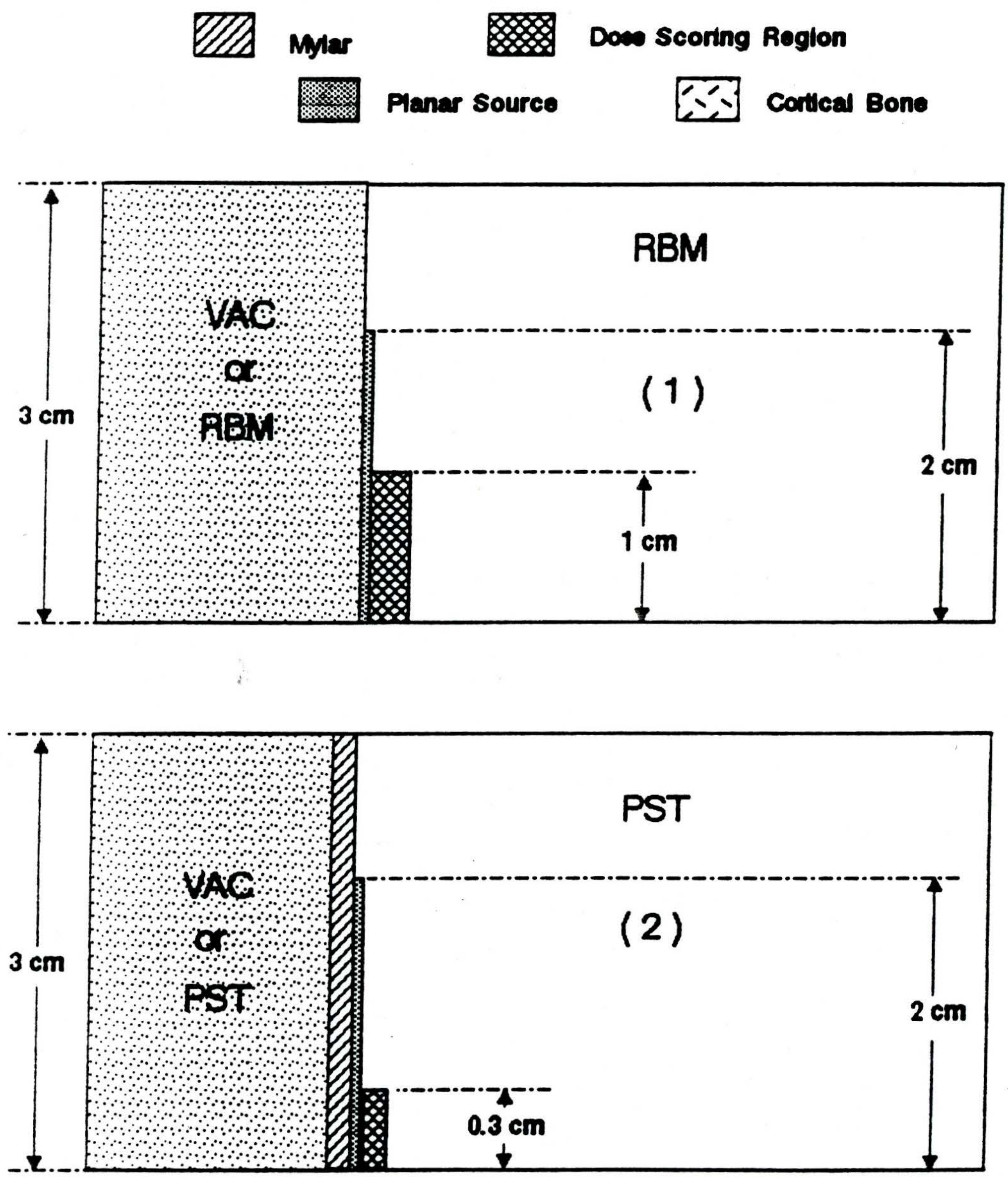

Figure 4.6 Geometries of the upper half cross section in the Monte Carlo calculations

CHAPTER 5

CONCLUSIONS

Tumor-associated monoclonal antibodies are potential carriers of ionizing radiation to the tumor site for cancer therapy. Practically, this technology is limited among other factors by radiotoxicity to the red bone marrow due to its high radiosensitivity and rapid entry of the labeled antibodies into the bone marrow from the circulation. Since the neighborhood of tumors may include air and bone interfaces, radiation dose near the interfaces should be quantitated.

In chapter 2, the dose near tissue interfaces due to a semi-infinite source of monoenergetic electrons was assumed to be linearly increased with electron energy from 0 to 0.1 MeV (see Figure 2.5). Since the function of variation of dose with electron energy was integrated with the spectrum of a beta source to calculate the average dose per beta decay, it is important to compare this function with other researchers' findings.

Berger [2] calculated the reduction factor $G(z)$ for a semi-infinite source of monoenergetic electrons in water as defined in equation 3.1, where z is the distance away from the source and is in scaled distance. The absorbed dose rate at z inside the source is equal to the equilibrium dose rate times $(1-G(z))$. Since the mass thickness of the DSRs was defined to be 12 mg/cm^2 in chapter 2, the maximum value of z, z_m, for the DSR at the interface for each monoenergetic electron source is equal to the mass thickness of the DSR divided by the CSDA range r_o of the electron in water. The r_o of electron in water was taken from ICRU report 37 [20].

The percentage of the equilibrium energy deposition, P, in the DSR at 0-12 mg/cm^2 from the interface for a monoenergetic electron source can be calculated by the following equation.

$$P = \frac{\int_0^{z_m} (1 - G(z))\, dz}{C} \times 100 \tag{5.1}$$

where $z_m = 0.012/r_o$

$C = 1$ if $z_m \leq 1$

$C = z_m$ if $z_m > 1$

Thus, the energy deposited in the DSR at 0-12 mg/cm^2 by one disintegration of the electron source is the product of P and the electron energy of the source. The normalized dose in table 5.1 was calculated by dividing the energy deposition for the monoenergetic electron sources by the highest energy deposition value among them. Likewise, the Monte Carlo results in table 2.3 were normalized in the same way. The normalized doses obtained by the two methods were plotted as a function of electron energy in Figure 5.1 for comparison.

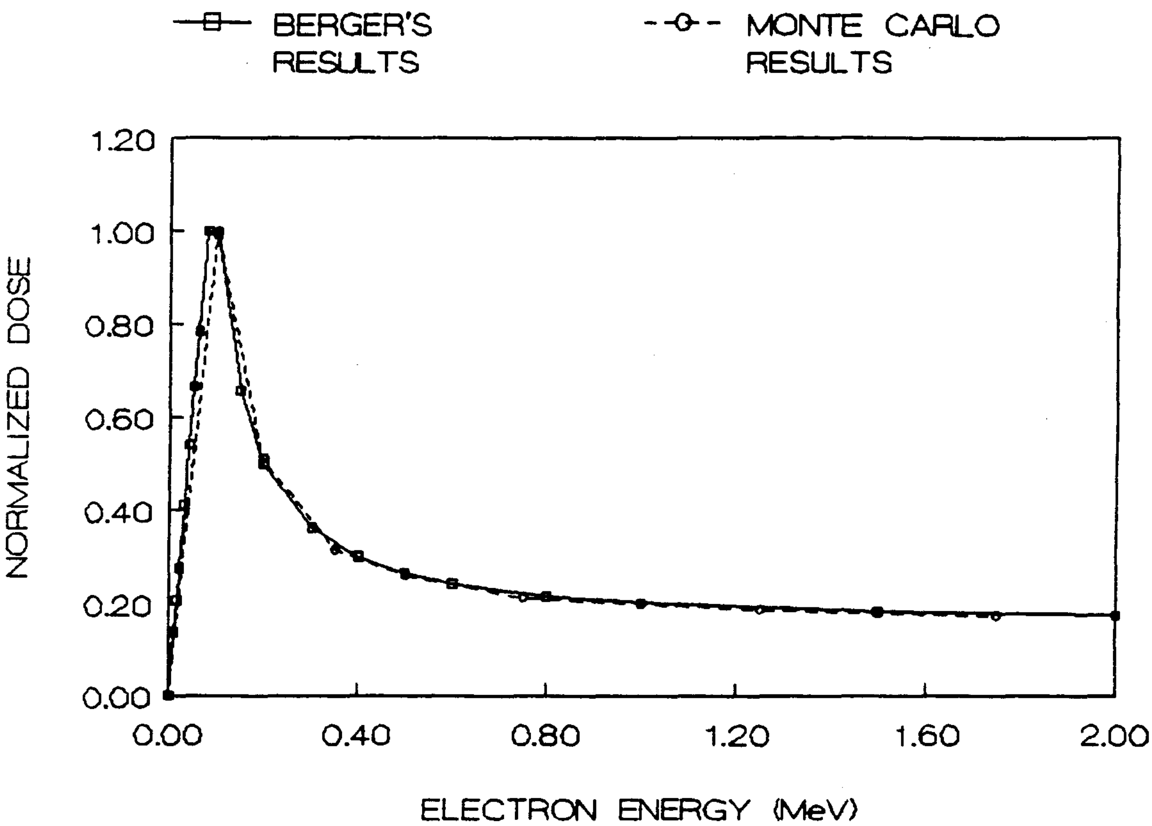

Figure 5.1 Comparison of Monte Carlo results with Bergers' results by plotting normalized dose at 0-12 mg/cm^2 as a function of electron energy

TABLE 5.1

Comparison of the Monte Carlo results with Bergers' results

Electron energy (MeV)	CSDA range in water (g/cm²)	% of total energy deposition	Normalized dose from Berger	Normalized dose from Monte Carlo
0.01	2.515E-4	99.732	0.1392	
0.015	5.147E-4	99.448	0.2083	
0.02	8.566E-4	99.078	0.2766	
0.03	1.756E-3	98.108	0.4109	
0.04	2.919E-3	96.860	0.5409	
0.05	4.320E-3	95.357	0.6656	
0.06	5.940E-3	93.623	0.7842	
0.08	9.773E-3	89.540	1.0000	
0.1	1.431E-3	71.065	0.9921	1.00±0.01
0.15	2.817E-2	31.358	0.6566	
0.2	4.487E-2	17.934	0.5007	0.50±0.01
0.3	8.421E-2	8.650	0.3623	
0.35	1.060E-1		0.3285*	0.323±0.006
0.4	1.288E-1	5.377	0.3003	
0.5	1.767E-1	3.804	0.2655	0.270±0.005
0.6	2.268E-1	2.905	0.2434	
0.75	3.046E-1		0.2218*	0.216±0.004
0.8	3.308E-1	1.943	0.2170	
1	4.378E-1	1.447	0.2020	0.201±0.004
1.25	5.731E-1		0.1921*	0.190±0.004
1.5	7.090E-1	0.877	0.1837	0.176±0.004
1.75	8.448E-1		0.1762*	0.175±0.004
2	9.801E-1	0.629	0.1756	

* interpolated values by using cubic spline fitting

From table 5.1 and Figure 5.1, it can be observed that both sets of results agree within one standard deviation except at 1.5 MeV and 0.75 MeV. For these electron energies, the normalized Monte Carlo dose is about two standard deviations less than the normalized dose from Bergers' results. Linear increase of dose from 0 to 0.08 MeV was observed from the Bergers' results. The actual highest dose occurs somewhere between 0.08 and 0.1 MeV. The assumption of linear increase of dose from 0 to 0.1 MeV in chapter 2 is therefore justified. The good agreement between the two approaches beyond 0.1 MeV implies that the method of data analysis for obtaining the dose due to a semi-infinite source of monoenergetic electrons described in chapter 2 was reliable. Therefore, the results for VAC-RBM and CB-RBM configurations are confidently acceptable.

In the Monte Carlo approach, the dose enhancement ratio for the CB-RBM interface increases with electron energy and reaches a plateau at 0.50 MeV while the dose reduction ratio for the VAC-RBM interface decreases and becomes steady from 1.00 MeV onwards. The dose enhancement ratios at 0-12, 79-91 and 157-169 mg/cm^2 separations from the CB-RBM interface due to a semi-infinite source of ^{32}P were calculated to be 1.07 $\pm$ 0.01, 1.02 $\pm$ 0.03 and 1.00 $\pm$ 0.03 respectively. The dose reduction ratios at those separations from the VAC-RBM interface due to a semi-infinite source of ^{32}P were calculated to be 0.87 $\pm$ 0.01, 0.97 $\pm$ 0.03 and 1.00 $\pm$ 0.03 respectively. The dose enhancement ratios and dose reduction ratios at 0-12 mg/cm^2 were calculated to be 1.02 $\pm$ 0.01 and 0.96 $\pm$ 0.01 respectively for ^{147}Pm and 1.04 $\pm$ 0.01 and 0.93 $\pm$ 0.01 respectively for ^{204}Tl. No dose enhancement or dose reduction were found at the other separations from the interfaces for ^{147}Pm and ^{204}Tl. (refer to chapter 2)

In the experimental approach, the dose enhancement ratios at 0-9, 79-88 and 157-166 mg/cm^2 separations from the CB-RBM interface due to a semi-infinite source of ^{32}P were measured to be 1.07 $\pm$ 0.01, 1.03 $\pm$ 0.03 and 0.99 $\pm$ 0.03 respectively. The dose reduction ratios at those separations from the VAC-RBM interface due to a semi-infinite source of ^{32}P were measured to be 0.82 $\pm$ 0.01, 0.94 $\pm$ 0.03 and 0.97 $\pm$ 0.03 respectively. (refer to chapter 3)

With a point source of monoenergetic electrons at a VAC-RBM interface, the same dose reduction ratio was observed for 9 mg/cm^2 and 12 mg/cm^2 thicknesses of the DSR. Since dose distribution near the VAC-RBM interface varies more rapidly than that near a CB-RBM interface, it is logical to expect no significant effect of the different mass thicknesses of the DSR on the dose enhancement ratio.

The dose enhancement ratio and the dose reduction ratio obtained by the Monte Carlo approach and the experimental approach agree within one standard deviation except for the dose reduction ratio at 0-12 mg/cm2 (i.e. Monte Carlo setting) or 0-9 mg/cm^2 from the interface (i.e. experimental setting). The experimental result, 0.82 $\pm$ 0.02, in this case is about three standard deviations less than the Monte Carlo result, 0.87 $\pm$ 0.01 (refer to chapter 4, section 4.2). Although the dose reduction ratios from the two approaches agree reasonably well for the semi-infinite source confriguration, there is still an unexplained discrepancy between Monte Carlo results and experimental results for the point source confriguration (refer to chapter 4, section 4.2). More research work for dose reduction near VAC-RBM is required to find out the cause of this discrepancy.

The trabecular bone is composed of thin lamellae of cortical bone with a wide range of thicknesses and they form a meshwork of interconnecting spaces which contain bone marrow. Using the Cyltran Monte Carlo code, the dose enhancement ratio at 0-20 micron separation from the CB-RBM interface due to a plane or point source of 0.5 MeV electrons at the interface, increases rapidly with the scaled CB thickness until a saturation value is reached (refer to chapter 4, section 4.1). The 99% saturation occurs approximately at 0.22 times the CSDA range for 0.5 MeV electrons for both plane source and point source configurations. The saturation dose enhancement ratio for both configurations is 1.06 ± 0.01.

The present work only investigated the thickness of CB required for the saturation of backscatter dose for 0.5 MeV electrons. Further investigation of the effect of the CB thickness on the dose enhancement ratio for other electron energies is recommended.

REFERENCES

[1] Glenn, F. Knoll. Radiation Detection and Measurement. John Wiley and Sons, Toronto, 1979. pp. 56-62.

[2] Berger, M.J. 1973. "Improved Point Kernels for Electron and Beta Ray Dosimetry". Washington, D.C. : U.S. National Bureau of Standards. NBSIR 73-107.

[3] Bialobzyski, P.J. 1987. Electron Dose Distribution Near Tissue-Bone Interfaces. M.Sc. Project Report, McMaster University.

[4] Blechinger, J.C., Madsen, E.L., Frank, G.R. "Tissue-mimicking gelatin-agar gels for use in magnetic resonance imaging phantoms". Medical Physics, Vol. 15, No. 4, Jul/Aug 1988.

[5] Wessels, B.W., Griffith, M.H. "Miniature Thermoluminescent Dosimeter Absorbed Dose Measurements in Tumor Phantom Models". The Journal of Nuclear Medicine, Vol. 27, No. 8, Aug 1986.

[6] Kastner, J., Hukkoo, R., Oltman, B.G., Dayal, Y. "Thermoluminescent Internal Beta-Ray Dosimetry". Radiation Research 32, pp. 625-640, 1967.

[7] Barber, D.E., Moore, R., Hutchinson, T. 1974. "Response of LiF To 1.0-4.0 KeV Electrons". Health Physics Pergamon Press 1975. Vol. 28 (Jan), pp. 13-15.

[8] Cameron, J.R., Suntharalingam, N., Kenney, G.N. "Thermoluminescent Dosimetry" Madison, Wisconsin, The University of Wisconsin Press, 1968.

[9] Daniels, F., Boyd, C.A., Saundas, D.F. "Thermoluminescence as a research tool". Science 117, 343-349 (1953).

[10] Kohler, G., Milstein, C. "Continuous culture of fused cells secreting antibody of proven defined specificity". Nature 256, pp. 495-497, 1975.

[11] Wessels, B.W., Roger, R.D. "Radionuclide selection and model absorbed dose calculations for radiolabelled tumor associated antibodies". Medical Physics, Vol. 11; pp. 638-645, 1984.

[12] Humm, J.L. "Dosimeteric Aspects of Radiolabelled Antibodies for Tumor Therapy". Journal of Nuclear Medicine, Vol. 27 : 1490-1497, 1986.

[13] Order, S.E., Klein, J.L., Ettinger, D., Alderson, P., Siegelman, S., Leichner, P. "Use of Isotopic Immunoglobulin in Therapy". Cancer Research 40 : 3001-3007, 1980.

[14] Order, S.E. "Monoclonal Antibodies : potential role in Radiation Therapy and Oncology". Internation Journal of Radiation Oncology, Biology, Physics, Vol. 8, PP. 1193-1201, 1981.

[15] William, F.B., Irving, L.S. "Studies Directed Toward The Use Of Antibodies As Carriers Of Radioactivity For Therapy". Advances in Biology & Medical Physics, pp. 285-356.

[16] Zamboni, L., Pease, D.C. "The vascular bed of red bone marrow". J Ultrastructure Research, 5 : 65-85, 1961.

[17] Dewey, W.C. "Vascular - extravascular exchange of I-131 plasma proteins in the rat". American Journal of Physiology, 197 : 423-431, 1959.

[18] Lord, B.I., Hendry, J.H. "The distribution of haemopoietic colony-forming units in mouse femur, and its modification by X rays". British Journal of Radiology, 45, pp. 110-115, 1972.

[19] Maloney, M.A., Lamela, R.A., Dorie, M.J., Patt, H.M. "Concentration Gradient of Blood Stem Cells in Mouse Bone Marrow - An Open Question". Blood, vol. 51, No. 3, 1978.

[20] International Commission on Radiation Units and Measurements, Stopping Powers For Electrons And Positions, ICRU report 37, Oct 1984.

[21] Kwok, C.S., Bialobzyski, P.J., Prestwich, W.V., "Effect of tissue inhomogeneity on dose distribution of low energy electrons", submitted to Medical Physics.

[22] Prestwich, W.V. Nunes, J. Kwok, C.S. "Beta Dose Point Kernels for Radionuclides of Potential Use in Radioimmunotherapy", accepted for publication in Journal of Nuclear Medicine.

[23] Wickramasinghe, S.N. Human Bone Marrow, Blackwell Scientific Publications, 1975.

[24] Stickney, D.R., Gridley, D.S., Kirk, G.A., Slater, J.M. "Enhancement of Monoclonal Antibody Binding to Melanoma With Single Dose Radiation or Hyperthermia", NCI Monographs, No. 3, 1987.

[25] Holliday, J.E., Sternglass, E.J. "Backscattering of 5-20 KeV Electrons form Insulators and Metals", Journal of Applied Physics, Vol. 28, No. 10, 1957.

[26] Al-Beteri, A.A., Raeside, D.E. "An Improved Electron Multiple-Scattering Distribution for Monte Carlo Transport Simulation", Medical Physics, Vol. 15, No. 3, 1988.

[27] Archard, G.D. "Back Scattering of Electrons", Journal of Applied Physics, Vol. 32, No. 8, 1961.

[28] "Private communication from Dr. C. S. Kwok : Physics Department, Ontario Cancer Foundation".

[29] Radiation Shielding Information Center Computer Code Collection 467, Integrated TIGER Series of Coupled Electron/Photon Monte Carlo Code System, Oak Ridge National Laboratory (1985).

[30] Ford, R.L., Nelson, W.R., "The EGS Code System", SLAC Report No.210 (1978)

APPENDIX A

In this appendix, the Monte Carlo results are tabulated in the form of the energy deposition per electron, S, in a dose scoring region due to a plane source of monoenergetic electrons with energy E at source position P for RBM-RBM, CB-RBM and VAC-RBM geometries. The positions of the DSR are listed as the nearest scaled distance of the DSR from the interface. The mass thickness and the mass of the DSR are 12 mg/cm^2 and 0.037695 g, respectively.

The following equation can be used to convert the unit of the results into Gray per electron.

$$\text{Dose} = \frac{S\left(\frac{\text{MeV}}{\text{electron}}\right) \times 1.602 \times 10^{-13}\left(\frac{\text{Joule}}{\text{MeV}}\right)\left(\frac{1\ \text{Gy}}{\text{Joule/Kg}}\right)}{3.7695 \times 10^{-5}(\text{ Kg })}$$

$$= 4.2499 \times 10^{-9} S \text{ (Gy/electron)} \qquad (A.1)$$

GEOMETRY : RBM-RBM DSR=0 MASS THICKNESS = 12mg/cm^2

P\E(MeV)	0.10	0.20	0.35	0.50	0.75	1.00	1.25	1.50	1.75
0	1.248E-02	1.484E-02	1.385E-02	1.351E-02	1.339E-02	1.402E-02	1.409E-02	1.387E-02	1.429E-02
1/18	1.461E-02	1.700E-02	1.632E-02	1.516E-02	1.139E-02	1.063E-02	9.861E-03	8.961E-03	8.882E-03
1/9	1.608E-02	1.791E-02	1.396E-02	1.085E-02	8.483E-03	7.848E-03	7.198E-03	7.278E-03	7.024E-03
1/6	1.724E-02	1.800E-02	1.081E-02	8.693E-03	7.069E-03	6.465E-03	6.096E-03	5.827E-03	5.935E-03
2/9	1.835E-02	1.662E-02	9.199E-03	7.605E-03	6.078E-03	5.633E-03	5.261E-03	5.044E-03	4.929E-03
1/3	1.943E-02	1.163E-02	6.902E-03	5.781E-03	4.506E-03	4.309E-03	4.021E-03	3.788E-03	3.756E-03
2/3	1.654E-02	4.827E-03	2.425E-03	1.775E-03	1.500E-03	1.278E-03	1.240E-03	1.109E-03	9.970E-04
1	6.238E-03	3.819E-04	3.432E-05	1.503E-05	7.117E-06	6.384E-06	3.081E-06	5.450E-06	2.645E-06
10/9	4.086E-03	6.372E-05	2.063E-06	2.368E-07	3.245E-07	9.936E-08	2.118E-07	8.977E-07	5.632E-07
4/3	1.264E-03	9.145E-07	2.190E-07	1.000E-08	1.000E-08	1.000E-08	1.000E-08	1.140E-06	3.113E-07

CORRESPONDING ABSOLUTE UNCERTAINTIES

P\E(MeV)	0.10	0.20	0.35	0.50	0.75	1.00	1.25	1.50	[illegible]
0	1.248E-04	2.968E-04	2.770E-04	1.351E-04	2.678E-04	1.402E-04	1.409E-04	1.387E-04	[illegible]
1/18	1.461E-04	1.700E-04	1.632E-04	1.516E-04	1.139E-04	1.063E-04	1.972E-04	1.792E-04	1.776E-04
1/9	1.608E-04	1.791E-04	1.396E-04	1.085E-04	8.483E-05	1.570E-04	7.198E-05	1.456E-04	1.405E-04
1/6	1.724E-04	1.800E-04	2.163E-04	1.739E-04	1.414E-04	1.293E-04	1.219E-04	1.748E-04	1.780E-04
2/9	1.834E-04	1.662E-04	9.199E-05	1.521E-04	1.216E-04	1.127E-04	1.052E-04	1.009E-04	9.858E-05
1/3	1.943E-04	2.325E-04	1.380E-04	1.156E-04	9.011E-05	8.618E-05	8.041E-05	1.136E-04	7.513E-05
2/3	1.654E-04	9.653E-05	7.275E-05	3.550E-05	5.998E-05	5.112E-05	6.199E-05	8.870E-05	3.988E-05
1	1.248E-04	3.819E-05	9.265E-06	5.711E-06	4.697E-06	3.383E-06	3.050E-06	3.706E-06	2.275E-06
10/9	8.172E-05	9.559E-06	1.898E-06	2.273E-07	2.726E-07	9.836E-08	1.843E-07	8.887E-07	4.393E-07
4/3	3.793E-05	7.041E-07	2.168E-07	9.900E-09	9.900E-09	9.900E-09	9.900E-09	1.083E-06	3.020E-07

GEOMETRY : CB-RBM   DSR=0   MASS THICKNESS = 12mg/cm^2

P\E(MeV)	0.10	0.20	0.35	0.50	0.75	1.00	1.25	1.50	1.75
0	1.360E-02	1.590E-02	1.556E-02	1.512E-02	1.417E-02	1.505E-02	1.431E-02	1.499E-02	1.523E-02
1/18	1.524E-02	1.798E-02	1.738E-02	1.599E-02	1.209E-02	1.045E-02	1.012E-02	1.015E-02	9.697E-03
1/9	1.662E-02	1.852E-02	1.446E-02	1.110E-02	9.191E-03	8.401E-03	7.989E-03	7.743E-03	7.290E-03
1/6	1.778E-02	1.846E-02	1.177E-02	9.657E-03	7.786E-03	7.171E-03	6.612E-03	6.476E-03	6.168E-03
2/9	1.859E-02	1.715E-02	9.717E-03	7.954E-03	6.893E-03	6.086E-03	5.861E-03	5.662E-03	5.328E-03
1/3	1.941E-02	1.222E-02	7.473E-03	6.169E-03	5.364E-03	4.852E-03	4.405E-03	4.153E-03	4.149E-03
2/3	1.684E-02	4.640E-03	2.503E-03	1.846E-03	1.606E-03	1.461E-03	1.418E-03	1.235E-03	1.062E-03
1	6.360E-03	3.920E-04	5.384E-05	1.782E-05	2.116E-06	5.999E-06	2.999E-06	2.097E-06	3.482E-06
10/9	4.220E-03	5.477E-05	1.632E-06	3.019E-07	4.032E-07	4.350E-07	4.563E-07	3.930E-07	4.610E-07
4/3	1.280E-03	6.906E-07	7.248E-07	1.799E-07	4.787E-07	1.000E-08	6.810E-07	9.975E-08	1.000E-07

CORRESPONDING ABSOLUTE UNCERTAINTIES

P\E(MeV)	0.10	0.20	0.35	0.50	0.75	1.00	1.25	1.50	1.75
0	2.721E-04	1.590E-04	1.556E-04	3.024E-04	1.417E-04	1.505E-04	1.431E-04	2.998E-04	3.045E-04
1/18	1.524E-04	1.798E-04	1.738E-04	1.599E-04	2.418E-04	1.045E-04	2.024E-04	2.030E-04	1.939E-04
1/9	1.662E-04	1.852E-04	1.446E-04	2.219E-04	1.838E-04	8.401E-05	7.989E-05	1.549E-04	7.290E-05
1/6	1.778E-04	1.846E-04	2.353E-04	1.931E-04	1.557E-04	1.434E-04	1.322E-04	1.943E-04	1.234E-04
2/9	1.859E-04	1.715E-04	1.943E-04	1.591E-04	1.379E-04	6.086E-05	1.172E-04	1.699E-04	1.598E-04
1/3	1.941E-04	2.443E-04	7.473E-05	1.234E-04	1.609E-04	9.704E-05	8.810E-05	8.305E-05	1.245E-04
2/3	3.367E-04	9.280E-05	7.509E-05	9.228E-05	4.817E-05	2.923E-05	5.670E-05	3.706E-05	4.248E-05
1	6.360E-05	3.136E-05	8.615E-06	6.238E-06	1.777E-06	2.700E-06	2.519E-06	1.531E-06	2.194E-06
10/9	8.440E-05	7.667E-06	1.142E-06	2.657E-07	3.991E-07	2.393E-07	3.057E-07	3.890E-07	4.102E-07
4/3	3.839E-05	6.837E-07	5.436E-07	1.781E-07	4.452E-07	9.900E-09	6.742E-07	9.875E-08	9.900E-08

GEOMETRY : VAC-RBM DSR=0 MASS THICKNESS = 12mg/cm^2

P\E(MeV)	0.10	0.20	0.35	0.50	0.75	1.00	1.25	1.50	1.75
0	9.886E-03	1.115E-02	9.329E-03	9.549E-03	9.216E-03	9.162E-03	9.332E-03	9.590E-03	9.431E-03
1/18	1.351E-02	1.477E-02	1.401E-02	1.276E-02	9.412E-03	7.825E-03	7.366E-03	7.082E-03	7.042E-03
1/9	1.549E-02	1.662E-02	1.250E-02	8.655E-03	6.825E-03	6.044E-03	5.759E-03	5.588E-03	5.363E-03
1/6	1.667E-02	1.680E-02	9.366E-03	7.199E-03	5.890E-03	5.258E-03	4.901E-03	4.714E-03	4.417E-03
2/9	1.756E-02	1.564E-02	8.000E-03	6.309E-03	4.929E-03	4.402E-03	4.208E-03	3.990E-03	4.035E-03
1/3	1.880E-02	1.095E-02	6.266E-03	4.922E-03	3.965E-03	3.481E-03	3.181E-03	3.139E-03	3.091E-03
2/3	1.635E-02	4.578E-03	2.244E-03	1.791E-03	1.327E-03	1.155E-03	1.066E-03	9.779E-04	9.274E-04
1	6.399E-03	3.724E-04	3.585E-05	1.527E-05	2.495E-06	2.263E-06	7.970E-06	7.105E-07	6.873E-06
10/9	4.246E-03	4.183E-05	2.834E-06	1.000E-07	1.000E-07	2.548E-07	1.847E-06	1.000E-06	1.000E-07
4/3	1.283E-03	4.966E-07	7.851E-07	1.823E-07	1.000E-07	3.046E-08	1.803E-06	1.000E-07	4.100E-07

CORRESPONDING ABSOLUTE UNCERTAINTIES

P\E(MeV)	0.10	0.20	0.35	0.50	0.75	1.00	1.25	1.50	1.75
0	9.886E-05	1.115E-04	1.866E-04	1.910E-04	1.843E-04	1.832E-04	1.866E-04	2.877E-04	9.431E-05
1/18	1.351E-04	1.477E-04	2.803E-04	2.552E-04	9.412E-05	1.565E-04	1.473E-04	1.416E-04	1.406E-04
1/9	1.549E-04	3.324E-04	2.500E-04	8.655E-05	1.365E-04	1.209E-04	1.152E-04	1.118E-04	5.363E-05
1/6	1.667E-04	1.680E-04	9.366E-05	7.199E-05	1.178E-04	1.577E-04	9.802E-05	9.428E-05	8.834E-05
2/9	1.756E-04	1.564E-04	8.000E-05	1.893E-04	1.479E-04	8.804E-05	1.262E-04	7.980E-05	8.070E-05
1/3	1.880E-04	1.095E-04	6.266E-05	9.844E-05	7.930E-05	6.962E-05	3.181E-05	6.278E-05	6.182E-05
2/3	1.635E-04	9.156E-05	6.733E-05	5.372E-05	5.308E-05	2.310E-05	5.329E-05	4.889E-05	2.782E-05
1	1.280E-04	2.234E-05	5.378E-06	5.346E-06	1.921E-06	1.584E-07	5.021E-06	4.974E-07	3.711E-06
10/9	8.493E-05	6.693E-06	1.984E-06	9.900E-08	9.900E-08	2.523E-07	8.313E-07	9.703E-07	9.900E-08
4/3	3.848E-05	3.327E-07	4.632E-07	1.804E-07	9.900E-08	3.015E-08	1.749E-06	9.900E-08	4.059E-07

GEOMETRY : RBM-RBM   DSR=1/9   MASS THICKNESS = 12mg/cm^2

P\E(MeV)	0.10	0.20	0.35	0.50	0.75	1.00	1.25	1.50	1.75
0	8.509E-03	1.054E-02	8.866E-03	8.292E-03	7.546E-03	7.192E-03	6.842E-03	6.671E-03	5.423E-03
1/18	1.021E-02	1.191E-02	1.079E-02	1.020E-02	9.258E-03	8.938E-03	8.540E-03	8.361E-03	6.754E-03
1/9	1.248E-02	1.487E-02	1.415E-02	1.387E-02	1.368E-02	1.375E-02	1.371E-02	1.430E-02	1.204E-02
1/6	1.463E-02	1.710E-02	1.632E-02	1.519E-02	1.125E-02	9.976E-03	9.568E-03	8.914E-03	7.476E-03
2/9	1.618E-02	1.803E-02	1.427E-02	1.062E-02	8.829E-03	8.079E-03	7.218E-03	7.276E-03	5.796E-03
1/3	1.829E-02	1.655E-02	9.153E-03	7.630E-03	6.342E-03	5.525E-03	5.414E-03	5.194E-03	3.892E-03
2/3	1.824E-02	6.729E-03	3.941E-03	2.946E-03	2.506E-03	2.120E-03	1.987E-03	1.914E-03	1.515E-03
1	8.974E-03	1.253E-03	2.918E-04	1.808E-04	1.212E-04	1.020E-04	9.632E-05	7.709E-05	7.396E-05
10/9	6.233E-03	3.800E-04	3.086E-05	1.416E-05	1.179E-05	1.067E-06	4.641E-06	6.024E-06	2.028E-06
4/3	2.435E-03	3.316E-06	1.964E-09	2.673E-08	1.874E-07	1.181E-09	4.666E-07	1.755E-06	4.267E-07

CORRESPONDING ABSOLUTE UNCERTAINTIES

P\E(MeV)	0.10	0.20	0.35	0.50	0.75	1.00	1.25	1.50	1.75
0	8.509E-05	2.108E-04	8.866E-05	1.658E-04	1.509E-04	2.158E-04	1.368E-04	6.671E-05	1.085E-04
1/18	1.021E-04	1.191E-04	2.158E-04	1.020E-04	1.852E-04	8.938E-05	1.708E-04	1.672E-04	1.351E-04
1/9	1.248E-04	1.487E-04	2.831E-04	1.387E-04	2.737E-04	2.750E-04	2.741E-04	2.860E-04	2.409E-04
1/6	1.463E-04	3.420E-04	1.632E-04	1.519E-04	2.250E-04	1.995E-04	1.914E-04	2.674E-04	2.243E-04
2/9	1.618E-04	1.803E-04	1.427E-04	1.062E-04	8.829E-05	1.616E-04	1.444E-04	7.276E-05	1.159E-04
1/3	1.829E-04	1.655E-04	1.831E-04	1.526E-04	1.268E-04	5.525E-05	1.083E-04	5.194E-05	1.168E-04
2/3	1.824E-04	1.346E-04	1.182E-04	5.892E-05	7.518E-05	6.359E-05	3.974E-05	5.743E-05	4.544E-05
1	8.974E-05	3.759E-05	2.335E-05	1.627E-05	2.666E-05	1.020E-05	1.926E-05	1.233E-05	1.331E-05
10/9	1.247E-04	2.280E-05	5.556E-06	5.238E-06	6.838E-06	4.696E-07	2.274E-06	3.193E-06	1.988E-06
4/3	4.871E-05	1.757E-06	1.944E-09	2.646E-08	1.855E-07	1.169E-09	3.126E-07	1.492E-06	3.755E-07

GEOMETRY : CB-RBM DSR=1/9 MASS THICKNESS = 12mg/cm^2

P\E(MeV)	0.10	0.20	0.35	0.50	0.75	1.00	1.25	1.50	1.75
0	9.211E-03	1.149E-02	9.994E-03	9.146E-03	8.107E-03	7.809E-03	7.556E-03	7.286E-03	5.708E-03
1/18	1.064E-02	1.279E-02	1.149E-02	1.038E-02	9.440E-03	9.499E-03	9.178E-03	8.905E-03	7.050E-03
1/9	1.267E-02	1.518E-02	1.417E-02	1.454E-02	1.388E-02	1.418E-02	1.412E-02	1.441E-02	1.203E-02
1/6	1.497E-02	1.737E-02	1.655E-02	1.547E-02	1.151E-02	1.084E-02	9.644E-03	9.570E-03	7.218E-03
2/9	1.634E-02	1.774E-02	1.435E-02	1.058E-02	8.782E-03	8.026E-03	7.631E-03	7.152E-03	5.627E-03
1/3	1.822E-02	1.687E-02	9.269E-03	7.513E-03	6.295E-03	5.882E-03	5.598E-03	5.254E-03	4.100E-03
2/3	1.867E-02	6.667E-03	3.956E-03	3.151E-03	2.590E-03	2.245E-03	2.125E-03	1.952E-03	1.549E-03
1	9.217E-03	1.254E-03	3.429E-04	1.781E-04	1.053E-04	9.588E-05	8.026E-05	7.836E-05	6.040E-05
10/9	6.340E-03	3.575E-04	2.995E-05	9.058E-06	3.766E-06	6.382E-06	5.924E-06	7.970E-06	4.965E-06
4/3	2.536E-03	2.234E-06	2.917E-07	4.917E-08	1.000E-07	2.407E-07	1.000E-07	3.953E-07	4.244E-07

CORRESPONDING ABSOLUTE UNCERTAINTIES

P\E(MeV)	0.10	0.20	0.35	0.50	0.75	1.00	1.25	1.50	1.75
0	9.211E-05	1.149E-04	1.999E-04	2.744E-04	8.107E-05	2.343E-04	7.556E-05	1.457E-04	1.142E-04
1/18	1.064E-04	1.279E-04	1.149E-04	2.076E-04	1.888E-04	1.900E-04	1.836E-04	1.781E-04	1.410E-04
1/9	1.267E-04	1.518E-04	1.417E-04	1.454E-04	2.776E-04	2.836E-04	1.412E-04	2.883E-04	2.406E-04
1/6	1.497E-04	1.737E-04	1.655E-04	1.547E-04	2.301E-04	1.084E-04	9.644E-05	1.914E-04	1.443E-04
2/9	1.634E-04	1.774E-04	1.435E-04	1.058E-04	8.782E-05	1.606E-04	7.631E-05	7.152E-05	1.125E-04
1/3	1.822E-04	1.687E-04	1.854E-04	1.508E-04	1.888E-04	1.166E-04	1.678E-04	1.051E-04	8.199E-05
2/3	1.867E-04	6.667E-05	7.911E-05	1.260E-04	5.179E-05	6.734E-05	8.500E-05	5.856E-05	6.195E-05
1	1.843E-04	5.017E-05	2.743E-05	1.731E-05	1.579E-05	9.588E-06	1.364E-05	1.761E-05	1.450E-05
10/9	1.268E-04	2.145E-05	3.295E-06	2.808E-06	2.084E-06	2.681E-06	3.199E-06	4.463E-06	3.029E-06
4/3	5.073E-05	1.765E-06	2.888E-07	4.868E-08	9.900E-08	2.383E-07	9.900E-08	3.518E-07	2.886E-07

GEOMETRY : VAC-RBM DSR=1/9 MASS THICKNESS = 12mg/cm^2

P\E(MeV)	0.10	0.20	0.35	0.50	0.75	1.00	1.25	1.50	1.75
0	7.263E-03	8.772E-03	7.079E-03	6.647E-03	5.753E-03	5.621E-03	5.559E-03	5.326E-03	4.178E-03
1/18	9.805E-03	1.108E-02	9.959E-03	9.021E-03	8.346E-03	8.193E-03	8.008E-03	7.980E-03	6.251E-03
1/9	1.241E-02	1.419E-02	1.349E-02	1.348E-02	1.336E-02	1.333E-02	1.347E-02	1.362E-02	1.221E-02
1/6	1.420E-02	1.687E-02	1.565E-02	1.454E-02	1.086E-02	9.825E-03	9.361E-03	8.895E-03	6.978E-03
2/9	1.590E-02	1.731E-02	1.366E-02	1.033E-02	8.105E-03	7.431E-03	7.364E-03	6.824E-03	5.228E-03
1/3	1.797E-02	1.640E-02	8.979E-03	7.463E-03	6.119E-03	5.338E-03	5.222E-03	4.880E-03	3.796E-03
2/3	1.814E-02	6.692E-03	3.823E-03	2.962E-03	2.465E-03	2.208E-03	2.022E-03	1.827E-03	1.545E-03
1	9.247E-03	1.273E-03	3.682E-04	1.752E-04	1.133E-04	1.054E-04	8.863E-05	8.122E-05	7.686E-05
10/9	6.436E-03	3.946E-04	4.074E-05	1.674E-05	7.119E-07	7.253E-06	1.034E-06	4.534E-07	1.518E-06
4/3	2.495E-03	8.539E-07	1.376E-06	5.998E-07	1.361E-08	2.334E-07	1.087E-06	1.000E-07	2.643E-07

CORRESPONDING ABSOLUTE UNCERTAINTIES

P\E(MeV)	0.10	0.20	0.35	0.50	0.75	1.00	1.25	1.50	[illegible]
0	7.263E-05	1.754E-04	1.416E-04	1.329E-04	1.726E-04	1.124E-04	1.112E-04	1.065E-04	[illegible]
1/18	1.961E-04	2.217E-04	2.988E-04	1.804E-04	2.504E-04	8.193E-05	1.602E-04	1.596E-04	[illegible]
1/9	1.241E-04	1.419E-04	2.699E-04	1.348E-04	2.672E-04	2.665E-04	4.042E-04	2.723E-04	[illegible]
1/6	1.420E-04	3.375E-04	1.565E-04	2.908E-04	2.172E-04	2.947E-04	1.872E-04	1.779E-04	[illegible]
2/9	1.590E-04	1.731E-04	1.366E-04	2.067E-04	1.621E-04	1.486E-04	1.473E-04	1.365E-04	1.568E-04
1/3	1.797E-04	1.640E-04	8.979E-05	1.493E-04	1.836E-04	1.068E-04	5.222E-05	9.759E-05	3.796E-05
2/3	1.814E-04	1.338E-04	1.529E-04	8.885E-05	9.859E-05	1.104E-04	4.043E-05	5.481E-05	6.180E-05
1	1.849E-04	3.819E-05	3.314E-05	2.102E-05	2.039E-05	1.264E-05	1.329E-05	7.310E-06	1.460E-05
10/9	1.287E-04	3.157E-05	7.740E-06	4.853E-06	4.841E-07	4.569E-06	1.013E-06	4.489E-07	1.123E-06
4/3	7.484E-05	5.550E-07	6.192E-07	5.938E-07	1.347E-08	2.310E-07	7.171E-07	9.900E-08	2.616E-07

GEOMETRY : RBM-RBM　　　DSR=2/9　　　MASS THICKNESS = 12mg/cm^2

P\E(MeV)	0.35	0.50	0.75	1.00	1.25	1.50	1.75
0	7.100E-03	6.322E-03	5.581E-03	5.262E-03	4.975E-03	4.768E-03	4.961E-03
1/18	8.006E-03	7.394E-03	6.612E-03	5.971E-03	5.912E-03	5.566E-03	5.290E-03
1/9	9.265E-03	8.956E-03	7.418E-03	7.112E-03	6.996E-03	6.730E-03	6.640E-03
1/6	1.089E-02	1.001E-02	8.954E-03	8.739E-03	8.707E-03	8.243E-03	8.526E-03
2/9	1.418E-02	1.354E-02	1.367E-02	1.365E-02	1.409E-02	1.434E-02	1.447E-02
1/3	1.403E-02	1.067E-02	8.487E-03	7.816E-03	7.664E-03	7.013E-03	6.761E-03
2/3	5.376E-03	4.345E-03	3.582E-03	3.041E-03	2.928E-03	2.814E-03	2.719E-03
1	1.228E-03	8.090E-04	6.027E-04	4.499E-04	5.074E-04	4.900E-04	4.342E-04
10/9	3.437E-04	2.044E-04	1.173E-04	9.190E-05	1.264E-04	8.235E-05	1.064E-04
4/3	3.296E-07	3.803E-08	3.552E-07	1.329E-06	2.909E-07	4.958E-07	2.131E-07

CORRESPONDING ABSOLUTE UNCERTAINTIES

P\E(MeV)	0.35	0.50	0.75	1.00	1.25	1.50	1.75
0	1.420E-04	6.322E-05	1.116E-04	1.579E-04	1.493E-04	9.536E-05	4.961E-05
1/18	8.006E-05	1.479E-04	1.322E-04	1.194E-04	1.182E-04	1.113E-04	5.290E-05
1/9	9.265E-05	8.356E-05	7.418E-05	1.422E-04	1.399E-04	1.348E-04	1.328E-04
1/6	1.089E-04	2.002E-04	1.791E-04	1.748E-04	8.707E-05	1.649E-04	1.705E-04
2/9	1.418E-04	1.354E-04	2.733E-04	2.730E-04	1.409E-04	2.868E-04	2.894E-04
1/3	1.403E-04	2.134E-04	8.487E-05	1.563E-04	1.533E-04	1.403E-04	2.028E-04
2/3	1.075E-04	4.345E-05	1.075E-04	6.082E-05	8.785E-05	5.629E-05	8.156E-05
1	2.456E-05	3.286E-05	5.424E-05	1.799E-05	2.537E-05	3.490E-05	2.605E-05
10/9	2.406E-05	1.839E-05	1.055E-05	1.287E-05	1.390E-05	1.318E-05	1.277E-05
4/3	3.263E-07	3.764E-08	3.516E-07	9.099E-07	2.763E-07	3.471E-07	2.110E-07

GEOMETRY : CB-RBM   DSR=2/9   MASS THICKNESS = 12mg/cm^2

P\E(MeV)	0.35	0.50	0.75	1.00	1.25	1.50	1.75
0	7.748E-03	6.926E-03	6.191E-03	5.853E-03	5.608E-03	5.168E-03	5.159E-03
1/18	8.271E-03	7.546E-03	6.795E-03	6.308E-03	6.198E-03	5.821E-03	5.765E-03
1/9	9.398E-03	8.705E-03	7.740E-03	7.233E-03	6.889E-03	6.725E-03	6.673E-03
1/6	1.079E-02	1.020E-02	9.312E-03	8.783E-03	8.565E-03	8.525E-03	8.215E-03
2/9	1.423E-02	1.399E-02	1.395E-02	1.402E-02	1.422E-02	1.388E-02	1.424E-02
1/3	1.356E-02	1.007E-02	8.558E-03	7.719E-03	7.411E-03	6.966E-03	7.134E-03
2/3	5.543E-03	4.446E-03	3.657E-03	3.180E-03	2.939E-03	2.967E-03	2.668E-03
1	1.168E-03	7.482E-04	6.502E-04	5.424E-04	5.025E-04	4.711E-04	5.065E-04
10/9	3.219E-04	1.866E-04	1.312E-04	1.104E-04	7.469E-05	9.693E-05	9.350E-05
4/3	4.814E-07	7.786E-07	3.552E-07	1.000E-08	4.695E-08	1.560E-06	1.876E-07

CORRESPONDING ABSOLUTE UNCERTAINTIES

P\E(MeV)	0.35	0.50	0.75	1.00	1.25	1.50	1.75
0	2.324E-04	1.385E-04	6.191E-05	1.756E-04	1.122E-04	1.034E-04	1.548E-04
1/18	1.654E-04	1.509E-04	1.359E-04	1.262E-04	6.198E-05	1.164E-04	5.765E-05
1/9	9.398E-05	1.741E-04	7.740E-05	7.233E-05	1.378E-04	1.345E-04	1.335E-04
1/6	1.079E-04	2.039E-04	1.862E-04	8.783E-05	2.569E-04	1.705E-04	1.643E-04
2/9	2.847E-04	1.399E-04	1.395E-04	1.402E-04	2.844E-04	1.388E-04	2.848E-04
1/3	1.356E-04	2.015E-04	8.558E-05	7.719E-05	1.482E-04	1.393E-04	1.427E-04
2/3	1.109E-04	8.893E-05	1.097E-04	6.361E-05	5.878E-05	5.934E-05	5.335E-05
1	5.842E-05	2.993E-05	5.852E-05	2.712E-05	3.517E-05	4.240E-05	2.533E-05
10/9	2.576E-05	2.239E-05	1.050E-05	1.657E-05	8.216E-06	8.724E-06	1.496E-05
4/3	3.947E-07	5.606E-07	3.516E-07	9.900E-09	4.648E-08	1.544E-06	1.857E-07

GEOMETRY : VAC-RBM DSR=2/9 MASS THICKNESS = 12mg/cm^2

P\E(MeV)	0.35	0.50	0.75	1.00	1.25	1.50	1.75
0	5.981E-03	5.375E-03	4.516E-03	4.535E-03	4.326E-03	4.246E-03	4.027E-03
1/18	7.720E-03	6.830E-03	6.271E-03	5.745E-03	5.477E-03	5.404E-03	5.243E-03
1/9	8.950E-03	8.140E-03	7.576E-03	7.040E-03	6.662E-03	6.447E-03	6.620E-03
1/6	1.056E-02	9.811E-03	9.043E-03	8.586E-03	8.171E-03	8.282E-03	8.076E-03
2/9	1.374E-02	1.387E-02	1.332E-02	1.397E-02	1.376E-02	1.407E-02	1.456E-02
1/3	1.391E-02	1.028E-02	8.593E-03	7.868E-03	7.122E-03	6.869E-03	7.038E-03
2/3	5.077E-03	4.258E-03	3.430E-03	3.275E-03	3.061E-03	2.794E-03	2.688E-03
1	1.156E-03	7.892E-04	6.433E-04	4.999E-04	4.446E-04	4.809E-04	5.017E-04
10/9	3.431E-04	2.014E-04	1.341E-04	1.022E-04	8.890E-05	8.376E-05	1.147E-04
4/3	2.894E-07	1.000E-07	7.354E-07	1.000E-07	1.371E-07	5.358E-07	1.000E-07

CORRESPONDING ABSOLUTE UNCERTAINTIES

P\E(MeV)	0.35	0.50	0.75	1.00	1.25	1.50	1.75
0	1.794E-04	1.075E-04	4.516E-05	9.069E-05	8.652E-05	8.492E-05	8.055E-05
1/18	1.544E-04	1.366E-04	6.271E-05	1.149E-04	5.477E-05	1.621E-04	1.049E-04
1/9	2.685E-04	2.442E-04	7.576E-05	1.408E-04	1.332E-04	1.934E-04	1.324E-04
1/6	2.111E-04	2.943E-04	1.809E-04	1.717E-04	1.634E-04	1.656E-04	1.615E-04
2/9	1.374E-04	2.775E-04	2.663E-04	1.397E-04	2.752E-04	4.220E-04	4.368E-04
1/3	1.391E-04	1.028E-04	1.719E-04	1.574E-04	1.424E-04	1.374E-04	2.111E-04
2/3	1.523E-04	8.517E-05	1.029E-04	6.549E-05	9.184E-05	5.588E-05	1.344E-04
1	4.626E-05	6.313E-05	2.573E-05	2.999E-05	2.223E-05	4.328E-05	4.014E-05
10/9	1.715E-05	2.416E-05	1.878E-05	1.635E-05	1.334E-05	1.256E-05	2.293E-05
4/3	2.662E-07	9.900E-08	4.780E-07	9.900E-08	1.357E-07	3.590E-07	9.900E-08

GEOMETRY : RBM-RBM   DSR=1/3   MASS THICKNESS = 12mg/cm^2

P\E(MeV)	0.35	0.50	0.75	1.00	1.25	1.50	1.75
0	5.466E-03	4.621E-03	4.421E-03	4.021E-03	3.725E-03	3.781E-03	3.636E-03
1/18	6.376E-03	5.570E-03	5.093E-03	4.614E-03	4.388E-03	4.185E-03	3.907E-03
1/9	7.276E-03	6.890E-03	5.657E-03	5.099E-03	5.020E-03	5.007E-03	4.559E-03
1/6	7.870E-03	7.274E-03	6.627E-03	6.168E-03	5.928E-03	5.740E-03	5.657E-03
2/9	9.231E-03	8.268E-03	7.743E-03	7.139E-03	6.738E-03	6.678E-03	6.808E-03
1/3	1.420E-02	1.390E-02	1.343E-02	1.351E-02	1.360E-02	1.414E-02	1.462E-02
2/3	6.992E-03	5.689E-03	4.608E-03	4.233E-03	3.832E-03	3.804E-03	3.794E-03
1	2.523E-03	1.877E-03	1.504E-03	1.133E-03	1.205E-03	1.145E-03	1.088E-03
10/9	1.292E-03	8.753E-04	6.168E-04	4.948E-04	4.461E-04	4.742E-04	4.585E-04
4/3	3.247E-05	9.163E-06	5.571E-07	3.200E-06	3.942E-06	6.916E-07	7.594E-06

CORRESPONDING ABSOLUTE UNCERTAINTIES

P\E(MeV)	0.35	0.50	0.75	1.00	1.25	1.50	1.75
0	1.093E-04	9.242E-05	8.842E-05	8.043E-05	7.450E-05	7.562E-05	1.091E-04
1/18	6.376E-05	5.570E-05	1.019E-04	9.227E-05	8.775E-05	1.256E-04	1.172E-04
1/9	1.455E-04	6.890E-05	1.131E-04	1.020E-04	1.004E-04	1.001E-04	1.368E-04
1/6	7.870E-05	2.182E-04	1.325E-04	1.233E-04	1.186E-04	1.722E-04	1.131E-04
2/9	9.231E-05	8.268E-05	7.743E-05	1.428E-04	1.347E-04	1.336E-04	1.362E-04
1/3	2.840E-04	1.390E-04	1.343E-04	1.351E-04	2.720E-04	1.414E-04	2.924E-04
2/3	1.398E-04	1.138E-04	4.608E-05	8.466E-05	1.150E-04	7.608E-05	1.138E-04
1	7.569E-05	5.631E-05	6.017E-05	3.398E-05	4.821E-05	4.580E-05	3.264E-05
10/9	5.169E-05	4.376E-05	4.318E-05	3.463E-05	8.922E-06	3.794E-05	2.292E-05
4/3	6.493E-06	8.574E-06	2.897E-07	2.464E-06	2.286E-06	6.847E-07	5.316E-06

GEOMETRY : CB-RBM DSR=1/3 MASS THICKNESS = 12mg/cm^2

P\E(MeV)	0.35	0.50	0.75	1.00	1.25	1.50	1.75
0	5.861E-03	5.305E-03	4.735E-03	4.348E-03	4.127E-03	3.841E-03	3.978E-03
1/18	6.325E-03	5.735E-03	5.040E-03	4.628E-03	4.482E-03	4.172E-03	4.259E-03
1/9	7.162E-03	6.500E-03	5.755E-03	5.354E-03	5.163E-03	5.041E-03	4.896E-03
1/6	7.763E-03	7.360E-03	6.396E-03	6.061E-03	5.718E-03	5.754E-03	5.413E-03
2/9	9.250E-03	8.494E-03	7.577E-03	7.254E-03	7.034E-03	6.552E-03	6.686E-03
1/3	1.403E-02	1.370E-02	1.399E-02	1.400E-02	1.385E-02	1.411E-02	1.452E-02
2/3	7.070E-03	5.792E-03	4.686E-03	4.310E-03	3.922E-03	3.865E-03	3.651E-03
1	2.539E-03	1.745E-03	1.453E-03	1.262E-03	1.207E-03	1.108E-03	1.054E-03
10/9	1.205E-03	8.324E-04	5.666E-04	5.378E-04	5.247E-04	5.197E-04	4.752E-04
4/3	2.933E-05	1.387E-05	1.021E-05	6.629E-06	7.361E-06	1.677E-06	1.739E-05

CORRESPONDING ABSOLUTE UNCERTAINTIES

P\E(MeV)	0.35	0.50	0.75	1.00	1.25	1.50	1.75
0	1.172E-04	1.061E-04	9.470E-05	8.696E-05	8.254E-05	7.681E-05	1.193E-04
1/18	1.265E-04	1.147E-04	1.008E-04	4.628E-05	1.345E-04	8.345E-05	8.518E-05
1/9	1.432E-04	1.300E-04	1.151E-04	1.071E-04	1.033E-04	1.008E-04	9.792E-05
1/6	7.763E-05	1.472E-04	1.279E-04	1.212E-04	1.716E-04	5.754E-05	1.624E-04
2/9	1.850E-04	8.494E-05	7.577E-05	7.254E-05	1.407E-04	1.310E-04	1.337E-04
1/3	1.403E-04	1.370E-04	2.798E-04	2.800E-04	2.770E-04	2.822E-04	2.904E-04
2/3	1.414E-04	1.158E-04	1.874E-04	8.620E-05	1.176E-04	1.160E-04	7.302E-05
1	7.616E-05	6.979E-05	5.812E-05	3.785E-05	4.830E-05	8.862E-05	6.325E-05
10/9	3.614E-05	2.497E-05	2.266E-05	2.689E-05	3.148E-05	3.118E-05	3.801E-05
4/3	7.625E-06	3.051E-06	5.617E-06	3.845E-06	4.784E-06	1.023E-06	7.649E-06

GEOMETRY : VAC-RBM DSR=1/3 MASS THICKNESS = 12mg/cm^2

P\E(MeV)	0.35	0.50	0.75	1.00	1.25	1.50	1.75
0	4.948E-03	4.410E-03	3.865E-03	3.695E-03	3.398E-03	3.341E-03	3.274E-03
1/10	6.220E-03	5.518E-03	4.930E-03	4.582E-03	4.169E-03	3.988E-03	4.115E-03
1/9	6.914E-03	6.319E-03	5.807E-03	5.218E-03	5.069E-03	4.791E-03	4.848E-03
1/6	8.155E-03	7.001E-03	6.576E-03	5.991E-03	5.601E-03	5.462E-03	5.448E-03
2/9	9.012E-03	8.308E-03	7.381E-03	7.120E-03	6.689E-03	6.588E-03	6.708E-03
1/3	1.389E-02	1.390E-02	1.303E-02	1.360E-02	1.399E-02	1.460E-02	1.460E-02
2/3	6.788E-03	5.666E-03	4.801E-03	4.486E-03	4.074E-03	3.753E-03	3.788E-03
1	2.462E-03	1.705E-03	1.437E-03	1.226E-03	1.074E-03	1.066E-03	1.089E-03
10/9	1.302E-03	8.093E-04	5.940E-04	4.828E-04	4.719E-04	4.663E-04	4.757E-04
4/3	3.372E-05	1.346E-05	6.686E-06	2.039E-06	1.000E-08	1.382E-06	1.487E-06

CORRESPONDING ABSOLUTE UNCERTAINTIES

P\E(MeV)	0.35	0.50	0.75	1.00	1.25	1.50	1.75
0	1.483E-04	8.819E-05	7.730E-05	1.108E-04	6.796E-05	1.002E-04	6.548E-05
1/10	1.866E-04	1.655E-04	9.861E-05	9.165E-05	8.387E-05	7.965E-05	1.285E-04
1/9	1.883E-04	1.264E-04	1.061E-04	1.565E-04	1.014E-04	9.581E-05	9.695E-05
1/6	1.631E-04	2.100E-04	1.973E-04	1.198E-04	1.680E-04	1.092E-04	5.448E-05
2/9	9.012E-05	1.661E-04	1.476E-04	1.424E-04	1.398E-04	1.976E-04	1.342E-04
1/3	1.389E-04	1.390E-04	1.303E-04	2.720E-04	1.399E-04	2.919E-04	2.919E-04
2/3	1.358E-04	1.193E-04	1.440E-04	4.486E-05	8.147E-05	1.126E-04	1.515E-04
1	7.387E-05	6.821E-05	7.183E-05	6.128E-05	5.868E-05	3.198E-05	4.358E-05
10/9	3.907E-05	4.047E-05	2.376E-05	3.379E-05	2.859E-05	4.197E-05	2.854E-05
4/3	8.429E-06	4.710E-06	2.674E-06	1.646E-06	9.900E-09	9.257E-07	1.294E-06

GEOMETRY : RBM-RBM DSR=4/9 MASS THICKNESS = 12mg/cm^2

P\E(MeV)	0.35	0.50	0.75	1.00	1.25	1.50	1.75
0	4.033E-03	3.453E-03	3.177E-03	3.076E-03	2.824E-03	2.740E-03	2.763E-03
1/18	4.883E-03	4.303E-03	3.807E-03	3.556E-03	3.185E-03	3.245E-03	3.107E-03
1/9	5.542E-03	4.801E-03	4.329E-03	4.123E-03	3.838E-03	3.659E-03	3.548E-03
1/6	6.212E-03	5.471E-03	5.006E-03	4.682E-03	4.724E-03	4.263E-03	4.197E-03
2/9	7.060E-03	6.270E-03	5.676E-03	5.131E-03	4.821E-03	4.838E-03	4.651E-03
1/3	9.058E-03	8.471E-03	7.757E-03	7.152E-03	6.890E-03	6.679E-03	6.585E-03
2/3	8.890E-03	7.512E-03	6.056E-03	5.621E-03	5.325E-03	5.104E-03	4.820E-03
1	3.854E-03	3.144E-03	2.422E-03	2.011E-03	2.088E-03	2.046E-03	1.863E-03
10/9	2.533E-03	1.786E-03	1.422E-03	1.341E-03	1.209E-03	1.109E-03	1.165E-03
4/3	3.464E-04	1.692E-04	1.036E-04	1.062E-04	7.500E-05	7.774E-05	9.324E-05

CORRESPONDING ABSOLUTE UNCERTAINTIES

P\E(MeV)	0.35	0.50	0.75	1.00	1.25	1.50	1.75
0	1.210E-04	1.036E-04	9.532E-05	6.151E-05	2.824E-05	8.220E-05	8.290E-05
1/18	1.465E-04	1.291E-04	7.614E-05	7.113E-05	1.274E-04	6.490E-05	9.321E-05
1/9	1.108E-04	9.603E-05	8.659E-05	8.246E-05	7.675E-05	3.659E-05	7.097E-05
1/6	1.242E-04	1.094E-04	1.001E-04	9.364E-05	9.447E-05	1.279E-04	8.393E-05
2/9	1.412E-04	6.270E-05	1.135E-04	1.026E-04	9.643E-05	9.677E-05	9.302E-05
1/3	9.058E-05	1.694E-04	1.551E-04	7.152E-05	1.378E-04	1.336E-04	1.317E-04
2/3	1.778E-04	1.502E-04	1.211E-04	1.124E-04	1.065E-04	1.021E-04	9.640E-05
1	7.707E-05	6.287E-05	2.422E-05	6.034E-05	6.264E-05	1.023E-04	7.451E-05
10/9	7.598E-05	5.357E-05	7.112E-05	5.363E-05	4.836E-05	3.326E-05	5.823E-05
4/3	3.117E-05	1.861E-05	1.866E-05	9.561E-06	1.275E-05	1.011E-05	1.305E-05

GEOMETRY : CB-RBM   DSR=4/9   MASS THICKNESS = 12mg/cm^2

P\E(MeV)	0.35	0.50	0.75	1.00	1.25	1.50	1.75
0	4.188E-03	3.714E-03	3.389E-03	3.102E-03	2.908E-03	2.765E-03	2.762E-03
1/18	4.795E-03	4.133E-03	3.631E-03	3.524E-03	3.315E-03	3.203E-03	3.032E-03
1/9	5.647E-03	4.893E-03	4.217E-03	4.099E-03	3.888E-03	3.756E-03	3.525E-03
1/6	6.128E-03	5.704E-03	4.878E-03	4.781E-03	4.101E-03	4.133E-03	4.009E-03
2/9	7.087E-03	6.431E-03	5.752E-03	5.212E-03	5.034E-03	4.994E-03	4.656E-03
1/3	9.255E-03	8.285E-03	7.571E-03	7.200E-03	6.917E-03	6.755E-03	6.689E-03
2/3	9.348E-03	7.635E-03	6.186E-03	5.518E-03	5.286E-03	5.054E-03	4.926E-03
1	3.711E-03	2.989E-03	2.384E-03	2.150E-03	2.053E-03	1.909E-03	2.057E-03
10/9	2.573E-03	1.785E-03	1.489E-03	1.290E-03	1.255E-03	1.091E-03	1.179E-03
4/3	3.045E-04	1.353E-04	1.408E-04	9.092E-05	1.047E-04	6.548E-05	8.810E-05

CORRESPONDING ABSOLUTE UNCERTAINTIES

P\E(MeV)	0.35	0.50	0.75	1.00	1.25	1.50	1.75
0	1.256E-04	7.429E-05	6.779E-05	9.307E-05	5.816E-05	1.106E-04	5.524E-05
1/18	9.590E-05	8.267E-05	7.262E-05	7.048E-05	9.945E-05	6.407E-05	6.064E-05
1/9	1.694E-04	9.787E-05	1.687E-04	1.230E-04	7.776E-05	7.511E-05	1.058E-04
1/6	6.128E-05	1.141E-04	1.463E-04	1.434E-04	8.203E-05	4.133E-05	1.203E-04
2/9	1.417E-04	6.431E-05	1.150E-04	1.042E-04	2.014E-04	9.988E-05	9.312E-05
1/3	1.851E-04	8.285E-05	1.514E-04	1.440E-04	1.383E-04	1.351E-04	1.338E-04
2/3	9.348E-05	7.635E-05	1.237E-04	1.104E-04	1.057E-04	1.011E-04	9.852E-05
1	1.113E-04	1.196E-04	7.153E-05	8.600E-05	4.106E-05	7.637E-05	6.170E-05
10/9	5.147E-05	5.356E-05	4.466E-05	3.869E-05	3.764E-05	4.364E-05	5.896E-05
4/3	1.523E-05	2.706E-05	2.112E-05	1.000E-05	1.152E-05	7.203E-06	1.586E-05

GEOMETRY : VAC-RBM   DSR=4/9   MASS THICKNESS = 12mg/cm^2

P\E(MeV)	0.35	0.50	0.75	1.00	1.25	1.50	1.75
0	3.940E-03	3.367E-03	3.023E-03	2.864E-03	2.633E-03	2.643E-03	2.420E-03
1/18	4.658E-03	4.250E-03	3.908E-03	3.477E-03	3.198E-03	2.926E-03	3.114E-03
1/9	5.301E-03	5.079E-03	4.141E-03	3.993E-03	4.051E-03	3.731E-03	3.675E-03
1/6	6.190E-03	5.505E-03	4.869E-03	4.588E-03	4.490E-03	4.060E-03	4.024E-03
2/9	6.952E-03	6.287E-03	5.512E-03	5.354E-03	5.105E-03	4.834E-03	4.726E-03
1/3	9.343E-03	8.400E-03	7.598E-03	7.102E-03	6.854E-03	6.701E-03	6.435E-03
2/3	9.177E-03	7.269E-03	6.470E-03	5.522E-03	5.235E-03	5.092E-03	4.755E-03
1	3.740E-03	2.962E-03	2.448E-03	2.064E-03	1.950E-03	1.888E-03	2.001E-03
10/9	2.564E-03	1.818E-03	1.391E-03	1.199E-03	1.196E-03	1.100E-03	1.127E-03
4/3	3.875E-04	2.080E-04	1.298E-04	1.022E-04	6.899E-05	1.047E-04	8.692E-05

CORRESPONDING ABSOLUTE UNCERTAINTIES

P\E(MeV)	0.35	0.50	0.75	1.00	1.25	1.50	1.75
0	7.880E-05	6.735E-05	9.069E-05	5.728E-05	7.898E-05	1.057E-04	4.839E-05
1/18	9.316E-05	8.500E-05	1.172E-04	6.954E-05	9.594E-05	8.777E-05	6.227E-05
1/9	1.060E-04	1.524E-04	8.283E-05	1.198E-04	1.215E-04	7.461E-05	7.350E-05
1/6	1.238E-04	1.101E-04	9.738E-05	9.176E-05	8.980E-05	8.120E-05	1.207E-04
2/9	1.390E-04	6.287E-05	1.102E-04	1.606E-04	1.532E-04	1.450E-04	1.418E-04
1/3	9.343E-05	1.680E-04	7.598E-05	2.131E-04	1.371E-04	1.340E-04	1.287E-04
2/3	1.835E-04	1.454E-04	2.588E-04	1.104E-04	1.047E-04	1.018E-04	1.427E-04
1	7.481E-05	1.481E-04	9.791E-05	6.191E-05	5.851E-05	7.553E-05	8.004E-05
10/9	5.127E-05	7.270E-05	4.174E-05	4.798E-05	5.982E-05	4.401E-05	7.887E-05
4/3	3.100E-05	2.288E-05	1.817E-05	1.532E-05	1.656E-05	1.884E-05	1.651E-05

GEOMETRY : RBM-RBM DSR=5/9 MASS THICKNESS = 12mg/cm^2

P\E(MeV)	0.35	0.50	0.75	1.00	1.25	1.50	1.75
0	2.516E-03	2.131E-03	2.177E-03	2.045E-03	1.906E-03	1.887E-03	1.760E-03
1/18	3.354E-03	2.858E-03	2.671E-03	2.440E-03	2.382E-03	2.345E-03	2.233E-03
1/9	3.848E-03	3.708E-03	3.339E-03	3.128E-03	2.970E-03	2.546E-03	2.746E-03
1/6	4.849E-03	4.273E-03	3.576E-03	3.516E-03	3.376E-03	3.241E-03	2.980E-03
2/9	5.480E-03	4.825E-03	4.369E-03	4.024E-03	3.839E-03	3.815E-03	3.688E-03
1/3	7.129E-03	6.299E-03	5.609E-03	5.171E-03	4.963E-03	4.726E-03	4.729E-03
2/3	1.376E-02	1.052E-02	8.789E-03	7.810E-03	7.371E-03	6.905E-03	6.674E-03
1	5.465E-03	4.363E-03	3.462E-03	3.054E-03	2.943E-03	2.901E-03	2.635E-03
10/9	3.923E-03	3.095E-03	2.596E-03	2.141E-03	2.046E-03	1.931E-03	1.926E-03
4/3	1.214E-03	7.226E-04	5.522E-04	5.213E-04	4.460E-04	4.734E-04	5.085E-04

CORRESPONDING ABSOLUTE UNCERTAINTIES

P\E(MeV)	0.35	0.50	0.75	1.00	1.25	1.50	1.75
0	7.549E-05	6.394E-05	8.706E-05	6.134E-05	5.717E-05	3.774E-05	5.280E-05
1/18	1.341E-04	1.143E-04	5.341E-05	9.760E-05	4.765E-05	9.378E-05	4.466E-05
1/9	7.695E-05	7.416E-05	1.002E-04	6.256E-05	8.910E-05	1.018E-04	5.491E-05
1/6	9.697E-05	1.282E-04	7.151E-05	7.031E-05	6.751E-05	9.723E-05	5.960E-05
2/9	1.096E-04	9.649E-05	4.369E-05	8.047E-05	7.679E-05	1.144E-04	1.106E-04
1/3	1.426E-04	1.260E-04	1.122E-04	1.034E-04	1.489E-04	9.451E-05	9.457E-05
2/3	2.752E-04	2.104E-04	1.758E-04	1.562E-04	7.371E-05	2.072E-04	1.335E-04
1	1.093E-04	1.309E-04	6.924E-05	9.161E-05	5.885E-05	1.160E-04	5.269E-05
10/9	1.177E-04	6.191E-05	5.192E-05	8.563E-05	8.184E-05	5.794E-05	5.778E-05
4/3	6.070E-05	2.890E-05	4.417E-05	3.649E-05	1.784E-05	2.840E-05	2.034E-05

GEOMETRY : CB-RBM DSR=5/9 MASS THICKNESS = 12mg/cm^2

P\E(MeV)	0.35	0.50	0.75	1.00	1.25	1.50	1.75
0	2.536E-03	2.376E-03	2.178E-03	2.073E-03	1.933E-03	1.826E-03	1.916E-03
1/18	3.245E-03	2.912E-03	2.627E-03	2.492E-03	2.362E-03	2.219E-03	2.204E-03
1/9	4.000E-03	3.561E-03	3.255E-03	2.982E-03	2.793E-03	2.668E-03	2.627E-03
1/6	4.833E-03	4.302E-03	3.716E-03	3.517E-03	3.267E-03	3.019E-03	3.019E-03
2/9	5.518E-03	4.838E-03	4.482E-03	4.163E-03	3.649E-03	3.808E-03	3.651E-03
1/3	7.191E-03	6.299E-03	5.470E-03	5.290E-03	4.989E-03	4.954E-03	4.880E-03
2/3	1.400E-02	1.035E-02	8.303E-03	7.924E-03	7.210E-03	7.049E-03	6.724E-03
1	5.216E-03	4.204E-03	3.510E-03	3.053E-03	2.961E-03	2.871E-03	2.569E-03
10/9	3.985E-03	3.040E-03	2.575E-03	2.250E-03	2.058E-03	1.975E-03	1.970E-03
4/3	1.191E-03	8.033E-04	5.672E-04	4.366E-04	4.466E-04	5.027E-04	4.274E-04

CORRESPONDING ABSOLUTE UNCERTAINTIES

P\E(MeV)	0.35	0.50	0.75	1.00	1.25	1.50	1.75
0	7.609E-05	7.129E-05	6.533E-05	8.290E-05	3.866E-05	7.305E-05	9.582E-05
1/18	6.491E-05	8.737E-05	7.879E-05	4.983E-05	7.087E-05	8.877E-05	6.611E-05
1/9	7.999E-05	1.068E-04	9.765E-05	5.964E-05	2.793E-05	1.067E-04	5.254E-05
1/6	9.666E-05	8.604E-05	1.115E-04	3.517E-05	9.800E-05	9.057E-05	1.207E-04
2/9	5.518E-05	9.676E-05	8.964E-05	8.325E-05	1.095E-04	7.617E-05	1.095E-04
1/3	7.191E-05	6.299E-05	1.094E-04	1.058E-04	9.978E-05	1.486E-04	9.759E-05
2/3	2.800E-04	1.035E-04	8.303E-05	1.585E-04	2.163E-04	1.410E-04	1.345E-04
1	1.043E-04	8.407E-05	1.053E-04	3.053E-05	5.921E-05	5.743E-05	5.138E-05
10/9	7.971E-05	6.080E-05	7.724E-05	6.751E-05	6.173E-05	3.950E-05	5.909E-05
4/3	5.957E-05	4.016E-05	3.970E-05	3.493E-05	2.233E-05	2.011E-05	3.420E-05

GEOMETRY : VAC-RBM DSR=5/9 MASS THICKNESS = 12mg/cm^2

P\E(MeV)	0.35	0.50	0.75	1.00	1.25	1.50	1.75
0	2.534E-03	2.323E-03	2.004E-03	1.918E-03	1.920E-03	1.791E-03	1.729E-03
1/18	3.169E-03	3.002E-03	2.711E-03	2.518E-03	2.282E-03	2.246E-03	2.419E-03
1/9	3.813E-03	3.743E-03	3.154E-03	2.902E-03	2.768E-03	2.839E-03	2.721E-03
1/6	4.507E-03	4.066E-03	3.865E-03	3.401E-03	3.371E-03	3.149E-03	3.038E-03
2/9	5.337E-03	4.760E-03	4.299E-03	4.014E-03	3.750E-03	3.780E-03	3.472E-03
1/3	6.976E-03	6.383E-03	5.558E-03	5.211E-03	4.947E-03	5.064E-03	4.615E-03
2/3	1.406E-02	1.041E-02	8.769E-03	7.833E-03	7.312E-03	6.983E-03	6.900E-03
1	5.371E-03	4.296E-03	3.608E-03	3.205E-03	2.840E-03	2.754E-03	2.719E-03
10/9	4.080E-03	3.030E-03	2.422E-03	2.136E-03	2.142E-03	1.934E-03	1.842E-03
4/3	1.312E-03	8.068E-04	6.213E-04	5.451E-04	4.916E-04	4.724E-04	5.096E-04

CORRESPONDING ABSOLUTE UNCERTAINTIES

P\E(MeV)	0.35	0.50	0.75	1.00	1.25	1.50	1.75
0	1.014E-04	6.969E-05	8.016E-05	3.836E-05	7.679E-05	3.583E-05	6.916E-05
1/18	6.338E-05	9.006E-05	8.132E-05	5.035E-05	6.847E-05	4.492E-05	4.838E-05
1/9	7.627E-05	7.485E-05	3.154E-05	5.805E-05	5.536E-05	8.516E-05	5.442E-05
1/6	1.352E-04	1.220E-04	1.159E-04	6.803E-05	1.011E-04	6.297E-05	6.076E-05
2/9	1.067E-04	9.520E-05	1.720E-04	8.027E-05	1.125E-04	7.560E-05	6.944E-05
1/3	1.395E-04	2.553E-04	5.558E-05	1.563E-04	9.894E-05	1.013E-04	9.229E-05
2/3	1.406E-04	2.082E-04	1.754E-04	1.567E-04	1.462E-04	1.397E-04	6.900E-05
1	1.611E-04	8.592E-05	1.082E-04	9.615E-05	5.680E-05	5.509E-05	5.438E-05
10/9	1.224E-04	1.212E-04	7.266E-05	1.068E-04	6.425E-05	5.803E-05	7.369E-05
4/3	5.249E-05	7.261E-05	4.970E-05	2.725E-05	1.966E-05	2.362E-05	3.567E-05

GEOMETRY : RBM-RBM DSR=2/3 MASS THICKNESS = 12mg/cm^2

P\E(MeV)	0.35	0.50	0.75	1.00	1.25	1.50	1.75
0	1.205E-03	1.069E-03	1.087E-03	9.761E-04	1.049E-03	1.026E-03	1.075E-03
1/18	1.957E-03	1.723E-03	1.685E-03	1.528E-03	1.540E-03	1.430E-03	1.432E-03
1/9	2.479E-03	2.343E-03	2.128E-03	1.977E-03	1.918E-03	1.900E-03	1.756E-03
1/6	3.044E-03	2.975E-03	2.601E-03	2.497E-03	2.313E-03	2.326E-03	2.233E-03
2/9	3.953E-03	3.569E-03	3.235E-03	2.921E-03	2.834E-03	2.723E-03	2.711E-03
1/3	5.416E-03	4.867E-03	4.372E-03	4.016E-03	3.776E-03	3.527E-03	3.566E-03
2/3	1.414E-02	1.367E-02	1.396E-02	1.390E-02	1.404E-02	1.403E-02	1.467E-02
1	7.072E-03	5.620E-03	4.688E-03	4.129E-03	3.859E-03	3.927E-03	3.481E-03
10/9	5.468E-03	4.411E-03	3.670E-03	3.132E-03	2.916E-03	2.925E-03	2.711E-03
4/3	2.530E-03	1.899E-03	1.390E-03	1.355E-03	1.201E-03	1.060E-03	1.121E-03

CORRESPONDING ABSOLUTE UNCERTAINTIES

P\E(MeV)	0.35	0.50	0.75	1.00	1.25	1.50	1.75
0	4.819E-05	5.344E-05	6.520E-05	2.928E-05	3.146E-05	4.102E-05	0.00004299
1/18	7.828E-05	6.893E-05	6.740E-05	3.056E-05	6.161E-05	4.290E-05	0.00005726
1/9	9.915E-05	7.028E-05	8.511E-05	7.908E-05	5.755E-05	5.701E-05	0.00003512
1/6	9.131E-05	8.924E-05	1.041E-04	9.988E-05	6.940E-05	6.977E-05	0.00006699
2/9	1.186E-04	7.138E-05	9.706E-05	5.842E-05	8.501E-05	8.169E-05	0.00008133
1/3	1.625E-04	9.733E-05	1.312E-04	8.032E-05	1.133E-04	1.058E-04	0.00010698
2/3	1.414E-04	2.734E-04	1.396E-04	1.390E-04	2.808E-04	2.805E-04	0.00014668
1	1.414E-04	1.686E-04	1.406E-04	1.239E-04	7.718E-05	7.854E-05	0.00006962
10/9	1.640E-04	8.822E-05	7.340E-05	1.253E-04	1.166E-04	8.776E-05	0.00005421
4/3	7.589E-05	5.696E-05	4.171E-05	8.128E-05	4.802E-05	7.417E-05	0.00004482

GEOMETRY : CB-RBM DSR=2/3 MASS THICKNESS = 12mg/cm^2

P\E(MeV)	0.35	0.50	0.75	1.00	1.25	1.50	1.75
0	1.094E-03	1.071E-03	1.226E-03	1.077E-03	1.138E-03	1.078E-03	1.057E-03
1/18	1.802E-03	1.660E-03	1.568E-03	1.513E-03	1.454E-03	1.375E-03	1.351E-03
1/9	2.594E-03	2.355E-03	2.056E-03	2.030E-03	1.886E-03	1.768E-03	1.802E-03
1/6	3.279E-03	2.758E-03	2.681E-03	2.523E-03	2.173E-03	2.223E-03	2.226E-03
2/9	3.918E-03	3.727E-03	3.285E-03	2.944E-03	2.925E-03	2.810E-03	2.566E-03
1/3	5.360E-03	4.765E-03	4.294E-03	3.946E-03	3.778E-03	3.657E-03	3.692E-03
2/3	1.398E-02	1.362E-02	1.354E-02	1.372E-02	1.416E-02	1.409E-02	1.460E-02
1	7.022E-03	5.510E-03	4.817E-03	4.083E-03	4.071E-03	3.807E-03	3.816E-03
10/9	5.419E-03	4.306E-03	3.622E-03	3.183E-03	2.919E-03	2.706E-03	2.825E-03
4/3	2.407E-03	1.743E-03	1.398E-03	1.300E-03	1.225E-03	1.133E-03	1.144E-03

CORRESPONDING ABSOLUTE UNCERTAINTIES

P\E(MeV)	0.35	0.50	0.75	1.00	1.25	1.50	1.75
0	3.281E-05	5.355E-05	6.132E-05	5.384E-05	3.413E-05	5.390E-05	5.285E-05
1/18	5.407E-05	8.300E-05	6.270E-05	4.538E-05	2.908E-05	5.498E-05	8.107E-05
1/9	7.783E-05	7.064E-05	6.169E-05	8.121E-05	5.657E-05	7.072E-05	7.206E-05
1/6	9.837E-05	8.274E-05	1.072E-04	7.570E-05	6.518E-05	6.670E-05	6.677E-05
2/9	7.836E-05	7.453E-05	6.571E-05	8.832E-05	8.776E-05	5.620E-05	7.699E-05
1/3	1.608E-04	9.530E-05	8.588E-05	7.891E-05	3.778E-05	1.097E-04	7.383E-05
2/3	1.398E-04	1.362E-04	1.354E-04	1.372E-04	1.416E-04	2.817E-04	1.459E-04
1	7.022E-05	1.102E-04	9.634E-05	4.083E-05	8.142E-05	1.142E-04	1.145E-04
10/9	1.084E-04	1.292E-04	7.244E-05	6.366E-05	5.837E-05	1.083E-04	5.650E-05
4/3	9.627E-05	5.228E-05	5.593E-05	3.899E-05	4.898E-05	4.532E-05	5.722E-05

GEOMETRY : VAC-RBM DSR=2/3 MASS THICKNESS = 12mg/cm^2

P\E(MeV)	0.35	0.50	0.75	1.00	1.25	1.50	1.75
0	1.220E-03	1.129E-03	1.101E-03	1.122E-03	1.097E-03	1.033E-03	9.545E-04
1/18	1.761E-03	1.751E-03	1.520E-03	1.553E-03	1.487E-03	1.402E-03	1.382E-03
1/9	2.438E-03	2.315E-03	2.097E-03	1.995E-03	2.006E-03	1.925E-03	1.674E-03
1/6	3.034E-03	2.851E-03	2.735E-03	2.400E-03	2.394E-03	2.319E-03	2.098E-03
2/9	3.902E-03	3.758E-03	3.131E-03	3.128E-03	2.815E-03	2.661E-03	2.506E-03
1/3	5.412E-03	4.889E-03	4.350E-03	3.996E-03	3.891E-03	3.692E-03	3.583E-03
2/3	1.443E-02	1.371E-02	1.341E-02	1.390E-02	1.407E-02	1.427E-02	1.439E-02
1	6.976E-03	5.608E-03	4.821E-03	4.227E-03	4.078E-03	3.826E-03	3.759E-03
10/9	5.497E-03	4.353E-03	3.507E-03	3.105E-03	2.936E-03	2.785E-03	2.744E-03
4/3	2.546E-03	1.827E-03	2.511E-03	1.357E-03	1.238E-03	1.188E-03	1.068E-03

CORRESPONDING ABSOLUTE UNCERTAINTIES

P\E(MeV)	0.35	0.50	0.75	1.00	1.25	1.50	1.75
0	4.880E-05	4.514E-05	5.503E-05	6.732E-05	5.484E-05	3.099E-05	1.909E [illegible]
1/18	7.045E-05	5.252E-05	7.598E-05	7.766E-05	4.460E-05	4.207E-05	4.145E-05
1/9	7.315E-05	6.946E-05	6.291E-05	5.984E-05	4.011E-05	5.775E-05	8.368E-05
1/6	9.102E-05	8.552E-05	1.094E-04	7.201E-05	7.182E-05	6.956E-05	4.196E-05
2/9	7.804E-05	1.127E-04	9.394E-05	3.128E-05	8.446E-05	7.984E-05	5.013E-05
1/3	1.082E-04	1.467E-04	8.699E-05	1.199E-04	1.556E-04	7.384E-05	1.075E-04
2/3	1.443E-04	2.741E-04	2.681E-04	2.780E-04	2.813E-04	2.854E-04	1.439E-04
1	1.395E-04	1.682E-04	9.642E-05	8.454E-05	8.155E-05	1.148E-04	7.519E-05
10/9	1.099E-04	1.741E-04	1.403E-04	9.314E-05	8.807E-05	5.571E-05	8.231E-05
4/3	1.018E-04	1.461E-04	1.256E-04	6.785E-05	7.427E-05	4.753E-05	6.405E-05

GEOMETRY : RBM-RBM   DSR=7/9   MASS THICKNESS = 12mg/cm^2

P\E(MeV)	0.35	0.50	0.75	1.00	1.25	1.50	1.75
0	3.618E-04	3.618E-04	4.398E-04	3.200E-04	3.550E-04	4.185E-04	3.999E-04
1/18	7.306E-04	6.550E-04	7.364E-04	6.717E-04	7.146E-04	6.922E-04	6.541E-04
1/9	1.217E-03	1.191E-03	1.100E-03	1.038E-03	1.058E-03	1.046E-03	1.021E-03
1/6	1.830E-03	1.778E-03	1.562E-03	1.591E-03	1.474E-03	1.475E-03	1.506E-03
2/9	2.390E-03	2.346E-03	2.124E-03	1.997E-03	1.918E-03	1.907E-03	1.905E-03
1/3	3.959E-03	3.805E-03	3.244E-03	2.855E-03	2.961E-03	2.598E-03	2.599E-03
2/3	9.214E-03	8.458E-03	7.800E-03	7.005E-03	6.857E-03	6.634E-03	6.504E-03
1	8.995E-03	7.577E-03	6.075E-03	5.529E-03	5.301E-03	5.205E-03	4.815E-03
10/9	6.954E-03	5.991E-03	4.732E-03	4.243E-03	3.950E-03	3.810E-03	3.601E-03
4/3	3.916E-03	2.974E-03	2.393E-03	2.257E-03	2.072E-03	2.041E-03	1.930E-03

CORRESPONDING ABSOLUTE UNCERTAINTIES

P\E(MeV)	0.35	0.50	0.75	1.00	1.25	1.50	1.75
0	3.980E-05	3.256E-05	3.958E-05	1.920E-05	2.840E-05	2.511E-05	2.799E-05
1/18	3.653E-05	3.275E-05	4.418E-05	2.687E-05	4.288E-05	4.153E-05	2.616E-05
1/9	4.867E-05	5.952E-05	6.598E-05	5.189E-05	3.175E-05	5.229E-05	8.170E-05
1/6	9.152E-05	7.110E-05	6.247E-05	7.954E-05	7.372E-05	4.425E-05	4.519E-05
2/9	7.169E-05	4.692E-05	6.371E-05	7.988E-05	5.754E-05	5.722E-05	5.716E-05
1/3	1.188E-04	7.609E-05	9.733E-05	8.564E-05	8.884E-05	7.795E-05	5.197E-05
2/3	1.843E-04	1.692E-04	1.560E-04	1.401E-04	1.371E-04	1.327E-04	1.301E-04
1	1.799E-04	7.577E-05	1.822E-04	1.106E-04	1.060E-04	1.041E-04	9.629E-05
10/9	2.086E-04	1.198E-04	9.463E-05	8.485E-05	7.899E-05	1.143E-04	1.080E-04
4/3	7.832E-05	8.922E-05	7.178E-05	6.772E-05	6.214E-05	6.122E-05	7.720E-05

GEOMETRY : CB-RBM DSR=7/9 MASS THICKNESS = 12mg/cm^2

P/E(MeV)	0.35	0.50	0.75	1.00	1.25	1.50	1.75
0	3.402E-04	4.082E-04	4.527E-04	3.343E-04	3.869E-04	3.732E-04	3.986E-06
1/18	6.405E-04	7.499E-04	6.566E-04	6.689E-04	6.295E-04	6.919E-04	6.751E-04
1/9	1.189E-03	1.225E-03	1.251E-03	1.105E-03	1.061E-03	1.070E-03	1.022E-03
1/6	1.835E-03	1.711E-03	1.551E-03	1.425E-03	1.324E-03	1.510E-03	1.370E-03
2/9	2.518E-03	2.360E-03	2.075E-03	2.055E-03	1.970E-03	1.787E-03	1.842E-03
1/3	3.823E-03	3.685E-03	3.233E-03	2.973E-03	2.762E-03	2.803E-03	2.596E-03
2/3	9.189E-03	7.947E-03	7.718E-03	7.031E-03	7.154E-03	6.615E-03	6.717E-03
1	9.154E-03	7.469E-03	6.244E-03	5.729E-03	5.166E-03	5.013E-03	4.751E-03
10/9	7.070E-03	5.458E-03	4.806E-03	4.081E-03	3.679E-03	3.782E-03	3.640E-03
4/3	3.795E-03	3.132E-03	2.414E-03	2.156E-03	1.977E-03	1.972E-03	2.013E-03

CORRESPONDING ABSOLUTE UNCERTAINTIES

P\E(MeV)	0.35	0.50	0.75	1.00	1.25	1.50	1.75
0	3.062E-05	2.449E-05	3.621E-05	3.009E-05	2.708E-05	4.105E-05	1.594E-07
1/18	3.843E-05	3.750E-05	3.939E-05	4.013E-05	3.147E-05	2.076E-05	4.050E-05
1/9	4.758E-05	8.572E-05	7.507E-05	5.524E-05	4.243E-05	6.420E-05	5.111E-05
1/6	5.505E-05	3.422E-05	4.653E-05	5.700E-05	6.618E-05	6.040E-05	5.480E-05
2/9	7.554E-05	9.440E-05	6.226E-05	6.164E-05	7.880E-05	7.149E-05	7.367E-05
1/3	1.529E-04	1.105E-04	9.698E-05	8.919E-05	8.286E-05	8.408E-05	7.788E-05
2/3	9.189E-05	2.384E-04	2.315E-04	1.406E-04	1.431E-04	1.323E-04	1.343E-04
1	9.154E-05	1.494E-04	1.249E-04	5.729E-05	1.033E-04	1.003E-04	9.502E-05
10/9	1.414E-04	1.092E-04	4.806E-05	8.162E-05	1.104E-04	3.782E-05	7.280E-05
4/3	7.590E-05	9.396E-05	7.241E-05	6.469E-05	5.931E-05	5.917E-05	6.038E-05

GEOMETRY : VAC-RBM   DSR=7/9   MASS THICKNESS = 12mg/cm^2

P\E(MeV)	0.35	0.50	0.75	1.00	1.25	1.50	1.75
0	3.793E-04	3.723E-04	3.612E-04	3.832E-04	4.168E-04	4.319E-04	3.771E-04
1/18	6.618E-04	7.270E-04	6.466E-04	7.188E-04	6.985E-04	6.865E-04	6.874E-04
1/9	1.189E-03	1.245E-03	1.147E-03	1.063E-03	1.062E-03	1.083E-03	9.816E-04
1/6	1.744E-03	1.765E-03	1.617E-03	1.499E-03	1.595E-03	1.365E-03	1.383E-03
2/9	2.390E-03	2.342E-03	2.005E-03	1.992E-03	1.907E-03	1.748E-03	1.765E-03
1/3	3.798E-03	3.544E-03	2.924E-03	2.919E-03	2.878E-03	2.823E-03	2.599E-03
2/3	9.206E-03	8.504E-03	7.162E-03	7.211E-03	6.724E-03	6.707E-03	6.667E-03
1	9.082E-03	7.314E-03	6.448E-03	5.930E-03	5.373E-03	4.787E-03	5.020E-03
10/9	6.876E-03	5.693E-03	4.748E-03	4.095E-03	3.859E-03	3.790E-03	3.658E-03
4/3	3.879E-03	3.124E-03	2.480E-03	2.291E-03	2.107E-03	1.944E-03	1.817E-03

CORRESPONDING ABSOLUTE UNCERTAINTIES

P\E(MeV)	0.35	0.50	0.75	1.00	1.25	1.50	1.75
0	2.276E-05	3.351E-05	3.251E-05	3.832E-05	3.335E-05	3.023E-05	2.639E-05
1/18	2.647E-05	4.362E-05	1.940E-05	2.875E-05	3.493E-05	4.119E-05	4.125E-05
1/9	5.945E-05	4.980E-05	2.293E-05	4.253E-05	5.311E-05	5.414E-05	3.926E-05
1/6	8.722E-05	7.060E-05	6.469E-05	7.495E-05	4.784E-05	4.096E-05	5.530E-05
2/9	9.560E-05	4.685E-05	8.018E-05	5.975E-05	3.814E-05	6.992E-05	8.823E-05
1/3	3.798E-05	7.087E-05	8.773E-05	8.756E-05	5.756E-05	5.645E-05	7.797E-05
2/3	1.841E-04	1.701E-04	1.432E-04	1.442E-04	6.724E-05	1.341E-04	1.333E-04
1	9.082E-05	1.463E-04	6.448E-05	1.186E-04	5.373E-05	9.574E-05	1.004E-04
10/9	2.063E-04	1.139E-04	9.497E-05	8.189E-05	7.717E-05	7.579E-05	7.316E-05
4/3	7.759E-05	9.373E-05	9.918E-05	6.872E-05	4.214E-05	7.777E-05	7.268E-05

GEOMETRY : RBM-RBM DSR=8/9 MASS THICKNESS = 12mg/cm^2

P\E(MeV)	0.35	0.50	0.75	1.00	1.25	1.50	1.75
0	3.662E-05	7.824E-05	5.445E-05	6.943E-05	7.159E-05	3.637E-05	8.008E-05
1/18	1.676E-04	1.447E-04	1.858E-04	2.112E-04	2.012E-04	2.188E-04	1.700E-04
1/9	3.940E-04	3.681E-04	3.971E-04	3.651E-04	3.544E-04	4.511E-04	3.724E-04
1/6	7.241E-04	7.469E-04	6.905E-04	6.892E-04	7.303E-04	7.312E-04	6.396E-04
2/9	1.159E-03	1.169E-03	1.201E-03	1.073E-03	9.778E-04	1.080E-03	1.056E-03
1/3	2.397E-03	2.430E-03	2.054E-03	1.965E-03	1.979E-03	1.857E-03	1.792E-03
2/3	7.301E-03	6.433E-03	5.861E-03	5.132E-03	4.791E-03	4.704E-03	4.632E-03
1	1.368E-02	1.022E-02	8.595E-03	7.616E-03	7.400E-03	6.926E-03	7.105E-03
10/9	9.179E-03	7.507E-03	6.229E-03	5.626E-03	5.183E-03	4.933E-03	4.989E-03
4/3	5.385E-03	4.393E-03	3.731E-03	3.209E-03	3.001E-03	2.872E-03	2.857E-03

CORRESPONDING ABSOLUTE UNCERTAINTIES

P\E(MeV)	0.35	0.50	0.75	1.00	1.25	1.50	1.75
0	6.226E-06	1.330E-05	7.078E-06	9.720E-06	1.145E-05	6.547E-06	9.610E-06
1/18	1.508E-05	1.591E-05	1.301E-05	2.323E-05	2.615E-05	1.969E-05	1.530E-05
1/9	3.152E-05	2.944E-05	3.574E-05	3.286E-05	1.418E-05	3.608E-05	1.862E-05
1/6	3.620E-05	4.482E-05	3.453E-05	2.757E-05	2.191E-05	5.119E-05	3.837E-05
2/9	4.637E-05	4.678E-05	6.004E-05	5.366E-05	5.867E-05	5.399E-05	6.337E-05
1/3	9.588E-05	7.291E-05	8.214E-05	5.894E-05	5.938E-05	7.429E-05	5.376E-05
2/3	1.460E-04	1.287E-04	1.172E-04	1.026E-04	9.582E-05	4.704E-05	1.390E-04
1	2.735E-04	1.022E-04	2.578E-04	7.616E-05	1.480E-04	1.385E-04	1.421E-04
10/9	9.179E-05	7.507E-05	1.246E-04	1.125E-04	1.037E-04	9.866E-05	9.977E-05
4/3	1.615E-04	1.318E-04	1.119E-04	1.284E-04	6.002E-05	5.744E-05	8.571E-05

GEOMETRY : CB-RBM DSR=8/9 MASS THICKNESS = 12mg/cm^2

P\E(MeV)	0.35	0.50	0.75	1.00	1.25	1.50	1.75
0	3.669E-05	4.854E-05	7.504E-05	5.424E-05	7.271E-05	6.162E-05	6.626E-05
1/18	1.574E-04	1.630E-04	1.207E-04	1.667E-04	2.075E-04	1.899E-04	1.588E-04
1/9	3.322E-04	3.931E-04	4.093E-04	4.049E-04	3.679E-04	4.241E-04	3.894E-04
1/6	7.229E-04	7.269E-04	6.807E-04	7.047E-04	6.052E-04	7.170E-04	6.918E-04
2/9	1.250E-03	1.215E-03	1.139E-03	1.066E-03	1.008E-03	1.060E-03	1.022E-03
1/3	2.384E-03	2.384E-03	2.134E-03	2.018E-03	1.953E-03	1.851E-03	1.897E-03
2/3	7.069E-03	6.328E-03	5.656E-03	4.985E-03	5.045E-03	4.906E-03	4.998E-03
1	1.399E-02	1.047E-02	8.532E-03	8.028E-03	7.371E-03	6.883E-03	6.861E-03
10/9	9.049E-03	7.174E-03	6.330E-03	5.597E-03	5.276E-03	4.950E-03	5.019E-03
4/3	5.327E-03	4.400E-03	3.516E-03	3.229E-03	2.954E-03	2.714E-03	2.800E-03

CORRESPONDING ABSOLUTE UNCERTAINTIES

P\E(MeV)	0.35	0.50	0.75	1.00	1.25	1.50	1.75
0	9.174E-06	8.738E-06	1.576E-05	9.763E-06	1.018E-05	1.232E-05	1.060E-05
1/18	2.046E-05	2.053E-05	2.053E-05	1.334E-05	2.282E-05	2.089E-05	2.859E-05
1/9	1.993E-05	3.145E-05	3.684E-05	2.025E-05	2.575E-05	2.969E-05	2.726E-05
1/6	2.892E-05	2.908E-05	4.084E-05	3.524E-05	3.026E-05	3.585E-05	3.459E-05
2/9	3.749E-05	3.645E-05	4.556E-05	3.199E-05	3.024E-05	5.300E-05	5.112E-05
1/3	9.537E-05	9.537E-05	8.536E-05	4.035E-05	5.859E-05	7.403E-05	5.692E-05
2/3	1.414E-04	1.266E-04	5.656E-05	9.969E-05	1.513E-04	9.811E-05	9.996E-05
1	1.399E-04	1.047E-04	1.706E-04	2.409E-04	1.474E-04	6.883E-05	6.861E-05
10/9	9.049E-05	1.435E-04	1.266E-04	5.597E-05	1.055E-04	9.900E-05	5.019E-05
4/3	1.065E-04	1.320E-04	7.032E-05	9.687E-05	8.863E-05	8.143E-05	8.399E-05

GEOMETRY : VAC-RBM DSR=8/9 MASS THICKNESS = 12mg/cm^2

P\E(MeV)	0.35	0.50	0.75	1.00	1.25	1.50	1.75
0	5.152E-05	6.217E-05	6.322E-05	7.065E-05	6.996E-05	6.029E-05	7.845E-05
1/18	1.514E-04	1.374E-04	2.076E-04	1.386E-04	1.597E-04	1.771E-04	1.981E-04
1/9	3.191E-04	4.731E-04	4.035E-04	3.497E-04	3.844E-04	3.602E-04	3.513E-04
1/6	6.736E-04	7.031E-04	7.306E-04	7.438E-04	6.778E-04	6.953E-04	6.429E-04
2/9	1.127E-03	1.114E-03	1.016E-03	1.144E-03	1.026E-03	9.896E-04	9.649E-04
1/3	2.514E-03	2.227E-03	1.984E-03	1.883E-03	1.932E-03	1.917E-03	1.782E-03
2/3	7.201E-03	6.265E-03	5.657E-03	5.223E-03	4.888E-03	4.792E-03	4.805E-03
1	1.379E-02	1.043E-02	8.679E-03	7.903E-03	7.418E-03	7.230E-03	6.820E-03
10/9	9.070E-03	7.415E-03	6.158E-03	5.438E-03	5.062E-03	5.005E-03	4.918E-03
4/3	5.378E-03	4.398E-03	3.630E-03	3.207E-03	3.000E-03	2.994E-03	2.719E-03

CORRESPONDING ABSOLUTE UNCERTAINTIES

P\E(MeV)	0.35	0.50	0.75	1.00	1.25	1.50	1.75
0	1.082E-05	1.554E-05	1.707E-05	1.272E-05	1.469E-05	9.044E-06	1.49[illegible]
1/18	1.666E-05	1.648E-05	1.868E-05	1.247E-05	1.118E-05	2.480E-05	1.783E-05
1/9	3.510E-05	4.731E-05	3.228E-05	2.448E-05	3.076E-05	3.242E-05	1.405E-05
1/6	4.042E-05	2.812E-05	5.114E-05	2.975E-05	4.067E-05	2.781E-05	4.501E-05
2/9	6.764E-05	5.568E-05	4.064E-05	4.576E-05	4.102E-05	3.958E-05	3.860E-05
1/3	7.541E-05	6.680E-05	9.920E-05	5.650E-05	7.726E-05	5.750E-05	8.909E-05
2/3	1.440E-04	1.253E-04	1.697E-04	1.045E-04	9.777E-05	1.438E-04	9.610E-05
1	1.379E-04	1.043E-04	1.736E-04	1.581E-04	1.484E-04	1.446E-04	1.364E-04
10/9	1.814E-04	1.483E-04	1.847E-04	1.631E-04	5.062E-05	1.001E-04	9.836E-05
4/3	1.076E-04	1.319E-04	7.260E-05	6.413E-05	6.000E-05	5.987E-05	8.157E-05

GEOMETRY : RBM-RBM DSR=1 MASS THICKNESS = 12mg/cm^2

P\E(MeV)	0.35	0.50	0.75	1.00	1.25	1.50	1.75
0	8.391E-09	1.132E-06	1.837E-06	7.377E-06	1.549E-06	2.572E-06	2.245E-06
1/18	1.024E-05	1.238E-05	2.894E-06	1.555E-05	7.881E-06	2.297E-05	1.216E-05
1/9	5.294E-05	3.625E-05	4.939E-05	7.703E-05	4.483E-05	6.109E-05	6.483E-05
1/6	1.438E-04	1.372E-04	1.440E-04	2.001E-04	2.194E-04	1.963E-04	1.700E-04
2/9	3.327E-04	3.532E-04	4.044E-04	3.480E-04	4.225E-04	4.211E-04	3.625E-04
1/3	1.198E-03	1.126E-03	1.043E-03	1.063E-03	9.830E-04	1.065E-03	1.022E-03
2/3	5.626E-03	4.975E-03	4.272E-03	3.945E-03	3.764E-03	3.550E-03	3.490E-03
1	1.421E-02	1.372E-02	1.356E-02	1.411E-02	1.388E-02	1.427E-02	1.466E-02
10/9	1.390E-02	1.071E-02	8.505E-03	7.627E-03	7.332E-03	6.937E-03	6.935E-03
4/3	7.113E-03	5.781E-03	4.757E-03	4.396E-03	4.027E-03	3.783E-03	3.880E-03

CORRESPONDING ABSOLUTE UNCERTAINTIES

P\E(MeV)	0.35	0.50	0.75	1.00	1.25	1.50	1.75
0	8.307E-09	8.374E-07	8.266E-07	3.836E-06	1.534E-06	1.852E-06	1.684E-06
1/18	4.200E-06	5.696E-06	1.707E-06	6.222E-06	2.443E-06	5.054E-06	4.133E-06
1/9	6.882E-06	6.888E-06	1.235E-05	1.695E-05	7.173E-06	1.955E-05	9.076E-06
1/6	1.150E-05	1.372E-05	1.728E-05	2.401E-05	1.974E-05	2.356E-05	2.210E-05
2/9	2.661E-05	2.119E-05	1.618E-05	2.088E-05	3.380E-05	4.632E-05	2.900E-05
1/3	4.794E-05	4.504E-05	4.174E-05	5.316E-05	3.932E-05	5.326E-05	4.087E-05
2/3	1.125E-04	9.950E-05	8.543E-05	1.184E-04	1.129E-04	1.065E-04	3.490E-05
1	2.842E-04	2.743E-04	2.711E-04	1.411E-04	2.776E-04	1.427E-04	4.397E-04
10/9	1.390E-04	2.142E-04	8.505E-05	1.525E-04	1.466E-04	1.387E-04	6.935E-05
4/3	2.134E-04	1.156E-04	9.514E-05	8.792E-05	1.208E-04	1.135E-04	1.164E-04

GEOMETRY : CB-RBM DSR=1 MASS THICKNESS = 12mg/cm^2

P\E(MeV)	0.35	0.50	0.75	1.00	1.25	1.50	1.75
0	1.503E-06	1.000E-07	4.343E-08	4.508E-07	2.442E-06	1.265E-06	8.750E-06
1/18	6.188E-06	5.797E-06	4.989E-06	4.529E-06	1.454E-05	1.903E-05	1.934E-05
1/9	6.211E-05	4.470E-05	8.035E-05	4.127E-05	4.619E-05	7.256E-05	7.988E-05
1/6	1.474E-04	1.523E-04	1.650E-04	1.851E-04	1.527E-04	1.920E-04	1.761E-04
2/9	3.405E-04	3.333E-04	4.200E-04	4.173E-04	3.563E-04	4.199E-04	3.811E-04
1/3	1.025E-03	1.233E-03	1.086E-03	1.085E-03	9.970E-04	9.996E-04	9.651E-04
2/3	5.438E-03	4.764E-03	4.184E-03	3.826E-03	3.875E-03	3.638E-03	3.722E-03
1	1.368E-02	1.375E-02	1.368E-02	1.415E-02	1.359E-02	1.442E-02	1.448E-02
10/9	1.381E-02	1.028E-02	8.725E-03	7.665E-03	7.496E-03	6.908E-03	6.808E-03
4/3	6.973E-03	5.843E-03	4.742E-03	4.467E-03	4.162E-03	3.635E-03	3.679E-03

CORRESPONDING ABSOLUTE UNCERTAINTIES

P\E(MeV)	0.35	0.50	0.75	1.00	1.25	1.50	1.75
0	7.965E-07	9.900E-08	4.300E-08	4.463E-07	2.174E-06	8.854E-07	5.688E-0[illegible]
1/18	2.475E-06	4.116E-06	4.490E-06	3.850E-06	5.234E-06	5.898E-06	6.190E-06
1/9	9.316E-06	1.028E-05	1.205E-05	7.429E-06	9.699E-06	1.306E-05	1.598E-05
1/6	1.474E-05	1.371E-05	2.310E-05	3.147E-05	1.527E-05	1.152E-05	1.056E-05
2/9	2.043E-05	2.666E-05	3.360E-05	4.173E-05	3.206E-05	3.359E-05	2.287E-05
1/3	4.098E-05	6.167E-05	3.259E-05	5.426E-05	6.979E-05	5.997E-05	5.790E-05
2/3	1.088E-04	1.429E-04	8.367E-05	7.652E-05	7.749E-05	7.276E-05	7.443E-05
1	1.367E-04	2.749E-04	2.736E-04	1.415E-04	2.717E-04	1.442E-04	1.448E-04
10/9	1.381E-04	1.028E-04	1.745E-04	1.533E-04	1.499E-04	1.382E-04	1.362E-04
4/3	1.395E-04	1.169E-04	1.423E-04	1.340E-04	8.324E-05	7.270E-05	1.104E-04

GEOMETRY : VAC-RBM DSR=1 MASS THICKNESS = 12mg/cm^2

P\E(MeV)	0.35	0.50	0.75	1.00	1.25	1.50	1.75
0	1.000E-07	3.171E-06	2.850E-06	2.234E-07	2.522E-06	1.961E-06	1.631E-06
1/18	1.082E-05	1.190E-05	1.027E-05	1.527E-05	1.412E-05	9.411E-06	1.456E-05
1/9	4.117E-05	8.223E-05	5.345E-05	5.029E-05	6.069E-05	4.943E-05	5.720E-05
1/6	1.521E-04	1.902E-04	2.058E-04	1.590E-04	1.629E-04	1.827E-04	2.101E-04
2/9	3.567E-04	3.517E-04	4.120E-04	4.113E-04	4.329E-04	4.163E-04	3.440E-04
1/3	1.285E-03	1.105E-03	1.158E-03	1.181E-03	1.033E-03	1.048E-03	1.027E-03
2/3	5.557E-03	4.601E-03	4.404E-03	3.892E-03	3.777E-03	3.837E-03	3.589E-03
1	1.386E-02	1.376E-02	1.343E-02	1.385E-02	1.391E-02	1.407E-02	1.449E-02
10/9	1.365E-02	1.026E-02	8.611E-03	7.592E-03	7.202E-03	6.796E-03	6.658E-03
4/3	6.875E-03	5.749E-03	4.837E-03	4.251E-03	4.061E-03	3.855E-03	3.658E-03

CORRESPONDING ABSOLUTE UNCERTAINTIES

P\E(MeV)	0.35	0.50	0.75	1.00	1.25	1.50	1.75
0	9.900E-08	3.139E-06	1.909E-06	2.212E-07	2.497E-06	1.941E-06	9.947E-[illegible]
1/18	5.412E-06	3.927E-06	4.314E-06	4.580E-06	6.211E-06	3.482E-06	4.515E-0[illegible]
1/9	7.410E-06	1.645E-05	1.015E-05	1.106E-05	9.710E-06	1.285E-05	1.087E-0[illegible]
1/6	2.129E-05	1.902E-05	2.469E-05	1.908E-05	2.280E-05	1.827E-05	2.101E-05
2/9	2.497E-05	3.869E-05	2.884E-05	2.056E-05	3.463E-05	2.498E-05	3.440E-05
1/3	5.139E-05	6.628E-05	5.788E-05	2.362E-05	4.131E-05	3.145E-05	6.163E-05
2/3	1.111E-04	9.202E-05	1.321E-04	7.784E-05	7.553E-05	7.674E-05	1.077E-04
1	2.773E-04	2.753E-04	2.686E-04	2.770E-04	1.391E-04	4.221E-04	1.449E-04
10/9	2.730E-04	2.052E-04	1.722E-04	1.518E-04	1.440E-04	1.359E-04	1.332E-04
4/3	1.375E-04	1.150E-04	1.451E-04	8.503E-05	8.121E-05	7.710E-05	1.097E-04

APPENDIX B

```
      PROGRAM POLY6
      DOUBLE PRECISION A(7,7),Y(7),C(7),DET(2)
      DOUBLE PRECISION WORK(7),SUM(20)
      DIMENSION IPVT(7)
      REAL X(10),Z(10),UNC(10),STD,UL,TOTAL
      DOUBLE PRECISION P(10),DOSE(10),ERR(10)
      DOUBLE PRECISION VAL(10),D(7),E
      CHARACTER IN*15,OUT*15
      PRINT*,'INPUT FILE?'
      READ*,IN
      PRINT*,'OUTPUT FILE?'
      READ*,OUT
      OPEN(UNIT=1,FILE=IN)
      OPEN(UNIT=2,FILE='B:\111\'//OUT)
      DO 5 I=1,20
      SUM(I)=0.0D0
5     CONTINUE
      WRITE(2,*) 'THE INPUT FILE : ',IN
      WRITE(2,*) ' '
      WRITE(2,*) 'THE DATA POINTS :'
      WRITE(2,*) '          X            Y
     +     UNCERTAINTY'
      DO 10 I=1,10
        READ(1,*) X(I),Z(I),UNC(I)
        WRITE(2,*) X(I),Z(I),UNC(I)
        P(I)=DBLE(X(I))
        DOSE(I)=DBLE(Z(I))
        ERR(I)=DBLE(UNC(I))
10    CONTINUE
      DO 15 I=1,10
        SUM(1)=SUM(1)+1.0/ERR(I)**2
        SUM(2)=SUM(2)+P(I)/ERR(I)**2
        SUM(3)=SUM(3)+P(I)**2/ERR(I)**2
        SUM(4)=SUM(4)+P(I)**3/ERR(I)**2
        SUM(5)=SUM(5)+P(I)**4/ERR(I)**2
        SUM(6)=SUM(6)+P(I)**5/ERR(I)**2
        SUM(7)=SUM(7)+P(I)**6/ERR(I)**2
        SUM(8)=SUM(8)+P(I)**7/ERR(I)**2
        SUM(9)=SUM(9)+P(I)**8/ERR(I)**2
        SUM(10)=SUM(10)+P(I)**9/ERR(I)**2
        SUM(11)=SUM(11)+P(I)**10/ERR(I)**2
        SUM(12)=SUM(12)+P(I)**11/ERR(I)**2
        SUM(13)=SUM(13)+P(I)**12/ERR(I)**2
        SUM(14)=SUM(14)+DOSE(I)/ERR(I)**2
        SUM(15)=SUM(15)+DOSE(I)*P(I)/ERR(I)**2
        SUM(16)=SUM(16)+DOSE(I)*P(I)**2/ERR(I)**2
        SUM(17)=SUM(17)+DOSE(I)*P(I)**3/ERR(I)**2
        SUM(18)=SUM(18)+DOSE(I)*P(I)**4/ERR(I)**2
        SUM(19)=SUM(19)+DOSE(I)*P(I)**5/ERR(I)**2
        SUM(20)=SUM(20)+DOSE(I)*P(I)**6/ERR(I)**2
15    CONTINUE
```

```
      DO 20 I=1,7
        DO 30 J=1,7
          A(I,J)=SUM(I+J-1)
30      CONTINUE
20    CONTINUE
      DO 40 I=1,7
        Y(I)=SUM(I+13)
40    CONTINUE
      N=7
      LD=N
      CALL DGEFA(A,LD,N,IPVT,INFO)
      JOB=11
      CALL DGEDI(A,LD,N,IPVT,DET,WORK,JOB)
      DO 50 I=1,7
        C(I)=0.0D0
        DO 60 J=1,7
          C(I)=C(I)+A(I,J)*Y(J)
60      CONTINUE
50    CONTINUE
      WRITE(2,*) ' '
      WRITE(2,*) '          X          CALCULATED Y
     +            % ERROR '
      WRITE(2,*) ' '
      STD=0.0
      DO 70 I=1,10
        VAL(I)=C(1)+C(2)*P(I)+C(3)*P(I)**2+C(4)*P(I)**3
     + +C(5)*P(I)**4+C(6)*P(I)**5+C(7)*P(I)**6
        WRITE(2,*) SNGL(P(I)),SNGL(VAL(I)),
     +  SNGL(ABS((Z(I)-VAL(I))*100/Z(I)))
       STD=STD+((Z(I)-VAL(I))**2)/3.0
70    CONTINUE
      WRITE(2,*) ' '
      WRITE(2,*) 'COEFFICIENTS AND THEIR UNCERTAINTY :'
      WRITE(2,*) ' '
      DO 55 I=1,7
       WRITE(2,*) SNGL(C(I)),'+/-',SNGL(SQRT(A(I,I)))
55    CONTINUE
      WRITE(2,*) ' '
      WRITE(2,*) 'VARIANCE OF THE FITTED CURVE :',STD
      UL=4/(3.0)
      TOTAL=C(1)*UL+(C(2)*UL**2)/2+(C(3)*UL**3)/3+
     +  (C(4)*UL**4)/4+(C(5)*UL**5)/5+(C(6)*UL**6)/6+
     +  (C(7)*UL**7)/7
      E=0.0D0
      DO 75 I=1,7
        D(I)=(UL**I)/REAL(I)
75    CONTINUE
      DO 80 I=1,7
        DO 85 J=1,7
          E=E+D(I)*A(I,J)*D(J)
85      CONTINUE
80    CONTINUE
```

```
      E=SQRT(E)
      WRITE(2,*) ' '
      WRITE(2,*) 'TOTAL DOSE : ',TOTAL,'+/-',SNGL(E)
      PRINT*,TOTAL
      WRITE(2,*) ' '
      PRINT*, ' '
      WRITE(2,*) '% ERROR : ',(SNGL(E)/TOTAL)*100
      PRINT*,(SNGL(E)/TOTAL)*100
      CLOSE(UNIT=1)
      CLOSE(UNIT=2)
      END


      SUBROUTINE DGEFA(A,LDA,N,IPVT,INFO)
      INTEGER LDA,N,IPVT(N),INFO
      DOUBLE PRECISION A(LDA,N)
      DOUBLE PRECISION T
      INTEGER IDAMAX,J,K,KP1,L,NM1
      INFO = 0
      NM1 = N - 1
      IF (NM1 .LT. 1) GO TO 70
      DO 60 K = 1, NM1
         KP1 = K + 1
         L = IDAMAX(N-K+1,A(K,K),1) + K - 1
         IPVT(K) = L
         IF (A(L,K) .EQ. 0.0D0) GO TO 40
            IF (L .EQ. K) GO TO 10
               T = A(L,K)
               A(L,K) = A(K,K)
               A(K,K) = T
   10       CONTINUE
            T = -1.0D0/A(K,K)
            CALL DSCAL(N-K,T,A(K+1,K),1)
            DO 30 J = KP1, N
               T = A(L,J)
               IF (L .EQ. K) GO TO 20
                  A(L,J) = A(K,J)
                  A(K,J) = T
   20          CONTINUE
               CALL DAXPY(N-K,T,A(K+1,K),1,A(K+1,J),1)
   30       CONTINUE
         GO TO 50
   40    CONTINUE
            INFO = K
   50    CONTINUE
   60 CONTINUE
   70 CONTINUE
      IPVT(N) = N
      IF (A(N,N) .EQ. 0.0D0) INFO = N
      RETURN
      END
```

```
      SUBROUTINE DGEDI(A,LDA,N,IPVT,DET,WORK,JOB)
      INTEGER LDA,N,IPVT(N),JOB
      DOUBLE PRECISION A(LDA,N),DET(2),WORK(N)
      DOUBLE PRECISION T
      DOUBLE PRECISION TEN
      INTEGER I,J,K,KB,KP1,L,NM1
      IF (JOB/10 .EQ. 0) GO TO 70
         DET(1) = 1.0D0
         DET(2) = 0.0D0
         TEN = 10.0D0
         DO 50 I = 1, N
            IF (IPVT(I) .NE. I) DET(1) = -DET(1)
            DET(1) = A(I,I)*DET(1)
            IF (DET(1) .EQ. 0.0D0) GO TO 60
   10       IF (DABS(DET(1)) .GE. 1.0D0) GO TO 20
               DET(1) = TEN*DET(1)
               DET(2) = DET(2) - 1.0D0
            GO TO 10
   20       CONTINUE
   30       IF (DABS(DET(1)) .LT. TEN) GO TO 40
               DET(1) = DET(1)/TEN
               DET(2) = DET(2) + 1.0D0
            GO TO 30
   40       CONTINUE
   50    CONTINUE
   60    CONTINUE
   70 CONTINUE
      IF (MOD(JOB,10) .EQ. 0) GO TO 150
         DO 100 K = 1, N
            A(K,K) = 1.0D0/A(K,K)
            T = -A(K,K)
            CALL DSCAL(K-1,T,A(1,K),1)
            KP1 = K + 1
            IF (N .LT. KP1) GO TO 90
            DO 80 J = KP1, N
               T = A(K,J)
               A(K,J) = 0.0D0
               CALL DAXPY(K,T,A(1,K),1,A(1,J),1)
   80       CONTINUE
   90       CONTINUE
  100    CONTINUE
         NM1 = N - 1
         IF (NM1 .LT. 1) GO TO 140
         DO 130 KB = 1, NM1
            K = N - KB
            KP1 = K + 1
            DO 110 I = KP1, N
               WORK(I) = A(I,K)
               A(I,K) = 0.0D0
  110       CONTINUE
```

```
         DO 120 J = KP1, N
            T = WORK(J)
            CALL DAXPY(N,T,A(1,J),1,A(1,K),1)
120      CONTINUE
         L = IPVT(K)
         IF (L .NE. K) CALL DSWAP(N,A(1,K),1,A(1,L),1)
130   CONTINUE
140   CONTINUE
150 CONTINUE
    RETURN
    END


    SUBROUTINE DAXPY(N,DA,DX,INCX,DY,INCY)
    DOUBLE PRECISION DX(1),DY(1),DA
    INTEGER I,INCX,INCY,IXIY,M,MP1,N
    IF(N.LE.0)RETURN
    IF (DA .EQ. 0.0D0) RETURN
    IF(INCX.EQ.1.AND.INCY.EQ.1)GO TO 20
    IX = 1
    IY = 1
    IF(INCX.LT.0)IX = (-N+1)*INCX + 1
    IF(INCY.LT.0)IY = (-N+1)*INCY + 1
    DO 10 I = 1,N
      DY(IY) = DY(IY) + DA*DX(IX)
      IX = IX + INCX
      IY = IY + INCY
 10 CONTINUE
    RETURN
      20 M = MOD(N,4)
         IF( M .EQ. 0 ) GO TO 40
         DO 30 I = 1,M
           DY(I) = DY(I) + DA*DX(I)
      30 CONTINUE
         IF( N .LT. 4 ) RETURN
      40 MP1 = M + 1
         DO 50 I = MP1,N,4
           DY(I) = DY(I) + DA*DX(I)
           DY(I + 1) = DY(I + 1) + DA*DX(I + 1)
           DY(I + 2) = DY(I + 2) + DA*DX(I + 2)
           DY(I + 3) = DY(I + 3) + DA*DX(I + 3)
50 CONTINUE
   RETURN
   END


   DOUBLE PRECISION FUNCTION DDOT(N,DX,INCX,DY,INCY)
   DOUBLE PRECISION DX(1),DY(1),DTEMP
   INTEGER I,INCX,INCY,IX,IY,M,MP1,N
   DDOT = 0.0D0
   DTEMP = 0.0D0
```

```
      IF(N.LE.0)RETURN
      IF(INCX.EQ.1.AND.INCY.EQ.1)GO TO 20
      IX = 1
      IY = 1
      IF(INCX.LT.0)IX = (-N+1)*INCX + 1
      IF(INCY.LT.0)IY = (-N+1)*INCY + 1
      DO 10 I = 1,N
        DTEMP = DTEMP + DX(IX)*DY(IY)
        IX = IX + INCX
        IY = IY + INCY
   10 CONTINUE
      DDOT = DTEMP
      RETURN
   20 M = MOD(N,5)
      IF( M .EQ. 0 ) GO TO 40
      DO 30 I = 1,M
        DTEMP = DTEMP + DX(I)*DY(I)
   30 CONTINUE
      IF( N .LT. 5 ) GO TO 60
   40 MP1 = M + 1
      DO 50 I = MP1,N,5
        DTEMP = DTEMP + DX(I)*DY(I) + DX(I+1)*DY(I+1) +
     *   DX(I+2)*DY(I+2) + DX(I+3)*DY(I+3) + DX(I+4)*DY(I+4)
   50 CONTINUE
   60 DDOT = DTEMP
      RETURN
      END


      SUBROUTINE  DSCAL(N,DA,DX,INCX)
      DOUBLE PRECISION DA,DX(1)
      INTEGER I,INCX,M,MP1,N,NINCX
      IF(N.LE.0)RETURN
      IF(INCX.EQ.1)GO TO 20
      NINCX = N*INCX
      DO 10 I = 1,NINCX,INCX
        DX(I) = DA*DX(I)
   10 CONTINUE
      RETURN
   20 M = MOD(N,5)
      IF( M .EQ. 0 ) GO TO 40
       DO 30 I = 1,M
       DX(I) = DA*DX(I)
   30 CONTINUE
      IF( N .LT. 5 ) RETURN
   40 MP1 = M + 1
      DO 50 I = MP1,N,5
        DX(I) = DA*DX(I)
        DX(I + 1) = DA*DX(I + 1)
        DX(I + 2) = DA*DX(I + 2)
        DX(I + 3) = DA*DX(I + 3)
```

```
      DX(I + 4) = DA*DX(I + 4)
   50 CONTINUE
      RETURN
      END


      SUBROUTINE  DSWAP (N,DX,INCX,DY,INCY)
      DOUBLE PRECISION DX(1),DY(1),DTEMP
      INTEGER I,INCX,INCY,IX,IY,M,MP1,N
      IF(N.LE.0)RETURN
      IF(INCX.EQ.1.AND.INCY.EQ.1)GO TO 20
      IX = 1
      IY = 1
      IF(INCX.LT.0)IX = (-N+1)*INCX + 1
      IF(INCY.LT.0)IY = (-N+1)*INCY + 1
      DO 10 I = 1,N
        DTEMP = DX(IX)
        DX(IX) = DY(IY)
        DY(IY) = DTEMP
        IX = IX + INCX
        IY = IY + INCY
   10 CONTINUE
      RETURN
   20 M = MOD(N,3)
      IF( M .EQ. 0 ) GO TO 40
      DO 30 I = 1,M
        DTEMP = DX(I)
        DX(I) = DY(I)
        DY(I) = DTEMP
   30 CONTINUE
      IF( N .LT. 3 ) RETURN
   40 MP1 = M + 1
      DO 50 I = MP1,N,3
        DTEMP = DX(I)
        DX(I) = DY(I)
        DY(I) = DTEMP
        DTEMP = DX(I + 1)
        DX(I + 1) = DY(I + 1)
        DY(I + 1) = DTEMP
        DTEMP = DX(I + 2)
        DX(I + 2) = DY(I + 2)
        DY(I + 2) = DTEMP
   50 CONTINUE
      RETURN
      END


      INTEGER FUNCTION IDAMAX(N,DX,INCX)
      DOUBLE PRECISION DX(1),DMAX
      INTEGER I,INCX,IX,N
      IDAMAX = 0
```

```
      IF( N .LT. 1 ) RETURN
      IDAMAX = 1
      IF(N.EQ.1)RETURN
      IF(INCX.EQ.1)GO TO 20
      IX = 1
      DMAX = DABS(DX(1))
      IX = IX + INCX
      DO 10 I = 2,N
         IF(DABS(DX(IX)).LE.DMAX) GO TO 5
         IDAMAX = I
         DMAX = DABS(DX(IX))
    5    IX = IX + INCX
   10 CONTINUE
      RETURN
   20 DMAX = DABS(DX(1))
      DO 30 I = 2,N
         IF(DABS(DX(I)).LE.DMAX) GO TO 30
         IDAMAX = I
         DMAX = DABS(DX(I))
   30 CONTINUE
      RETURN
      END
```

APPENDIX C

The fitting function used for $D_{SI}(X(E),E)$ interpolations :

For 0.35 MeV, fitting function : $Y = A + BX + CX^2$

where Y = dose x 10^{11} Gy per electron

X = scaled distance S from 0 to 2/3

A, B and C are fitting parameters

for RBM-RBM geometry

$A = 2.46 \pm 0.04$

$B = 4.1 \pm 0.4$

$C = -2.1 \pm 0.6$

for VAC-RBM geometry

$A = 2.19 \pm 0.01$

$B = 5.3 \pm 0.1$

$C = -3.3 \pm 0.2$

for CB-RBM geometry

$A = 2.61 \pm 0.05$

$B = 3.4 \pm 0.4$

$C = -1.3 \pm 0.6$

For 0.50 MeV, fitting function : $Y = A -$ [illegible] $- \exp(-CX))$

where Y = dose x 10^{11} Gy per electron

X = scaled distance S from 0 to 8/9

A, B and C are fitting parameters

for RBM-RBM geometry

$A = 2.01 \pm 0.06$

$B = 1.51 \pm 0.03$

$C = 3.7 \pm 0.2$

for VAC-RBM geometry

$A = 1.72 \pm 0.02$

$B = 1.72 \pm 0.03$

$C = 4.3 \pm 0.2$

for CB-RBM geometry

$A = 2.14 \pm 0.02$

$B = 1.30 \pm 0.03$

$C = 3.6 \pm 0.2$

For 0.75 MeV, fitting function : $Y = A + BX + CX^2 + DX^3$

where Y = dose x 10^{11} Gy per electron

X = scaled distance S from 0 to 2/3

A, B, C and D are fitting parameters

for RBM-RBM geometry

$A = 1.59 \pm 0.03$

$B = 6.6 \pm 0.6$

$C = -17 \pm 2$

$D = 18 \pm 2$

for VAC-RBM geometry

$A = 1.35 \pm 0.03$

$B = 8.1 \pm 0.5$

$C = -20 \pm 2$

$D = 19 \pm 2$

for CB-RBM geometry

$A = 1.76 \pm 0.03$

$B = 5.5 \pm 0.6$

$C = -15 \pm 2$

$D = 16 \pm 2$

For 1.00 MeV, fitting function : $Y = A + BX$

where Y = dose x 10^{11} Gy per electron

X = scaled distance S from 0 to 4/9

A and B are fitting parameters

for RBM-RBM geometry

$A = 1.59 \pm 0.02$

$B = 2.07 \pm 0.09$

for VAC-RBM geometry

$A = 1.32 \pm 0.02$

$B = 2.75 \pm 0.07$

for CB-RBM geometry

$A = 1.71 \pm 0.01$

$B = 1.84 \pm 0.05$

For 1.25 MeV, fitting function : $Y = A + BX$

where Y = dose x 10^{11} Gy per electron

X = scaled distance S from 0 to 4/9

A and B are fitting parameters

for RBM-RBM geometry

$A = 1.52 \pm 0.02$

$B = 2.02 \pm 0.08$

for VAC-RBM geometry

$A = 1.23 \pm 0.02$

$B = 2.66 \pm 0.08$

for CB-RBM geometry

$A = 1.62 \pm 0.02$

$B = 1.72 \pm 0.08$

For 1.50 MeV, fitting function : $Y = A + BX$

where Y = dose x 10^{11} Gy per electron
X = scaled distance S from 0 to 4/9
A and B are fitting parameters

for RBM-RBM geometry

$A = 1.43 \pm 0.02$
$B = 1.97 \pm 0.08$

for VAC-RBM geometry

$A = 1.19 \pm 0.02$
$B = 2.58 \pm 0.07$

for CB-RBM geometry

$A = 1.56 \pm 0.02$
$B = 1.71 \pm 0.08$

For 1.75 MeV, fitting function : $Y = A + BX$

where Y = dose x 10^{11} Gy per electron
X = scaled distance S from 0 to 4/9
A and B are fitting parameters

for RBM-RBM geometry

$A = 1.31 \pm 0.02$
$B = 2.04 \pm 0.08$

for VAC-RBM geometry

$A = 1.11 \pm 0.02$
$B = 2.56 \pm 0.07$

for CB-RBM geometry

$A = 1.38 \pm 0.02$
$B = 1.92 \pm 0.08$

The fitting functions for D(r,E) :

For 0-0.05 mm, fitting function : Y = A + B * exp (-CX)

where Y = dose x 10^{11} Gy per electron

X = scaled distance S from 0 to 8/9

A, B and C are fitting parameters

for RBM-RBM geometry

A = 1.8 ± 0.1

B = 7.6 ± 0.9

C = 2.8 ± 0.4

for VAC-RBM geometry

A = 1.6 ± 0.2

B = 6.8 ± 0.9

C = 2.4 ± 0.5

for CB-RBM geometry

A = 1.8 ± 0.2

B = 8 ± 1

C = 3.0 ± 0.6

For 0.75–0.80 mm, fitting function : $Y = A + B * \exp(-CX)$

where Y = dose x 10^{11} Gy per electron

X = scaled distance S from 0 to 8/9

A, B and C are fitting parameters

for RBM-RBM geometry

$A = 1.56 \pm 0.02$

$B = 8.5 \pm 0.2$

$C = 3.17 \pm 0.09$

for VAC-RBM geometry

$A = 1.32 \pm 0.03$

$B = 7.7 \pm 0.5$

$C = 2.71 \pm 0.07$

for CB-RBM geometry

$A = 1.66 \pm 0.02$

$B = 8.9 \pm 0.2$

$C = 3.37 \pm 0.09$

For 1.50-1.55 mm, fitting function : $Y = A - B \times \exp(-CX)$

where Y = dose x 10^{11} Gy per electron

X = scaled distance S from 0 to 8/9

A, B and C are fitting parameters

for RBM-RBM geometry

$A = 1.58 \pm 0.03$

$B = 11.0815 \pm 0.0009$

$C = 2.8 \pm 0.1$

for VAC-RBM geometry

$A = 1.58 \pm 0.03$

$B = 11.200 \pm 0.001$

$C = 0.2 \pm 0.1$

for CB-RBM geometry

$A = 1.87 \pm 0.03$

$B = 0.794 \pm 0.001$

$C = 3.2 \pm 0.1$

APPENDIX D

For mass density of TLD = 1.71 mg/cm^3

Fitting function : $Y = A + BX + CX^2$

where Y = energy deposition (MeV/electron)

X = electron energy (MeV)

A, B and C are fitting parameters

PST-PST geometry	VAC-PST geometry
$A = 0.0468 \pm 0.0006$	$A = 0.0498 \pm 0.0006$
$B = -0.043 \pm 0.004$	$B = -0.084 \pm 0.004$
$C = 0.037 \pm 0.004$	$C = 0.083 \pm 0.004$

For mass density of TLD = 2.39 mg/cm^3

Fitting function : $Y = A + BX + CX^2 + DX^3$

where Y = energy deposition (MeV/electron)

X = electron energy (MeV)

A, B, C and D are fitting parameters

PST-PST geometry	VAC-PST geometry
$A = 0.037 \pm 0.001$	$A = 0.044 \pm 0.001$
$B = 0.17 \pm 0.01$	$B = 0.10 \pm 0.01$
$C = -0.44 \pm 0.04$	$C = -0.32 \pm 0.04$
$D = 0.32 \pm 0.03$	$D = 0.25 \pm 0.03$